2012

MnSOD AND AUTOPHAGY IN PREVENTION OF OXIDATIVE MITOCHONDRIAL INJURIES INDUCED BY UVB IN MURINE SKIN

Vasudevan Bakthavatchalu
University of Kentucky, vasuvijai@gmail.com

MNSOD AND AUTOPHAGY IN PREVENTION OF OXIDATIVE
MITOCHONDRIAL INJURIES INDUCED BY UVB IN MURINE SKIN

———————————

DISSERTATION

———————————

A dissertation submitted in partial fulfillment of the
requirements for the degree of Doctoral of Philosophy in the
College of Medicine
at the University of Kentucky

By
Vasudevan Bakthavatchalu

Lexington, Kentucky

Director: Dr. Daret St Clair, Professor, Graduate Center for Toxicology

Lexington, Kentucky

2012

ABSTRACT OF DISSERTATION

MnSOD AND AUTOPHAGY IN PREVENTION OF OXIDATIVE
MITOCHONDRIAL INJURIES INDUCED BY UVB IN MURINE SKIN

UVB radiation is a known environmental carcinogen that causes DNA damage and increase ROS generation in mitochondria. Accumulating evidence suggests that mtDNA damage and increased ROS generation trigger mitochondrial translocation of p53. Within mitochondria, p53 interacts with nucleoid macromolecular complexes such as mitochondrial antioxidant MnSOD, mitochondrial DNA polymerase Polγ, and mtDNA. Mitochondria are considered to be a potential source for damage-associated molecular patterns (DAMPs) such as mtDNA, cytochrome C, ATP, and formyl peptides. Intracytoplasmic release of DAMPs can trigger inflammasome formation and programmed cell death processes. Autophagic clearance of mitochondria with compromised integrity can inhibit inflammatory and cell death processes.

In this study we investigated whether and how MnSOD plays a protective role in UVB-induced mitochondrial damage. The possibility of MnSOD participating in the mtDNA repair process was addressed *in vivo* using transgenic and pharmacological approaches. The results demonstrate that MnSOD functions as a fidelity protein that maintains the activity of Polγ by preventing UVB-induced nitration and inactivation of Polγ and that MnSOD coordinates with p53 to prevent mtDNA damage.

We also investigated whether autophagy is an adaptive response mechanism by which skin cells respond to mitochondrial injury, using mouse keratinocytes (JB6 cells) and C57/BL6 mice as *in vitro* and *in vivo* models. The results demonstrate that UVB induces autophagy initiation in murine skin tissues and that down regulation of AKT-mTOR levels triggers initiation of autophagy processes. These results suggest that autophagy may play a role in scavenging damaged mitochondria.

Taken together, the results from these studies suggest that MnSOD plays a protective role against UVB-induced mitochondria injury beyond its known antioxidant function. Within the mitochondrial matrix, MnSOD acts as an antioxidant and fidelity protein by prevention of UVB-induced nitration of Polγ. The functions of MnSOD may be to enhance mitochondrial membrane integrity and to prevent the genesis of oxidatively damaged mitochondrial components and subsequent intracytoplasmic spillage. Activation of autophagy serves as an additional response that scavenges damaged mitochondria.

KEYWORDS: MnSOD, Polymerase gamma, Autophagy, UVB, Mitochondria

<div align="right">

Vasudevan Bakthavatchalu
Student's Signature

Date

</div>

MnSOD AND AUTOPHAGY IN PREVENTION OF OXIDATIVE
MITOCHONDRIAL INJURIES INDUCED BY UVB IN MURINE SKIN

By

Vasudevan Bakthavatchalu

Dr. Daret St Clair
Director of Dissertation

Dr. Liya Gu
Director of Graduate Studies

Date

......This Dissertation is dedicated to my family and friends

Acknowledgements

I owe my gratitude to all the people who assisted me throughout my graduate training and with the successful completion of my dissertation. First and foremost, I would like to tender my sincere thanks to my mentor Dr. Daret K St. Clair for guiding me to be a self-motivated and independent researcher. I would also like to thank my Ph.D. committee members Dr. Mary Vore, Dr. Michael Reid, Dr. John D'Orazio, and Dr. Hsin-Sheng Yang for their time and effort to comment and review my research work. I would like to express my gratitude and thanks to Dr. Mary Vore, Director Graduate Center for Toxicology for giving me an opportunity to be a part of the Toxicology graduate program. My special thanks to Dr. D'Orazio for helping me to standardize UVB exposure studies in mice. I am thankful to Dr. Patrick Sullivan for agreeing to be my outside examiner.

Special thanks to Dr. William St. Clair and Edward Kasarskis for their valuable suggestions, criticisms and advice in our "Friday lab presentations". I also sincerely thank Dr. Ines Batinic-Haberle for kindly providing MnSOD mimetic used in this study. I would like to thank my present advisor Dr. Neil M. Williams, Associate Director, UKVDL, for his patience, faith, and support.

I would like to thank all my colleagues and friends of Dr. St Clair's lab especially Dr. Sanjit K Dhar, Dr. Sumitra Miriyala, Dr. Raman, Dr. Yulan Sun, Dr. Joyce Marie-Velez, and Dr. Noot. I would like to thank Dr. Yong Xu for his invaluable guidance and motivation and Teresa Noel for helping me with the invivo studies. I would like to thank Dr. Paiboon Jungsuwadee for helping me in standardizing mitochondrial isolation and Polγ reverse transcriptase assay. Special thanks to my good friend Lu Miao for her support and help to successfully complete

Table of Contents

List of Figures

List of Tables

List of Abbreviations

DAMP's	Damage associated molecular patterns
H_2O_2	Hydrogen peroxide
LC3-I, II	Microtubule-associated light chain 3
$Mn^{III}TE\text{-}2\text{-}PyP^{5+}$	Mn(III) meso-tetrakis(*N*-ethylpyridinium-2-yl) porphyrin
MnSOD	Manganese superoxide dismutase
mtDNA	Mitochondrial DNA
mTOR	Mammalian target of rapamycin
$O_2^{\cdot-}$	Superoxide
$OONO^-$	Peroxynitrite
PI3K	Phosphoinositide 3-kinase
Polγ	Polymerase gamma
ROS	Reactive oxygen species
UVB	Ultraviolet B radiation

1   Chapter One

1.1   Introduction

Skin being the largest organ of the body forms an anatomical barrier against environmental toxicants such as xenobiotics, UV and ionizing radiation. These environmental agents either directly or indirectly increase generation of reactive oxygen species (ROS). Interestingly, UV radiation mimics ROS and at the same time mediates ROS generation that triggers a cascade of signaling pathways involved in inflammation, apoptosis, DNA repair, proliferation and cell cycle arrest. These signaling molecules involved in mediating these events include NFκB, COX-2, Bax, Bcl2, MAPK, AP-1, p53, and p21 mediated pathways. ROS plays a critical role in the pathogenesis of various skin diseases such as photoaging and skin cancer. (Briganti and Picardo 2003, Trouba et al 2002, Zhou et al 2009).

Mitochondria are semi-autonomous organelles and the primary site for ROS generation in the cell. Mitochondrial DNA and proteins are more susceptible to oxidative damage. Exposure to agents such as UV, ionizing radiation, and chemical carcinogens favors increased ROS generation that results in mitochondrial dysfunction. The manganese superoxide dismutase (MnSOD) is a critical antioxidant against ROS-mediated damage by preventing the harmful effects of superoxide ($O_2^{-\bullet}$) through dismutation.

Recent studies have shown MnSOD association with mtDNA to be an integral constituent of nucleoids in the protection of mtDNA from ROS-mediated insults (Kienhofer et al 2009). Depletion and/or inactivation of the antioxidant system, particularly MnSOD in mitochondria due to ROS overload, results in damage to mtDNA and mitochondrial proteins. A breach in the first line of defense that prevents ROS-mediated damages triggers mitochondrial translocation of the tumor suppressor protein p53 that assists mtDNA repair by interacting with mtDNA repair proteins (Zhao et al 2005b). Factors that overwhelmingly increase oxidative stress results in activation of transcription-independent apoptosis by mitochondrial p53 and/or oxidative stress-mediated activation of autophagy. Autophagy is a catabolic pathway involved in clearance of damaged proteins and organelles such as mitochondria to ensure cell survival.

1.2   Ultraviolet radiation

Ultraviolet radiation is a constituent of the electromagnetic spectrum of sunlight. UVB lies between the visible spectrum and x-ray region and the wavelengths between 400 and 100 nm are divided into three regions, namely UVA between 400-320 nm, UVB between 320-280 nm, and UVC between 280-200 nm. UVC is completely prevented from reaching the earth by ozone layer. Approximately, 1-10% of UVB and more than 90% of UVA reaches the earth's atmosphere (Bowden 2004). High energy UVB radiation can penetrate up to the epidermal layer of the skin. UVB radiation causes DNA damage, denaturation of protein, and lipid peroxidation due to direct absorption by DNA, proteins, and lipids. UVA radiation can penetrate up to dermis and increases ROS production. These results in indirect DNA damage (oxidative DNA damage) and damage to elastin and collagen fibers. Acute exposure to UV results in both beneficial and harmful effects. Beneficial effects from acute UV exposure include skin pigmentation (tanning), bactericidal effects, and Vitamin D production.   The harmful effects of UV radiation are DNA damage, sunburn, erythema (inflammation), and immunosuppression. Chronic exposure to UV leads to photo aging and has been strongly associated with skin carcinogenesis. UV radiation has been used in phototherapy of disease conditions such as psoriasis, vitiligo, and atopic dermatitis.

1.2.1   The role of UV in skin cancer

Skin is the organ most exposed to UV radiation. Non-melanoma skin cancer accounts for 96% of skin cancer and the remaining 4% are attributed to melanoma. Every year approximately a million cases of skin cancer are diagnosed in United States. The ability to produce pigment and degree of pigmentation are the two important risk factors that determine skin cancer development (Gloster and Brodland 1996, Rigel 2008).

1.2.2   Mechanisms of DNA damage and DNA repair

The aromatic rings in the purines and pyrimidines structures in DNA absorb high-energy UV photons (maximum between 245 and 290 nm wavelength) (Tornaletti and Pfeifer 1996). This results in base adducts, strand breaks, and adjacent base

dimerization. The most common mutagenic lesions induced by UVB radiation are 6-4 photoproducts and cyclobutane pyrimidine dimers (CPD). The CPDs are formed by cyclobutane rings connecting the C4 and C5 carbon atoms of adjacent pyrimidines, as shown in Figure 1A. The 6-4 photoproducts are formed by a four -member ring intermediate between the C6 carbon of the 5' pyrimidine base and the C4 carbon of the 3' pyrimidine base (Pfeifer 1997), as shown in Figure 1B. Of these two photo lesions, CPDs occur more frequently, 6-4 photoproducts are repaired easily (Matsumura and Ananthaswamy 2002). When photo lesions are not repaired, UVB-induced signature mutations result in the form of C-T and CC-TT transitions. The nature of the DNA lesion determines the type of repair mechanism to be activated. Bulky adducts such as CPDs and 6-4 photoproducts are removed by the NER system. The photo lesions within the actively transcribed region are removed by transcription-coupled repair (TCR). The global genome repair pathway (GGR) repairs lesions in the non-transcribed region. The NER sub-pathways differ in their initial lesion recognition step. In GGR, the lesion is recognized by XPC/HHR23B. In TCR, the lesion is recognized by RNA polymerase II (Petit and Sancar 1999, van Hoffen et al 1995).

A
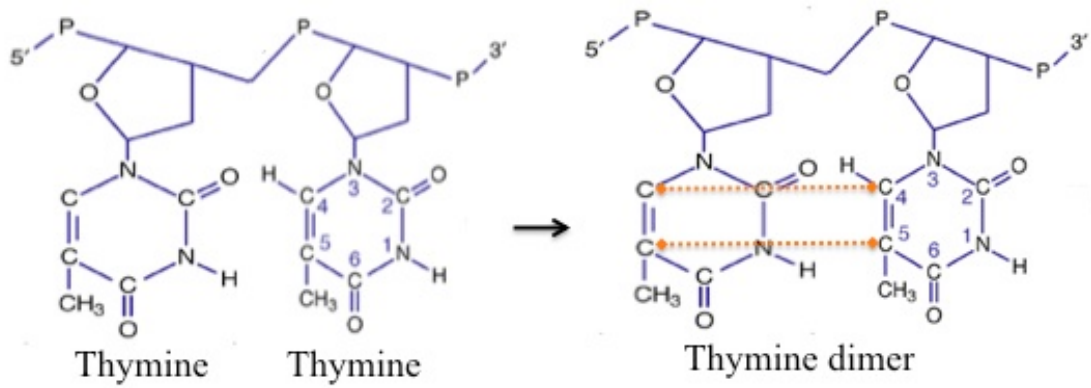
B
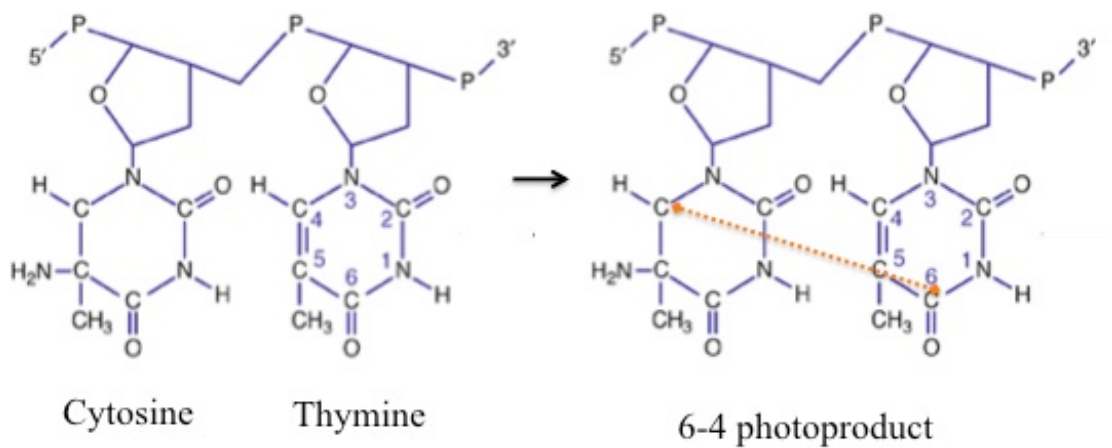
Figure 1.1 UV radiation induces mutagenic cyclopyrimidine dimers (CPDs) and 6-4 photoproducts between adjacent pyrimidine dimers in the DNA.

A. The CPDs are formed between C4 and C5 of adjacent pyrimidine dimers forming a four-ringed structure.

B. The 6-4 photoproducts are formed between C4 of 5' pyrimidine residue and C6 of 3' pyrimidine residue (adapted with permission from Matsumura Y and Ananthaswamy HN 2002. Expert Rev. Mol. Med. 4(26): 1-22).

1.2.3 p53-mediated gene regulation in UVB-exposed keratinocytes

Although keratinocytes have the ability to repair DNA damage caused by UV radiation, some cells retain the DNA lesions. Uncontrolled replication of these keratinocytes always results in skin cancer. However, skin has adaptive mechanisms to tightly regulate proliferation, differentiation, and cell death in different growth compartments of epidermis. Tumor suppressor protein p53 plays a critical role in mediating this temporo-spatial regulation of proliferation, differentiation, and cell death in keratinocytes. The initial response to UVB-induced DNA damage is p53 stabilization by phosphorylation of serine 15 and 20 residues that results in nuclear translocation of p53. As a transcription factor, p53 up-regulates expression of cell cycle control proteins such as p21/WAF1 (el-Deiry et al 1993) and GADD45 (Smith et al 1994). p21 (wild-type p53 activated fragment1)/CIP1 inhibits cyclin dependent kinase (CDK) and cause cell cycle arrest at G1-S phase (Harper et al 1993). GADD45 inhibits transition from G0-S phase and G2-M phases, by interacting with proliferating cell nuclear antigen (PCNA). GADD45 also stimulates the NER repair pathway (Maeda et al 2002). By regulating the cell cycle, p53 provides sufficient time for DNA repair before the S phase. In cells with severe DNA damage, p53 upregulates transcriptional dependent and transcriptional independent apoptotic pathways (Mihara et al 2003).

1.2.4 Differential function of p53 in UVB exposed skin

UVB-induced p53 protein plays a significant role in regulating apoptosis and DNA repair in the undifferentiated and differentiated compartments of epidermis. Loss of p53 decreases UVB induced DNA repair while the apoptotic rate remains unchanged (Li et al 1996). In the undifferentiated compartment, p53-independent apoptosis is minimal, while p53-dependent DNA repair is predominant. On the other hand, in the differentiated compartment p53-dependent apoptosis is predominant. Further, there is reduced activation of the NER pathway, which is p53 independent in the differentiated compartment (Li et al 1997). Apoptosis effectively eliminates damaged keratinocytes in differentiated compartment. On the other hand, DNA repair system effectively repairs the damaged keratinocytes in the basal compartment. This complex mechanism ensures epidermal integrity by protecting the epidermal stem cell population in the basal cell layer that is responsible for replenishing the epidermal

keratinocytes and is therefore critical to maintain homeostasis, as shown in Figure 2 (Tron et al 1998). UVB-induced mutation in p53 results in disruption of temporo-spatial regulation resulting in proliferation of basal cells with DNA damage and resistance to apoptosis. This gives a selective advantage to the p53-mutated clones over normal cells that undergo apoptosis when exposed to subsequent UVB radiation. The net result of keratinocyte proliferation-apoptosis dysregulation is the clonal expansion of p53-mutated cells that causes skin cancer.
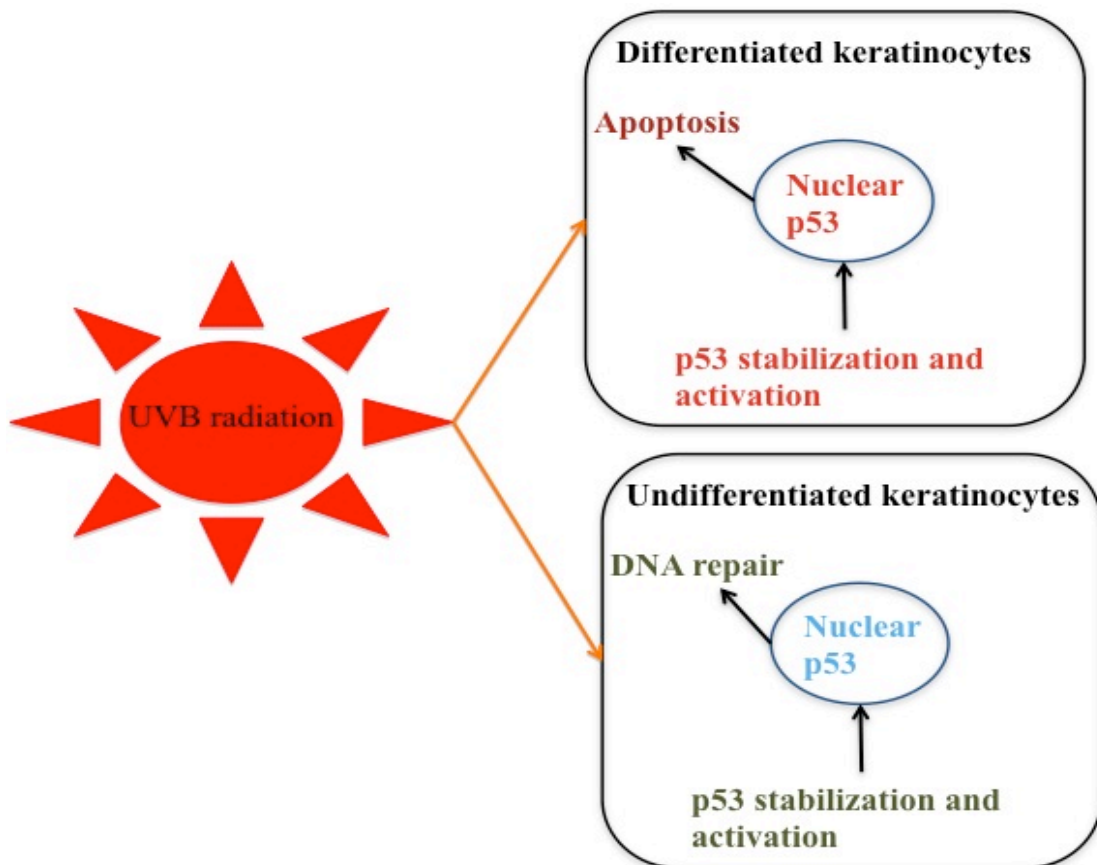
Figure 1.2 UVB induced cellular changes in epidermis

In the differentiated compartment of epidermis UVB-induced p53 causes increase in apoptosis. In the undifferentiated compartment of epidermis UVB-induced p53 causes increase in DNA repair (adapted from Tron VA et.al., 1998. Am. J. Pathol. 153(2): 579-585)

1.2.5   Effects of UVB-induced ROS generation in skin

Generation of ROS is the most immediate consequence of UV exposure in skin (Herrling et al 2006). Absorption of shorter wavelength UV radiation by conjugated bonds of organic molecules within the cells generates ROS. Keratinocytes exposed to UVB radiation activate xanthine oxidase and nitric oxide synthase (cNOS) to generate increased levels of $NO^{\bullet}$ and $O_2^{-\bullet}$ which in turn react to form peroxynitrite (Deliconstantinos et al 1996). Endogenous sensitizers, such as porphyrin and NADH, absorb energy from UV radiation and react with oxygen molecules to produce ROS (de Gruijl 2000). UV radiation can act both as a complete and incomplete carcinogen by causing damage to DNA, protein, and lipids. The endogenous photosensitizers, such as flavins, quinones, and porphyrins, absorb energy from UV radiation. These excited photosensitizers transfer energy to O_2 molecule by type II photosensitization mechanism to generate singlet and triplet oxygen. The guanine nucleotide has the lowest ionization potential, hence it is targeted by ROS generated by type II photosensitization mechanism. This results in increased formation of 8- oxo-7,8,-dihydro-2'-deoxyguanosine (8-oxo-dG) (Cadet et al 2000). 8-oxo-dG is the major oxidative base modification produced by hydroxy radicals and/or singlet oxygen on the C8 position of the 2'-deoxyguanosine (2-dG) in the nucleotide pool or within DNA (Cadet et al 2000, Hayakawa et al 1995, Kasai and Nishimura 1983). 8-oxo-dG plays a critical role in mutagenesis and carcinogenesis by pairing with adenine and cytosine (Shibutani et al 1991). Chronic exposure to UVB causes increased 8-oxo-dG formation. Hence, failure to remove 8-oxo-dG results in increased skin tumor formation (Kunisada et al 2005). Oxidation of guanine in DNA or formation of 8-oxo-dG in the nucleotide pool can cause G:C to T:A or A:T to C:G transversions. The 8-oxo-dG in the nucleotide pool is hydrolyzed to 8-oxo-dGMP by MTH1 protein (Nakabeppu 2001) and prevents spontaneous incorporation of 8-oxo-dG during DNA replication. 2-OH-A/adenine DNA glycosylase (MUTYH), 8-oxoG DNA glycosylase (OGG1), and apurinic/apyrimidinic (AP) endonuclease (APEX2) (Ide et al 2003) are involved in the removal to 8-oxo-dG from DNA as shown in Figure 3. All these enzymes are identified both in the nucleus and mitochondria (Tsuchimoto et al 2001).
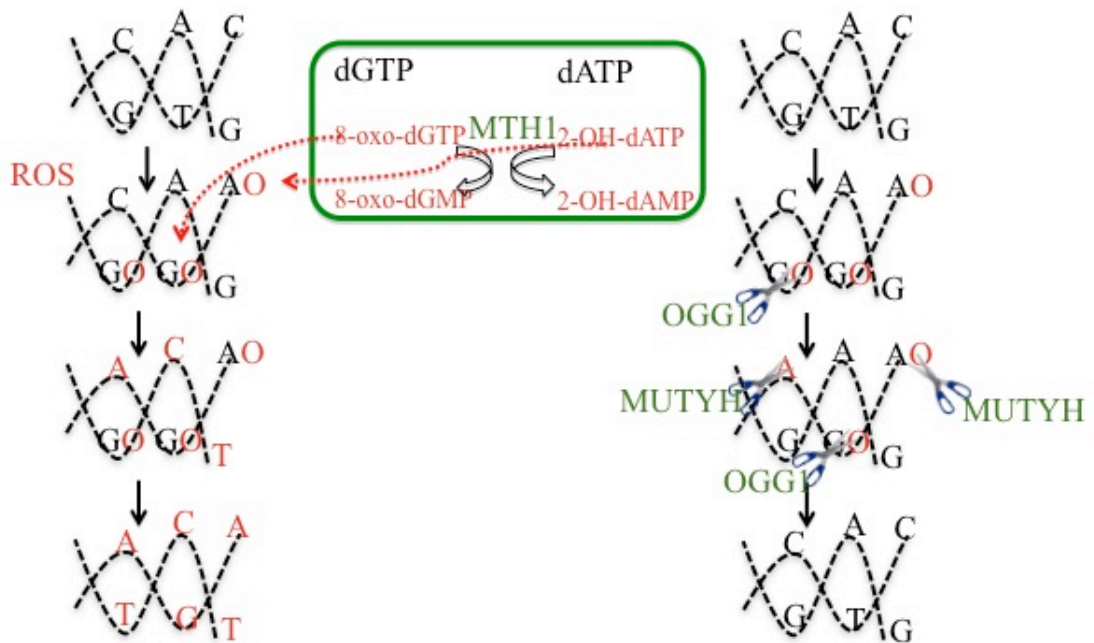
Figure 1.3 ROS-induced oxidative DNA damage and DNA repair mechanism.

Reactive oxygen species form 8-oxo-dG and 2-OH-A in the nucleotide pool and in the DNA strands. This results in G:C to A:T or A:T to G:C transversions. The 8-oxo-dG and 2-OH-A are removed by OGG1 and MUTYH respectively from the DNA strands. MTH1 hydrolyzes 8-oxo-dG, 8-oxo-dA and 2-OH-A, making them unavailable for incorporation during replication (adapted from Nakabeppu Y et al., 2004. Ann. NY. Acad. Sci. 1011:101-111).

1.2.6 UVB-induced ROS in skin carcinogenesis

Murine multistep skin carcinogenesis studies suggest that UV radiation is a complete carcinogen (Willis et al 1981). UV induced photoproducts and oxidative damage to DNA produce mutations in proto-oncogenes and tumor suppressor genes. The C-T and CC-TT transition mutation in hot spot regions of the p53 gene is an early event and p53 mutations are observed in more than 50% of actinic keratosis. Mutated undifferentiated cells (initiated cells) in the basal compartment of epidermis appear as early as 8 weeks (Berg et al 1996, Ziegler et al 1993, Ziegler et al 1994). The initiated cells have the following physical characteristics:

a. Unlimited proliferative potential

b. Increased resistance to UVB induced apoptosis compared to adjacent normal keratinocyte

c. Ability to generate and withstand ROS mediated damage

Clonal expansion of initiated cells results in UVB induced tumor promotion. UVB as tumor promoter can cause clonal expansion of initiated cells (Cerutti 1985, Zhang et al 2001). UVB-induced ROS mediated MAPK kinase activation plays a crucial role in AP-1 and NFκB activation. UVB activates ERK1/2, p38, and JNK signaling pathways by ROS generation (Bode and Dong 2003). UVB-induced ROS also stimulates the epidermal growth factor receptor (EGFR) by phosphorylation (Bode and Dong 2003, Cooper and Bowden 2007, Peus et al 1998). The activation of proliferation signaling cascades lead to skin cancer.

1.3 Tumor suppressor p53

p53 regulates the cell cycle and mutations that causes loss of the function of p53 often results in carcinogenesis. The ability of wild-type p53 to inhibit transformation induced by oncogenes, and deletion or mutation of wild-type p53 allele in different tumor types classified p53 as a tumor suppressor protein (Levine et al 1991).

p53 is activated in response to a tumor associated stress signal or various other cellular stress signals, such as hypoxia, irradiation, and DNA damage. p53 is described as "guardian of the genome" due to the fact that the biochemical function of p53 as a transcription factor can translate in to biological function by regulating cell cycle. (Lane 1992, Vousden and Lu 2002). UVB- induced skin cancer studies with

p53 knock-out mice reveal a decrease in apoptotic keratinocytes. In UVB exposed skin tissue, p53 induces apoptosis and not DNA repair in differentiated layers of epidermis. This results in efficient elimination of damaged keratinocytes. Hence, p53 has been named the "guardian of the tissue" in skin (Ziegler et al 1994). More than 90% of skin squamous cell carcinomas have mutated p53 (Brash et al 1991, Ziegler et al 1993).

Equal erythemogenic doses of UVA, UVB, and UVC induce p53 in a wavelength specific pattern. UVC increased p53 stabilization in the upper epidermal layer, while UVB increased p53 stabilization throughout the epidermis and UVA increased p53 stabilization only in basal layers of epidermis. However, the mechanism of p53 induction by UVA is different from that of UVB and UVC (Campbell et al 1993).

1.3.1 Post-translational p53 modification by UV radiation

In more than 50% of cancer, p53 mutation results in disruption of the apoptotic process. In normal cells, p53 is inactive and maintained at low concentrations by Mdm2 mediated polyubiquitination and degradation. Cellular stress factors such as hypoxia, metabolic stress, and DNA damage induced by UV radiation, ionizing radiation, and ROS result in p53 activation, stabilization, and by rapid accumulation of p53 in the cell (Harris and Levine 2005, Prives and Hall 1999). This increase in p53 level is due to decreased p53-Mdm2 interaction that results in decreased ubiquitination and degradation of p53 (Momand et al 2000). The above mentioned cellular stress factors employ different post-translational modifications of p53 to induce p53 activation. Various post-translational modifications of p53, such as phosphorylation, methylation, monoubiquitylation, sumoylation, and acetylation have been identified and are well elucidated. UV mediates phosphorylation of 2 threonine and 7 serine residues in the N-termini and 2 serine residues in the C-termini. This leads to increased p53 transcription, stabilization, and increased p53-mediated transcription. This results in increases in DNA repair, cell cycle control, and apoptotic proteins (Appella and Anderson 2001). UV radiation mediates acetylation of 2 lysine residues in the C-terminal domain. Acetylation of p53 results in increased transcriptional activity of p53 by an increase in its DNA binding property (Sakaguchi et al 1998). Methylation of lysine 372 residue by Set9methyl transferase increases nuclear localization and p53 stability (Chuikov et al 2004).

1.3.2   Translocation of p53 to mitochondria

Although mitochondrial translocation of p53 is a well-established phenomenon, the role of post-translational modification in translocation is still debated. Recent studies suggest monoubiquitylation as one of the possible mechanisms that may target p53 to mitochondria (Marchenko et al 2007). Mitochondria are the major source of ROS. ROS regulate communication between mitochondria and nucleus by redox modulation of various proteins such as phosphatases, kinases, and transcriptional factors (Liu et al 2008, Storz 2006). ROS mediate loss of zinc ions and oxidation of cysteine residues (Cys 227) in the DNA binding domain of the p53 protein. This interferes with the DNA binding properties of p53. (Fojta et al 1999). In the oxidized state, p53 interacts with thymine containing response elements. On the other hand, in the reduced state, p53 interacts with cytosine containing p53 response elements. These findings suggest modification of p53 transcriptional activity by ROS (Buzek et al 2002). Our laboratory findings show p53 translocation to mitochondria in JB6 cells and mice skin tissue exposed to the known oxidative stress inducer, TPA (Zhao et al 2005b). Mitochondrial localization of p53 has wide-ranging effects, from inducing apoptosis to mtDNA repair. As a transcriptional factor, p53 regulates the expression of the synthesis of cytochrome c oxidase 2 (SCO2) and regulates energy metabolism. SCO2 is required for cytochrome c oxidase complex formation and increased mitochondrial oxygen consumption (Matoba et al 2006). Apart from SCO2, p53 also regulates expression of key glycolytic enzymes. p53 negatively regulates phosphoglyceromutase and regulates the Tp53-induced glycolytic and apoptotic regulator (TIGAR). TIGAR dephosphorylates fructose-2, 6- bisphosphate to fructose-6-phosphate that is utilized in the pentose pathway (Bensaad et al 2006, Kondoh et al 2005).

1.3.3 p53 in mtDNA homeostasis

p53 plays an important role in mtDNA homeostasis. Studies with p53 knock-out mice fibroblasts show 50% reduction in mtDNA copy numbers and 40% reduction in mitochondrial mass. Similar results were observed in p53 deficient human fibroblasts. A decrease in p53 levels causes a decrease in mtDNA transcription and decrease in mtDNA-packaging factor (mtTFA) levels, and p53-regulated subunit of ribonucleotide reductase (p53R2) levels. mtTFA and p53R2 play critical roles in mtDNA maintenance (Lebedeva et al 2009). Increase in ROS and mtDNA damage triggered by DNA damaging agents, such as ethidium bromide, triggers mitochondrial translocation of p53. Mitochondrial p53 rescues mtDNA by interacting with Polγ and participating in the mitochondrial base excision repair (mtBER) process (Achanta et al 2005). The role of p53 in mtBER involves:

(i)   Stimulating nucleotide incorporation by Polγ

(ii)   Increasing glycosylase activity of mtBER

(iii)   Enhancing polymerization and 3'-5' exonuclease activity of Polγ (Chen et al 2006, de Souza-Pinto et al 2004).

Further, mitochondrial p53 reduces incorporation of nucleoside analog in mtDNA (Bakhanashvili et al 2008) and interacts with mitochondrial single stranded binding protein (mtSSB) to excise 8-oxodG from mtDNA (Wong et al 2009).

1.3.4 p53 mediated apoptosis

1.3.4.1 Transcription-dependent apoptosis

p53 mediates the intrinsic and extrinsic apoptotic pathways by transcriptional regulation of pro-apoptotic and anti-apoptotic proteins such as Bax (Miyashita and Reed 1995), Fas/Apo-1 (Owen-Schaub et al 1995), insulin- like growth factor binding protein 3 (IGF-BP3) (Buckbinder et al 1995), Killer/DR5 (Wu et al 1997), Noxa (Oda et al 2000a), the p53-regulated apoptosis inducing protein-1 (p53-AIP1) (Oda et al 2000b), PERP (Attardi et al 2000), and Bcl-2 (Haldar et al 1994).

p53 regulates the mitochondria mediated intrinsic apoptotic pathway by transcription dependent and transcription independent mechanisms (Moll and Zaika 2001). p53

13

regulates transcription of apoptotic protease activating factor-1 (APAF-1), a scaffolding protein that complexes with cytochrome c released from mitochondria and caspase-9 to form apoptosome (Robles et al 2001). Similarly, p53 regulates transcription of p53 upregulated modulator of apoptosis (PUMA), a BH3 domain containing protein. Mitochondrial translocation of PUMA causes induction of cytochrome C release to trigger activation of the intrinsic pathway (Nakano and Vousden 2001).

1.3.4.2 Transcription-independent apoptosis

The transcription independent pro-apoptotic function of p53 involves a direct translocation of p53 to mitochondria and the outer mitochondrial membrane. The p53 translocation event precedes alterations in mitochondrial membrane potential and the cytochrome c release associated with apoptosis (Erster et al 2004, Marchenko et al 2000). Cytoplasmic p53 is sequestered through its interaction with Bcl-xL. Nuclear translocation of p53 by the genotoxic stress signal results in transcriptional upregulation of PUMA. PUMA interaction with Bcl-xL aids disruption of cytoplasmic sequestration of p53 by Bcl-xL. This results in p53 translocation to the outer mitochondrial membrane. p53 interacts and activates Bax to induce mitochondrial outer membrane potential (MOMP) (Chipuk et al 2004, Chipuk et al 2005). Within the outer mitochondrial membrane, p53 activates Bak by disrupting its interaction with Mcl1 (Leu et al 2004).

1.3.5 p53 regulates mitochondrial ROS

p53 is essential for mitochondrial biogenesis and ROS homeostasis. Lack of p53 leads to decreased mitochondrial mass, indicative of reduction in mitochondrial oxidative capacity (Lebedeva et al 2009). Mitochondrial antioxidant MnSOD activity is increased in p53 deficient cells, which is also a common feature in most cancer cell types with p53 mutations. These p53 deficient cells are capable of surviving in conditions that induce cell death in normal cells (Pani et al 2000). An increase in p53 expression reduces MnSOD expression and activity. p53 interaction with Sp-1, a transcription factor that binds to the MnSOD promoter, is attributed to the p53-induced suppression of MnSOD gene expression (Dhar et al 2006).

1.4 Mitochondrial structural organization and function

Mitochondria are organelles approximately 0.5 to 1 μm in diameter and up to 5 μm long. The morphology, activity, and distribution of mitochondria are regulated by fusion and fission process (Chan 2006, Okamoto and Shaw 2005). Mitochondria have two phospholipid bilayer membranes. The outer and inner mitochondrial membranes are separated by intermembrane space and have distinct physiochemical properties based on their phospholipid composition and protein-to-lipid ratio. The outer membrane contains porin, a protein that forms nonspecific pores that are widely permeable to ions and larger molecules. The outer membrane has a protein-to-lipid ratio of 50:50. The inner membrane has an 80:20 protein-to-lipid ratio and is less permeable to ions and small molecules. The mitochondrial matrix is composed of mtDNA and an array of enzymes involved in carbohydrate, lipid, and amino acid oxidation. The inner membrane is organized into numerous projections called cristae. The cristae compartmentalize the mitochondrial matrix and increase the surface area of the inner membrane. The inner membrane contains respiratory complexes responsible for oxidative phosphorylation. The NADH and FADH2 produced in the mitochondrial matrix by the citric acid cycle are used as substrates for oxidative phosphorylation. Oxidative phosphorylation is a chemiosmotic process in which electrons are transferred through a series of respiratory protein complexes (Lenaz et al 2010) to oxygen and thereby reducing oxygen to water. The electron transfer by respiratory complexes is coupled to the transfer of protons against the electrochemical gradient from matrix to the intermembrane space. The electrochemical gradient that results from proton transfer across the inner membrane enables F1F0ATP synthase to generate ATP (Krauss 2001).

1.4.1 Mitochondrial respiratory complexes in ROS generation

Complex I is considered to be one of the main sites of ROS production and are involved in lipid peroxide production (Takeshige and Minakami 1979). Electron leak from complex I and transport of electron from succinate to NAD^+ are two possible mechanisms by which complex I generate $O_2^{-\bullet}$. Compounds like Adriamycin generate

$O_2^{-\bullet}$ via complex I by a redox cycling mechanism. This involves transfer of an electron to Adriamycin, resulting in semiquinone formation. The semiquinone radical subsequently reacts with oxygen to regenerate Adriamycin and $O_2^{-\bullet}$. (Salvatorelli et al 2006).

$O_2^{-\bullet}$ generation by complex III involves the Q cycle with transfer of electron against the electrical gradient. In state 4 mitochondrial respiration, the very high electrochemical potential inhibits the transfer and allows sufficient time for semiquinone to react with oxygen, resulting in $O_2^{-\bullet}$ generation (Jezek and Hlavata 2005). Increased electron flow through complex II and auto-oxidation of flavin in complex II cause complex II to generate $O_2^{-\bullet}$ (McLennan and Degli Esposti 2000, Zhang et al 1998). In addition to respiratory complexes, mitochondrial glycerophosphate dehydrogenase and dihydroorotate dehydrogenase are also involved in $O_2^{-\bullet}$ generation in mitochondria.

1.4.2   Pathological conditions associated with ROS-induced mtDNA damage

The mitochondrial genome consists of multiple copies of circular DNA that encodes 13 polypeptides required for oxidative phosphorylation, and 2 RNAs and 22 tRNAs required for their translation. The mitochondrial genome follows a non-Mendelian pattern of inheritance. About 93% of the mitochondrial genome is composed of coding DNA and no introns, with a gene density of 1 gene per 450 base pairs. The mitochondrial genome is not protected by histone proteins, however it is associated with several proteins to form nucleoids. Mitochondrial replication is based on strand-coupled and strand-displacement models. All genes are transcribed as large polycistrons.

mtDNA is a target for most chemical carcinogens and mtDNA is implicated as having a causal role in metastasis and oncogenic transformation (Allen and Coombs 1980, Backer and Weinstein 1980). Most tumors have a high frequency of homoplasmic point mutations in mtDNA (Coller et al 2001, Fliss et al 2000). mtDNA mutations and deletions are implicated in a number of hereditary disease conditions, such as Leber's hereditary optic neuropathy (LHON) (Wallace et al 1988) and spontaneous neuromuscular diseases such as chronic progressive ophthalmoplegia (CPEO), and

Kearns-Sayresyndrome (KSS) (Holt et al 1988, Wallace 1999). mtDNA deletions such as 4977-bp (Yang et al 1994) and 3895-bp (Krishnan et al 2004) in skin mitochondria are used as biomarkers for cumulative exposure to sun that is indicative of photo-aging. The implication of mitochondria in diseases is due to its ability generate ROS. ROS induced damage to mtDNA results in alteration of polypeptides encoded by mtDNA for respiratory complexes. These results in a further decrease of electron transfer activity and increases ROS generation. This establishes a "vicious cycle" of oxidative stress (Levine et al 1991) and decline in energy production (Achanta et al 2005, Lenaz and Genova 2010).

1.5 Reactive Oxygen Species (ROS) and Reactive Nitrogen Species (RNS)

When the balance between pro-oxidant and antioxidant is tipped toward pro-oxidant, oxidative stress results. This may be due either to increased production of pro-oxidants like reactive oxygen species (ROS) and reactive nitrogen species (RNS) or due to depletion of the antioxidant system. Aerobic metabolic processes, such as respiration, that involves mitochondria and microsomes, are responsible for ROS generation. $O_2^{-\bullet}$ is formed by transfer of an electron to ground state molecular oxygen Sequential reduction of $O_2^{-\bullet}$ results in formation of various ROS and water as shown in Figure 4. Approximately 1-2% of the oxygen consumed for mitochondrial respiration is converted to $O_2^{-\bullet}$ or into its dismutation product hydrogen peroxide (H_2O_2) (Boveris and Chance 1973). Further, in the presence of such metal ions such as Fe (III) or Cu (III), oxygen and H_2O_2 can generate hydroxyl ions that target the amino acid side chains at metal-binding site and cause protein oxidation (Stadtman 1990). This results in loss of enzyme function, cell integrity, and genomic instability (Hensley et al 2000). ROS is implicated in tumor initiation, promotion and progression stages of multistage carcinogenesis model. ROS can modulate cell growth, cell proliferation, and cell survival molecules such as c-FOS, c-JUN, c-MYC and AKT (Cerutti 1985, Cerutti and Trump 1991).
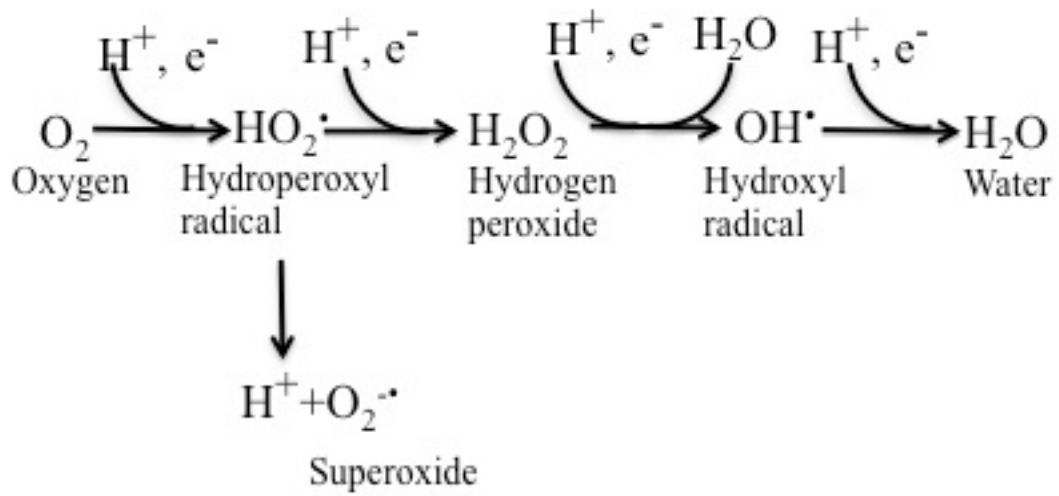
Figure 1.4 Sequential reduction of oxygen to water

Conversion of molecular oxygen to water requires sequential addition of 4 electrons that results in formation of different intermediate ROS molecules such as superoxide, peroxide, and hydroxyl radical, respectively. (Adapted from Imlay JA 2008. Annu. Rev. Biochem. 77:755-776.

1.5.1 Peroxynitrite and its effects on cellular components

Peroxynitrite (OONO$^-$) is an anion and a strong oxidant. Unlike OH$^\bullet$, OONO$^-$ can diffuse within a cell to cause oxidative damage and nitration (Radi 1998). The OONO$^-$ anion is formed at diffusion-controlled rates by the reaction between O$_2^{-\bullet}$ and NO$^\bullet$. The site of OONO$^-$ formation is spatially associated with O$_2^{-\bullet}$. This is due to the limited ability of O$_2^{-\bullet}$ to diffuse across membranes and its short half-life. The sources of O$_2^{-\bullet}$ are mitochondria, NADPH oxidase, and xanthine oxidase. The OONO$^-$ is produced at the rate of 50-100 μM per minute (Alvarez et al 2004, Nalwaya and Deen 2005, Quijano et al 2005). Although OONO$^-$ has a very short half-life at physiological pH (approximately 10 ms), its ability to diffuse through cell membrane up to 5- 20 μm has wide-ranging effects on adjacent cells. Within cells, OONO$^-$ cause antioxidant depletion and inhibition, protein aggregation, cytosolic enzyme activation and inhibition, enzyme cofactor impairment, modification of molecular mediators of cell signaling pathways, lipid peroxidation, calcium dysregulation, mitochondrial dysfunction, and DNA damage (Szabo et al 2007).

1.5.1.1 Direct oxidation by peroxynitrite

Oxidation reactions of OONO$^-$ are pH dependent and both OONO$^-$ and OONOH participate in oxidation of biomolecules with thiol groups and transition metal centers. Peroxynitrite reacts with thiol containing proteins such as glutathione and cysteine (Carballal et al 2003, Quijano et al 1997). The important cellular reaction involved in scavenging OONO$^-$ is glutathione oxidation. Seleno compounds and selenoproteins such as glutathione peroxidase are also involved in reducing OONO$^-$ and are recycled by glutathione. OONO$^-$ disrupts transition metal centers of proteins, such as alcohol dehydrogenase (Zn-S center) and aconitase (4Fe-4S cluster) (Szabo et al 2007). Heme-containing proteins, such as oxyhemoglobin (Romero et al 2003), peroxidases, and cytochrome c^{2+}, are also oxidized by peroxynitrite (Szabo et al 2007).

1.5.1.2 Nitration reactions by peroxynitrite

The Fe, Zn, Cu, and Mn containing superoxide dismutase enzymes are nitrated by OONO$^-$. MnSOD nitration leads to subsequent inactivation of its enzymatic activity (MacMillan-Crow et al 1998). In the presence of transition metals, metalloproteins,

and carbon dioxide, OONO⁻ can cause nitration of tyrosine (Ischiropoulos et al 1992), tryptophan residues of proteins, guanine residues of DNA (8-oxo and 8-nitro guanine) (Burney et al 1999, Szabo and Ohshima 1997), and aliphatic groups of sugars and fatty acids.

1.5.1.3 Peroxynitrite-carbon dioxide reaction

The OONO⁻ reaction with carbon dioxide gains more importance because:

1. It accounts for 30-40% (intracellular) and 90% (extracellular) of OONO⁻ reactivity.

2. There is an abundant availability of carbon dioxide in both intra- and extra -cellular compartments.

The OONO⁻ and CO_2 yields an adduct nitrosoperoxocarbonate (ONOOCO$_2^-$). The ONOOCO$_2^-$ decomposes to carbonate ($CO_3^{\bullet-}$) and nitrogen dioxide ($^{\bullet}NO_2$) radicals, which are one-electron oxidants (Goldstein et al 2005, Lymar and Hurst 1998). Compared with OONO⁻ anion, the oxidation reactions that form these radicals have lower yield. However, the nitration reaction has a higher yield and is accelerated by a factor of 2 in the presence of carbon dioxide (Radi et al 2001).

A small fraction of OONO⁻ also undergoes slow homolytic fission and proton-catalyzed decomposition to form one-electron oxidants $^{\bullet}NO_2$ and $CO_3^{\bullet-}$. This reaction assumes significance due to the fact that this reaction initiates lipid peroxidation processes (Mustafa et al 2010). Peroxynitrite can also nitrosate thiols, lipids, and sugars that elicit strong biological responses, such as vasodilation (Radi 1998).

1.5.2 Peroxynitrite in mitochondria

Mitochondria remain the primary site for formation and interaction of peroxynitrite. Cells exposed to $^{\bullet}NO$ have decreased mitochondrial respiration due to inactivation of succinate dehydrogenase, NADH dehydrogenase and ATPase by OONO⁻ formed from the reaction between $O_2^{\bullet-}$ and $NO^{\bullet}$ (Radi et al 1994). Peroxynitrite inhibits glutamate/malate and succinate supported oxygen consumption and also enhances generation of ROS such as $O_2^{\bullet}$ and H_2O_2 in a complex-II dependent mechanism. In addition to increasing the generation of ROS, OONO- also inactivates the mitochondrial antioxidant MnSOD by nitration of Tyr34 residue. This further aggravates mitochondrial injury by failure to detoxify the accumulating $O_2^{\bullet-}$ within

mitochondria (MacMillan-Crow et al 1996, Yamakura et al 1998). Recently, cytochrome c has been identified as a target for peroxynitrite induced nitration. Nitration of cytochrome c at Tyr67 residue is critical due to its ability to promote conformational change by disrupting the heme-methionine bond (Batthyany et al 2005, Cassina et al 2000). Nitration of cytochrome c increases its peroxidase activity. This adds further insult to the mitochondrial oxidative injury caused by peroxynitrite (Jang and Han 2006).

1.6   Antioxidant systems

1.6.1   MnSOD in normal cellular homeostasis and various disease processes

Manganese superoxide dismutase (MnSOD) is a nuclear encoded mitochondrial antioxidant protein. MnSOD is essential to protect aerobic life from adverse effects of oxygen by catalyzing the dismutation of $O_2^{\bullet-}$ generated by oxidative phosphorylation. MnSOD is a 96 kDa homotetramer transported to mitochondria by an amino-terminal mitochondrial target sequence. The importance of MnSOD to aerobic life forms is well demonstrated by MnSOD gene knock-out studies in mice and *Drosophila* models (Duttaroy et al 2003, Li et al 1995). In mice, deletion mutation of the MnSOD gene results in embryonic lethality at 5-21 days after birth and exhibits several pathologic lesions that include myocardial injury, left ventricular dilation and hypertrophy, severe anemia due to bone marrow depletion, neurodegeneration, severe mitochondrial damage, and lipid peroxidation (Lebovitz et al 1996, Li et al 1995). Several important mitochondrial enzymes involved in oxidative phosphorylation and the citric acid cycle such as succinate dehydrogenase and aconitase activities are significantly reduced in MnSOD knock-out mice and *Drosophila* (Li et al 1995, Paul et al 2007). MnSOD enzymatic activity is decreased by nitration of tyrosine residues, resulting in decreased mitochondrial activity (MacMillan-Crow et al 1998, MacMillan-Crow and Thompson 1999). Inactivation of MnSOD by nitration has been implicated in Alzheimer's disease pathogenesis (Anantharaman et al 2006). Long-term heterozygous MnSOD knock-down studies reveal increased oxidative DNA damage to both nuclear and mitochondrial DNA and a higher incidence of carcinogenesis (Van Remmen et al 2003). In condition such as diabetes, cancer, radiation injury, neuronal disease, and cardiovascular diseases there is a decrease in MnSOD expression or activity. Treatment with SOD mimetics such as 5, 10, 15, 20-

tetrakis (4-benzoic acid) porphyrin (MnTBAP), $Mn^{III}TE-2-PyP^{5+}$, and MnTnHex-2-PyP^{5+} prevents the adverse effects of decreased MnSOD expression or activity. (Batinic-Haberle et al 2010, Batinic-Haberle et al 2011).

1.6.2 Role of MnSOD as tumor suppressor

The role of MnSOD in cancer has been unclear until now due to the fact that MnSOD expression and/or activity increases or decreases in different tumor types (Chung-man Ho et al 2001, Oberley et al 1978, Oberley and Buettner 1979, Zhong et al 1999). The decrease may be attributed to either defects in MnSOD gene expression due to mutation in the promoter region (Wan et al 1994) or to inactivation by nitration (Vickers et al 1999). Tumors that have increased metastatic potential and poor prognosis have increased MnSOD expression (Janssen et al 2000, Malafa et al 2000). Further, over-expression of MnSOD alters many physical properties of tumors such as increased proliferation, decreased apoptosis, anaplasia, invasiveness, and anchorage independent growth (Chuang et al 2007, Church et al 1993). The role of MnSOD tumor initiation and promotion has been well studied by a murine multistep chemical skin carcinogenesis model. There was decreased incidence and number of papillomas in MnSOD over-expressing mice compared to the non-transgenic genotype due to a decrease in the level of 4-HNE modified proteins by tumor promoter treatment (Zhao et al 2001). With MnSOD knock-down mice, the incidence and number of papillomas were similar to that of wild-type mice and this might be due to an increase in both apoptosis and proliferation after tumor promoter treatment. (Zhao et al 2002). The increase in apoptosis might suppress the increased proliferation in MnSOD knock-down mice. Further, apoptosis precedes proliferation as apoptosis peaks at 6 h post treatment while mitosis peaks at 24 h post treatment. An intervention of the proliferative phase was made by treatment with MnSOD mimetic 12 h after tumor promoter treatment. The mimetic treatment reduces proliferation without affecting the apoptotic process resulting in a 50% decrease in tumor incidence. This provides a possible mechanism by which MnSOD acts as a tumor suppressor by reducing the oxidative stress-mediated tumorigenesis process (Zhao et al 2005a).

1.6.3 Regulation of transcription factors by MnSOD in tumor suppression

Another mechanism by which MnSOD causes tumor suppression is by altering the expression or activity of other tumor suppressors, oncogenes, and transcription factors (Chuang et al 2007, Kiningham and St Clair 1997, Li et al 1998). Regulation of transcription factors such as AP-1 and p53 by MnSOD has been well studied in our laboratory using a murine multi-stage skin carcinogenesis model. Treatment with DMBA and TPA activates AP-1 and p53, resulting in increased proliferation and apoptosis in the basal layers of the epidermis. Compared to wild-types, the increase in AP-1 activation in MnSOD knock-down is much greater. The increased AP-1 activation can be prevented by treatment with $Mn^{III}TE-2-PyP^{5+}$. This demonstrates the role of MnSOD in modulating AP-1 activity in multi-stage skin carcinogenesis (Zhao et al 2005a).

1.6.4 Modulation of ROS by MnSOD in tumor suppression

MnSOD acts as a tumor suppressor primarily by modulating ROS generation. (Oberley 2005). In most of the tumor types, over-expression of MnSOD causes partial suppression of tumor phenotype. Alteration in MnSOD enzymatic activity by polymorphisms such as I58T or V9A plays a significant role in tumor suppression (Ambrosone et al 1999, Borgstahl et al 1996). This suggest that increase in MnSOD level results in tumor suppression in different tumor types (Oberley 2005). Modulation of the signal transduction pathway by redox regulation is attributed to non-cytotoxic tumor suppression by increased MnSOD levels.

1.6.5 Alteration of MnSOD expression in carcinogenesis

Our laboratory has extensively studied alterations in the regulation of MnSOD gene expression. Sp-1 and AP-2 binding sites have been identified in the MnSOD GC-rich promoter region (Wan et al 1994). Sp-1 is a transcriptional activator of basal and TPA-induced MnSOD expression and Sp-1 interaction with transcription factors such as p53 repress MnSOD gene expression. AP-2, on the other hand, is a transcriptional repressor of MnSOD expression (Dhar et al 2006, Porntadavity et al 2001, Xu et al 2002). An NF-κB response element identified in the intron 2 region confers NF-κB-mediated MnSOD expression to which nucleophosmin is an important cofactor (Dhar

et al 2004, Xu et al 1999a, Xu et al 2007b). Transition, insertion, and transversion mutations to the GC rich promoter region have been identified in different tumor cell types. These mutations in the promoter result in at least 50% reduction in MnSOD transcription compared to the normal promoter (Xu et al 1999b). The C$\rightarrow$G transversion at -38 site in several human colorectal carcinomas creates a binding site for both Sp-1 and AP-2. Hence, the relative levels of Sp-1 and AP-2 determine MnSOD expression (Xu et al 2008). The insertion of A in the 11-straight G region at -93 site disrupts the nucleophosmin mediated interaction between the 11G loop at the promoter region and the enhancer region in the intron 2, resulting in decreased MnSOD expression (Xu et al 2007b).

Four kinds of single nucleotide polymorphisms (SNP) have been identified in the MnSOD gene. The Ala16Val SNP due to C$\rightarrow$G transition in the mitochondrial signal sequence affecting MnSOD translocation to mitochondria is well understood and studied in different tumor types. The Ala16 wild-type variant forms a partial α-helical structure that localizes in the mitochondrial matrix. The Val16 variant forms a β-sheet structure that localizes in the mitochondrial inner membrane and has decreased MnSOD activity (Rosenblum et al 1996, Sutton et al 2003). The Val16 SNP has been implicated in ovarian, lung, pancreatic, and prostate cancer (Bag and Bag 2008, Johnatty et al 2007, Wang et al 2001, Woodson et al 2003). Other MnSOD SNPs affect MnSOD transcription, enzyme activity and thermal stability, and create potential glucocorticoid receptor binding sites (Borgstahl et al 1996, Hernandez-Saavedra and McCord 2003, Hernandez-Saavedra and McCord 2009, Ho and Crapo 1988). Recent studies have identified MnSOD as an integral constituent of nucleoids. As a constituent of nucleoid MnSOD plays a vital part in protecting mtDNA and associated proteins from oxidative stress (Kienhofer et al 2009).

1.7   Mitochondrial DNA polymerase gamma

DNA polymerase gamma (Polγ) is the mitochondrial polymerase enzyme responsible for mtDNA replication, repair, and the recombination process (Graziewicz et al 2006, Kaguni 2004). Polγ was first identified as a RNA-dependent DNA polymerase present in mitochondria that represents 1% of the total cellular polymerase activity (Bolden et al 1977, Fridlender et al 1972). Polγ belongs to the A group family of polymerases. Polγ catalytic subunit shares structural homology with other polymerases in the group

that includes *Escherichia coli* DNA polymerase I, *Thermus aquaticus*DNA polymerase, and bacteriophage T7 DNA polymerase (Lecrenier et al 1997). The human Polγ catalytic subunit is mapped to chromosomal location 15q24 and the accessory subunit is mapped to chromosomal location 17q23-24. The Polγ encodes 1239 amino acids and has a 13-glutamine stretch in the N-termini encoded by CAG repeats in exon 2 (Lecrenier et al 1997, Ropp and Copeland 1996). Polγ is a heterotrimer composed of a 140 kDa catalytic unit and a dimer of 55 kDa accessory subunits (Bolden et al 1977, Gray and Wong 1992, Lim et al 1999, Wang et al 1997, Yakubovskaya et al 2006).

A wide range of substrates that includes homopolymers such as poly(dA).oligo(dT) and poly(dC).oligo(dG), single primed M13 DNA, and activated DNA is utilized by Polγ. Polγ possesses a unique reverse transcriptase activity that enables it to utilize poly(rA).oligo(dT) homopolymer. The ability of Polγ to utilize poly(rA).oligo(dT) is often used in assays to differentiate Polγ from other DNA polymerases (Graziewicz et al 2006). The N-terminal region contains an exonuclease domain with conserved motifs I, II, and III. The C-terminal region has a polymerase domain with conserved motifs A, B, and C and 6 conserved sequence elements (γ1, γ2, γ3, γ4, γ5, and γ6) (Kaguni 2004). Extended spacer region separates the polymerase and exonuclease domain (Yakubovskaya et al 2007). The catalytic subunit interacts with the accessory subunits by spacer region. It is thought that the spacer element might be involved in functional linking between polymerase and exonuclease activities, DNA binding, and subunit interaction (Graziewicz et al 2006).

The polymerase activity of Polγ has a fidelity of 1 error in 2.8 million base pairs incorporated (Johnson and Johnson 2001). Mutations in the conserved sequence elements and spacer region affect processivity, DNA binding affinity, polymerase activity, and exonuclease activity. Hence Polγ mutations have been implicated in various mitochondrial disorders (Luo and Kaguni 2005). Polγ is active between pH 7.5 and 9.5 and requires divalent cation (Mg^{2+}/Mn^{2+}). The two tyrosine residues (Tyr 951 and 955) along with glutamine residue (Glu 895) form a hydrophobic pocket in the active site of Polγ. The amino acid residues in the active site are responsible for interaction and selection of nucleotides by Polγ (Bienstock and Copeland 2004, Graziewicz et al 2004). Polγ activity is inhibited by dideoxynucleotides, sulfhydryl

blocking agent N-ethylmaleimide (NEM), ROS, and high salt concentration. However, it is resistant to inhibition by aphidicolin. The inhibitory effects of NEM, ROS and high salt concentration are attributed to the absence of an accessory subunit. Further, the presence of an accessory subunit confers resistance to inhibition in the holoenzyme (Graziewicz et al 2002, Lim et al 1999) .

The presence of a Polγ accessory subunit also stimulates processivity, polymerase and exonuclease activity of the catalytic subunit (Carrodeguas et al 1999, Johnson et al 2000, Wang and Kaguni 1999). The catalytic subunit of Polγ has intrinsic 5'-deoxyribose phosphate (dRP) lyase activity that is involved in mtDNA repair by a base excision repair pathway (Longley et al 1998). The intrinsic dRP-lyase activity allows Polγ to catalyze and remove the 5'-dRP sugar moiety from an incised apurinic/apyrimidinic site and incorporates appropriate nucleotides. The accessory subunit enhances the lyase activity of the catalytic subunit (Longley et al 1998, Pinz and Bogenhagen 1998).

Mutations in the *POLG* gene are extensively studied and lead to mtDNA depletion and deletion disorders. Mutations in *POLG* are associated with diseases such as progressive external ophthalmoplegia (PEO), Alper's syndrome, premature menopause, Parkinsonism, sensory ataxia neuropathy, dysarthria and ophthalmoparesis (SANDO), and mitochondrial neurogastrointestinal encephalopathy (MNGIE) (Graziewicz et al 2006). Mutations in *POLG* can be classified as 3 types; namely,

(i)   Class I mutations that occur in the Polγ catalytic site and reduce Polγ enzymatic activity

(ii)   Class II mutations that occur in the DNA binding channel and interfere with DNA binding affinity

(iii)   Class III mutations that interfere with interaction between the catalytic subunit and the accessory subunit and decrease processivity (Lee et al 2009).

Mutations in the polymerase domain that cause PEO, such as Y955C and R943H, decrease polymerase activity. The decrease in the polymerase activity of Polγ is due to amino acid substitution that interferes with enzyme translocation and interaction

with nucleotides. This results in decreased affinity of incoming nucleotides, increased error rates, and reduced catalysis (Ponamarev et al 2002). Mutations in the spacer region are classified as either a class II or class III mutation. Mutations in the global intrinsic region and/or accessory intrinsic region results in decreased Polγ affinity for mtDNA (Lee et al 2009). Mutations in the linker region that results in replacement of a neutral amino acid residue by a positively charged amino acid residue such as W748S destabilize DNA binding and decrease enzyme activity by decreasing processivity (Chan et al 2006). Mutations such as A467T in motif A of the polymerase domain are class III mutations that decrease Polγ processivity (Chan et al 2005).

Anti-retroviral drugs, such as the nucleoside reverse transcriptase inhibitor (NRTI) cause mitochondrial toxicity that mimic hereditary mitochondrial disease. Mitochondrial toxicity is attributed to Y951, Y955, and E895 residues in the active site of Polγ that result in increased sensitivity to NRTI inhibition. The Y951 residue stabilizes the incoming nucleotide analogue, while Y955 and E895 interact and form a steric block at the active site (Graziewicz et al 2004) . This may cause termination of DNA replication by incorporating terminal dideoxynucleotides into the replicating DNA strand. This also causes increased Polγ error by misincorporation, inefficient removal of nucleotides from the mtDNA, and inhibition of nucleotide incorporation by Polγ by steric inhibition of the active site (Graziewicz et al 2006). Studies with cardiac- targeted Y955C mutation in transgenic mice explored the features of cardiomyopathy caused by NTRIs. Transgenic mice with cardiac- targeted Y955C mutation in Polγ exhibited mtDNA depletion, oxidative stress, and mitochondrial damage to cardiomyocytes (Lewis et al 2007).

1.8   Autophagy

Autophagy is defined as a programmed cell death (type II) or a pro-survival pathway in a different physiological and pathological context (Ferraro and Cecconi 2007). Autophagy is a catabolic pathway involved in the degradation and recycling of cellular components such as long-lived and damaged organelles and proteins. Organelles such as mitochondria are the source and primary target for ROS. Studies have shown that autophagy efficiently removes defective mitochondria that generate more ROS and less ATP with high levels of mtDNA mutations. Such an effective

mechanism of mitochondrial turnover by autophagy ensures cell survivability by maintaining mtDNA integrity and thereby mitochondrial function (Gu et al 2004, Kroemer et al 2010, Yen and Klionsky 2008). Studies show that mitochondrial ROS-induced lipid peroxidation products activate autophagy (Scherz-Shouval and Elazar 2007). Furthermore, mitochondria are considered to be a potential source of damage associated with molecular patterns (DAMPs) such as mtDNA, cytochrome c, ATP, and formyl peptides (Zitvogel et al 2010). Intracytoplasmic release of DAMPs and/or exposure to UVB triggers formation of the NLR (nucleotide-binding domain, leucine-rich-repeat-containing) family, pyrin domain containing 3 (NRLP3) inflammasome. Activation of the inflammasome leads to activation of pro-inflammatory cytokines by Caspase-1 (Feldmeyer et al 2007, Keller et al 2008, Nestle et al 2009). Release of DAMPs into the extracellular milieu triggers a systemic inflammatory response syndrome (SIRS) (Krysko et al 2011, Zhang et al 2010). Autophagic clearance of damaged mitochondria inhibits NRLP3 inflammasome formation and activation of pro-inflammatory mediators (Nakahira et al 2011, Zhou et al 2011). UVB-induced inflammation plays an important role in enhancement of tumor growth (Sluyter and Halliday 2000, Sluyter and Halliday 2001). UVB radiation regulates signaling pathways that stimulate production of inflammatory mediators. Further inhibition of inflammation with anti-inflammatory agents inhibits skin carcinogenesis, especially during the tumor promotion and progression stages (Halliday and Lyons 2008).

1.8.1   General features of autophagy

Cellular homeostasis is completely dependent on synthesis and degradation of organelles and macromolecules that are vital for cellular functions. Within eukaryotic cells, lysosomal autophagy process and/or proteosomal ubiquitination degrade cellular components. While the transient proteins are degraded by the proteosomal ubiquitination pathway (Ciechanover et al 2000), the lysosomal autophagy pathway is involved in degrading macromolecules and turnover of cellular organelles (Mizushima et al 2008). Three major forms of autophagy occur in mammalian cells based on acquisition of substrate by lysosomes: macroautophagy, chaperone-mediated autophagy and microautopahgy (Cuervo 2004). Chaperone-mediated autophagy involves transport of proteins with a specific motif across lysosomal membranes aided by chaperone proteins that interact with lysosomal membrane proteins.

Microautopahgy is a process that involves cytoplasmic intake by lysosomal invagination. Macroautophagy is a process that involves sequestration of cytoplasmic contents in double membrane vesicles called autophagosomes. Autophagosomes mature through fusion with lysosomes to deliver the contents for degradation by lysosomal acid proteases (Levine and Klionsky 2004). The amino acids and other degradation byproducts are exported to the cytoplasm for synthesis of macromolecules and for metabolism by lysosomal permeases and transporters (Mizushima 2007). Thus, autophagy replenishes cellular energy reserved by ATP generation and recycles damaged and non-functional proteins and organelles.

1.8.2 Molecular mechanism of autophagy

At the molecular level, the autophagy pathway involves the following steps:

1. Nucleation or formation of phagophore.

2. Ubiquitin-like conjugation and formation of Atg5-Atg12-Atg16L complex and its association with extending phagophore membrane.

3. LC3 lipidation and association with growing phagophore membrane.

4. Acquisition of macromolecule targets for degradation.

5. Autophagosome-lysosomal fusion and degradation of macromolecule.

1.8.3 Phagophore formation

Phagophore membranes are derived from endoplasmic reticulum, trans-golgi apparatus and endosomes. Vesicular protein sorting 34 (VPS34), a class III PI3 kinase, and its binding partner Beclin-1, a known tumor suppressor, is involved in phagophore formation. VPS34 uses phosphatidylinositol (PI) to generate phosphotidyl inositol triphosphate (PI3P) for phagophore elongation. VPS34 interacts with Beclin-1 to recruit Atg proteins to the phagophore. Bcl2 disrupts beclin-1 interaction with VPS34 by its interaction mediated by the BH3 domain (Pattingre et al 2005). Bcl2-VPS34 interaction is disrupted by Jnk1-mediated phosphorylation of Bcl2 in response to nutrient stress signal. VPS34-Beclin-1 complex recruits additional pro-autophagic regulatory proteins such as UV radiation resistance associated proteins (UVRAG), a tumor suppressor (Liang et al 2006), BAX-interacting factor-1

(BIF-1), Ambra1 (Fimia et al 2007), Atg14L (Matsunaga et al 2009), and autophagy inhibitory proteins such as RUN domain and cysteine-rich domain containing Beclin-1 interacting protein (Rubicon) (Matsunaga et al 2009) and Bcl2 (Pattingre et al 2005).

1.8.4 Formation of Atg5-Atg12-Atg16L multimeric complex

The Atg5-Atg12 complex is formed by a ubiquitin-like conjugation system that involves Atg7, which functions like the E1 ubiquitin activation enzyme. Atg7 binding to its C-termini glycine residue activates Atg12 in an ATP-dependent manner. Atg12 is transferred to Atg10 that covalently links Atg12 to Atg5 at K130 residue. Atg10 acts as an E2-like ubiquitin carrier protein. Atg5-Atg12 complex forms the Atg5-Atg12-Atg16L multimeric complex with Atg16L dimers. The Atg5-Atg12-Atg16L complex is targeted to the extending phagophore. Association of the Atg5-Atg12-Atg16L complex with growing phagophore induces asymmetric recruitment of processed LC3II protein (Kirkin et al 2009, Mizushima 2007).

1.8.5 LC3 lipidation

Processing and conjugation of microtubule-associated light chain 3 protein (LC3) to autophagosomes are critical steps in the autophagy pathway and involve an ubiquitin-like conjugation system. LC3 protein is a mammalian homologue to the yeast Atg8 protein. The cytosolic full length LC3 protein is proteolytically cleaved by cysteine protease Atg4 that exposes the C-terminal G120 residue. Atg7, an E1-like ubiquitin activation enzyme, activates the cleaved LC3 in an ATP-dependent manner. Activated LC3-I (18kDa) protein is conjugated with phospotidylethanolamine (PE) at an exposed carboxyl glycine and transferred to Atg3. The lipidated LC3-II (14-16 kDa) is targeted to the autophagosome, which in turn is dependent on the Atg5-Atg12 complex (Kirkin et al 2009).

1.8.6 Acquisition of macromolecule targets for degradation

LC3-II acts as a receptor molecule for the adaptor molecule p62/SQSTM1 that promotes turnover of poly-ubiquitinated protein aggregates.

1.8.7   Autophagosome-lysosomal fusion

After the growing ends of the autophagosome completely fuse, the autophagosomes combine with the endosomal compartment of lysosome to form the autolysosome. The Lamp1 and Lamp2 proteins play a critical role in the maturation of the autolysosomes (Tanaka et al 2000). During the maturation process, the macromolecules within the vesicles are delivered to the endosomal compartment that lowers the pH and facilitates the degradation process carried out by acid proteases (Eskelinen 2005).

1.8.8   Autophagy regulation by signaling pathways

Autophagy is strongly induced as an adaptive response mainly to starvation signals. The mammalian target of rapamycin (mTOR) plays a critical role in nutrient sensing, cell growth, and autophagy regulation (Jin 2006). The mTOR signaling pathway is activated by AKT-PI3 kinase, a growth factor signaling pathway. mTOR acts as a downstream control point for hypoxia, ATP levels, insulin signaling, and growth factor receptor signaling that promotes cellular growth through regulation of ribosomal protein expression and protein translation (Sabatini 2006, Shaw 2009). In normal growth promoting conditions, mTOR inhibits autophagy through its inhibitory effects on Atg1 kinase. A decrease in AKT signaling and activation of adenosine 5'-monophosphate (AMP)-activated protein kinase (AMPK) by decreased ATP levels inhibit mTOR and upregulate the catabolic process through activation of autophagy. Hypoxia induces autophagy through activation of hypoxia inducing factor-1 (HIF1). Activated HIF1 targets include Bcl2/adenovirus E1B 19 kDa interacting protein (BNIP3) and BNIP3L, both of which are involved in mitochondrial clearance through mitophagy (Schweers et al 2007, Tracy et al 2007). In cardiac and skeletal muscles, BNIP3 activates mitochondrial clearance in response to ROS (Hamacher-Brady et al 2006, Mammucari et al 2007), and involves interaction with the LC3 related molecule Gamma amino butyric acid-A-receptor associated protein (GABARAP) (Schwarten et al 2009).

Activation of oncogenic signaling pathways such as PI3K-AKT and growth factor receptor suppress autophagy. Hence, autophagy is implicated in cancer as a tumor suppressor. In addition, proteins involved in regulation of autophagy, such as Beclin-1, UVRAG, Bif1 and Atg4C, are considered to be tumor suppressors. This is based on

the fact that inactivation of these protein results in tumor promotion. Mitochondria and peroxisomes produce ROS as a part of their normal oxidative function that are considered to be a potential source for DNA damage. Mitochondria and peroxisomes damaged by ROS are recycled by autophagy and favor genetic stability in normal cells. On the other hand, suppression of autophagy increases DNA damage, and the loss or gain of chromosomes thereby increases genetic instability and leads to tumor promotion (Brech et al 2009). Mitochondrial recycling by autophagy is a selective process of mitochondrial quality control through which autophagy selectively removes damaged mitochondria. As shown in Figure 6, autophagy exerts its tumor suppressor function through regulation of mitochondria within the cells (Jin 2006).
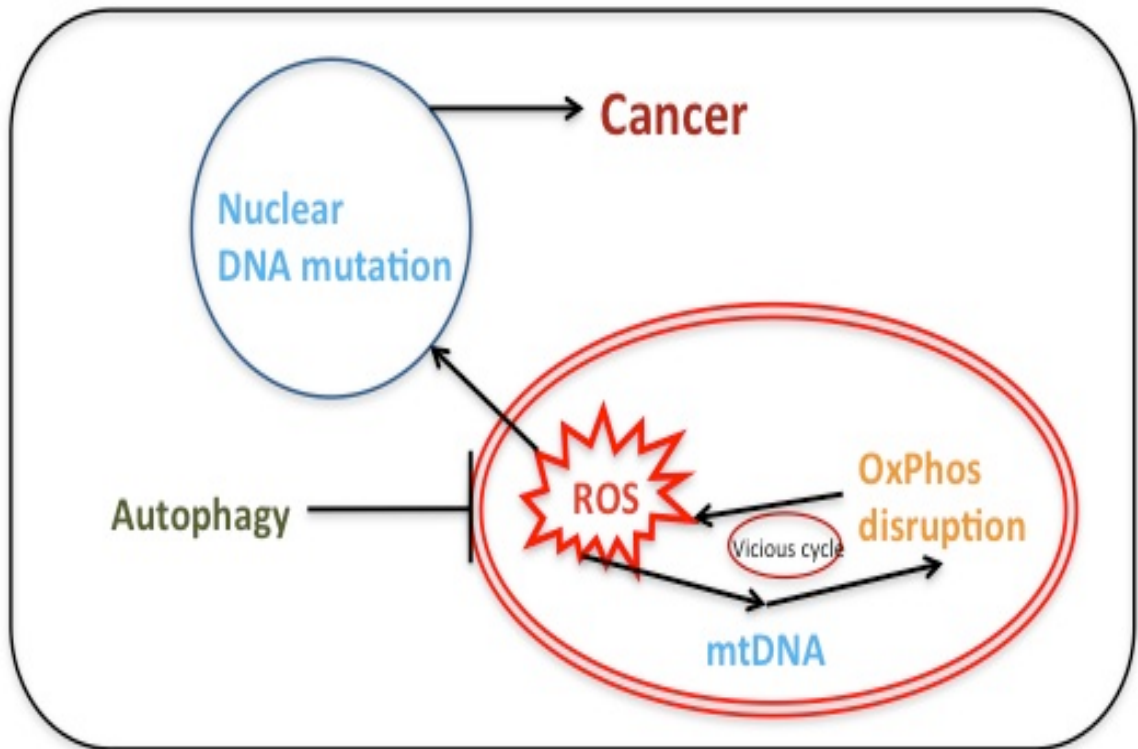
Figure 1.5 Schematic representation that illustrates carcinogenesis suppression by autophagy

Autophagy selectively degrades defective mitochondria and inhibits the vicious cycle of ROS generation and mitochondrial damage, thereby preventing nuclear DNA (Adapted from Jin S. 2006 Autophagy. 2(2): 80-84).

1.9   Research objectives

Although UVB-induced oxidative stress and cancer are well documented in murine skin carcinogenesis models, the survival mechanisms involved in those keratinocytes that survive the UVB insult remain unclear. This dissertation addresses the following hypotheses:

1.9.1   Manganese superoxide dismutase is a mitochondrial fidelity protein that protects Polγ against UV-induced inactivation

In chapter two we provide experimental data that suggest that epidermal cells use a novel dual-step approach to counteract UVB insult, which involves tumor suppressor protein p53 and mitochondrial antioxidant protein MnSOD. The mtDNA damage by UVB recruits p53 to mitochondria where p53 might provide support to mitochondrial DNA polymerase Polγ in repairing the damaged mtDNA and help Polγ in maintaining mtDNA integrity. We also demonstrate that UV-mediated peroxynitrite production in mitochondria inactivates redox sensitive proteins such as Polγ and impairs its ability to maintain mtDNA integrity, and that MnSOD acts as a nucleoid protector by interacting with Polγ and protecting it from oxidative stress induced inactivation.

1.9.2   AKT is a target for UVB- induced autophagy in mouse skin

In chapter three we investigate an autophagic mechanism that may contribute to the survival of keratinocytes after UVB exposure. Our results suggest that AKT inhibition triggers activation of autophagy and the removal of compromised mitochondria from keratinocytes exposed to UVB. The overall goal of this research is to investigate how mitochondrial redox status can be modulated to prevent the development of cancer. The data provide insights into the mechanisms leading to the survival of damaged cells. The data also suggest the potential use of Mn-porphyrin based mimetics for the prevention of skin cancer.

2　Chapter Two

Manganese superoxide dismutase is a mitochondrial fidelity protein that protects Polγ against UV-induced inactivation

2.1　Highlights

Manganese superoxide dismutase is a nuclear encoded primary antioxidant enzyme localized exclusively in the mitochondrial matrix. Genotoxic agents, such as UV radiation, generate oxidative stress and cause mitochondrial DNA (mtDNA) damage. The mitochondrial DNA polymerase (Polγ), a major constituent of nucleoids, is responsible for the replication and repair of the mitochondrial genome. Recent studies suggest that mitochondria contain fidelity proteins, and that MnSOD constitutes an integral part of the nucleoid complex. However, it is not known whether or how MnSOD participates in the mitochondrial repair processes. Using skin tissue from C57/BL6 mice exposed to UVB radiation, we demonstrate that MnSOD plays a critical role in preventing mtDNA damage by protecting the function of Polγ. Q-PCR analysis shows an increase in mtDNA damage after UVB exposure. Immunofluorescence and immunoblotting studies demonstrate p53 translocation to mitochondria and interaction with Polγ after UVB exposure. The mtDNA immunoprecipitation assay with Polγ and p53 antibodies in $p53^{+/+}$ and $p53^{-/-}$ mice demonstrates an interaction between MnSOD, p53, and Polγ. The results suggest that these proteins form a complex for the repair of UVB-associated mtDNA damage. The data also demonstrate that UVB exposure injures the mtDNA D-loop in a p53-dependent manner. The study used MnSOD-deficient mice and demonstrates that UVB-induced mtDNA damage is MnSOD-dependent. Exposure to UVB results in nitration and inactivation of Polγ, which is prevented by addition of the MnSOD mimetic $Mn^{III}TE$-2-PyP^{5+}. These results demonstrate for the first time that MnSOD is a fidelity protein that maintains the activity of Polγ by preventing UVB-induced

nitration and inactivation of Polγ. The data also demonstrate that MnSOD plays a role along with p53 to prevent mtDNA damage.

2.2 Introduction

Ultraviolet (UV) radiation is a pro-oxidant and carcinogen that induces oxidative stress and DNA damage (Aitken et al 2007, Bickers and Athar 2006). UV irradiation leads to increased stabilization and accumulation of tumor suppressor protein p53 in the skin. The main contributing factor to non-melanoma skin cancer is UVB-induced signature mutations in the p53 gene (Brash et al 1991, Hall et al 1993, Liu et al 1994). N-acetyl cysteine (NAC), superoxide dismutase mimetic, and catalase mimetic attenuate UVB-induced p53 stabilization without altering the transcriptional activation and cell cycle arrest functions of p53, suggesting a role for oxidative stress in UVB-induced p53 stabilization and accumulation (Decraene et al 2004a, Renzing et al 1996). Increased cellular stress by ROS triggers p53 translocation to mitochondria, leading to apoptosis and mitochondrial DNA (mtDNA) repair (Mihara et al 2003, Mihara and Moll 2003, Waster and Ollinger 2009, Zhao et al 2002, Zhao et al 2005b).

mtDNA is organized in the inner mitochondrial membrane as nucleoids. The nucleoids consist of mtDNA-protein macromolecular complexes containing 2-8 mtDNA molecules associated with various proteins such as mitochondrial transcription factor A (mTFA), a mitochondrial single-strand DNA-binding protein (mtSSB) and mitochondrial DNA polymerase gamma (Polγ) (Chen and Butow 2005, Garrido et al 2003, Legros et al 2004). mtDNA is more susceptible to UV-induced damage than nuclear DNA because it lacks histone and an elaborate repair system (Brown et al 1979, Shokolenko et al 2009, Yakes and Van Houten 1997).

Polγ is the only known polymerase enzyme responsible for replication and repair of mtDNA (Bogenhagen et al 2001, Hubscher et al 1979, Stuart et al 2004). The Polγ holoenzyme is a heterotrimer consisting of 1 catalytic subunit and 2 accessory subunits (Carrodeguas et al 1999, Gray and Wong 1992, Yakubovskaya et al 2006). The Polγ catalytic subunit has polymerase and proofreading activity for mtDNA

replication, and 5'-deoxyribose-5-phosphate lyase activity for base excision repair. The accessory subunits bind nucleotide to mtDNA for faster replication, increased processivity and protection of the catalytic subunit from ROS-mediated oxidative damage (Johnson et al 2000) . Polγ is susceptible to oxidative modifications due to the presence of 31 tyrosine residues in the catalytic subunit, including the two highly conserved tyrosine residues in the active site responsible for catalytic efficiency (Graziewicz et al 2002, Graziewicz et al 2004, Lewis et al 2006, Lim et al 2003, Van Goethem et al 2001).

UV irradiation triggers $NO^\bullet$ production in keratinocytes, which combines with $O_2^{-\bullet}$ to form the powerful oxidant peroxynitrite (Maglio et al 2005, Wu et al 2010). Inactivation of proteins by tyrosine nitration is regarded as a marker of nitrosative stress. The importance of nitration to protein structure or function depends on the location of tyrosine residues in the proteins; for example, its location in a loop or hydrophobic milieu such as the active site of an enzyme (Alvarez and Radi 2003).

ROS produced in mitochondria are detoxified by enzymatic and non-enzymatic antioxidant defense systems. The major constituents of the enzymatic system are MnSOD (Weisiger and Fridovich 1973), glutathione peroxidase (Esworthy et al 1997) and members of the thioredoxin family (Holmgren 1985). MnSOD forms the first line of defense against the $O_2^{-\bullet}$ produced in the mitochondria. Lack of MnSOD causes accumulation of oxidative mtDNA damage as well as inactivation of respiratory and Krebs cycle enzymes (Li et al 1995, Melov et al 1999). Recent studies have identified MnSOD as a nucleoid complex component that may protect mtDNA and proteins associated with mtDNA from oxidative damage (Kienhofer et al 2009). Further MnSOD enzymatic activity is regulated by mitochondrial SIRT3 to maintain ROS levels and mitochondrial homeostasis (Ozden et al 2011, Tao et al 2010). We propose that epidermal cells use the following novel dual-step strategy to counteract a UVB insult involving tumor suppressor protein p53 and MnSOD

 1) Damaged mtDNA recruit p53 to mitochondria where p53 enhances mitochondrial DNA polymerase Polγ repair activity

2) MnSOD may act as a fidelity protein by interacting with Polγ and protecting it from oxidative stress-induced inactivation.

2.3   Material and Methods

2.3.1   Materials

All chemicals and reagents were purchased from Sigma-Aldrich (St. Louis, MO) with exception of the following: protease inhibitor set III from Calbiochem (La Jolla, CA), dithiothreitol from BioRad (Carlsbad, CA), rabbit poly-clonal anti-MnSOD from Upstate Technology (Lake Placid, NY), Protein A/G agarose from Santa Cruz Biotechnology (Santa Cruz, CA), rabbit poly-clonal anti-nitrotyrosine antibody from Cayman Chemical (Ann Arbor, MI), rabbit poly-clonal anti-Polyγ antibody from Pierce Biotechnology (Rockford, IL), mouse monoclonal anti-p53 (1C12) antibody from Cell Signaling Technology Inc. (Danvers, MA), Monoclonal p53 antibody (DO-1) from Santa Cruz Biotechnology (Santa Cruz, CA), poly(rA).oligo(dT)$_{12\text{-}18}$ from Midland Certified Reagent Company (Midland, TX), and DNase I from New England Biolabs Inc. (Ipswich, MA).

2.3.2   Animal studies

Heterozygous MnSOD knockdown mice (MnSOD$^{+/-}$) (Li et al 1995, Van Remmen et al 1999) and p53 knock-out mice (p53$^{-/-}$) (Jacks et al 1994) were generated and genotyped as described. The animal experimental procedures used in this study were approved by the Institutional Animal Care and Use Committee of the University of Kentucky.

2.3.3   UV exposure

Depilated mice in the resting phase of hair cycle and JB6 cells were exposed to ultraviolet irradiation in a Plexiglass cabinet (Plastic Design Corporation, MA). A single dose of 5kJ/m^2 (mice) or 400mJ/cm^2 (JB6 cells) was delivered by UVB lamps (Black light blue lamp, Sankyo Denkco Ltd., Japan). The UV emittance was measured using a UVB photometer radiometer (International Light Technologies, Peabody, MA) equipped with a UVB measuring head.

2.3.4 Isolation of mitochondrial fraction from mouse skin tissue

The skin mitochondria were isolated as previously described (Zhao et al 2002). Briefly, the tissue was homogenized and diluted in 5 mL of ice-cold mitochondrial isolation buffer containing 0.225 mol/L mannitol, 0.075 mol/L sucrose, and 1 mmol/L EGTA (pH 7.4) The cytoplasmic, nuclear and tissue contaminants were removed by centrifugation at $576 \times g$ (Sorvall 5B centrifuge) for 5 minutes. Intact mitochondria were isolated from the filtered supernatant and subsequently washed with 1 ml mitochondrial isolation buffer by centrifugation at $9,000 \times g$ for 5 minutes. The protein concentration was determined by Bradford assay (Bio-Rad, Richmond, CA).

2.3.5 mtDNA isolation and mtDNA damage analysis using quantitative PCR (Q-PCR)

The Q-PCR to analyze mtDNA damage using Pico-Green dye was performed as described previously (Kovalenko and Santos 2009). mtDNA was isolated from mouse skin tissue using a genomic DNA extraction kit (QIAGEN, Chatsworth, VA). The mtDNA and PCR products were quantified using the PicoGreen dsDNA Quantitation kit (Invitrogen Corp., Carlsbad, CA). The fluorescence values of PCR products from UVB- treated samples and the control samples were used to calculate relative amplification and lesion frequency.

2.3.6 Mitochondrial fractionation

The subcellular fractionation of enriched mitochondria was performed as described previously (Mihara and Moll 2003). Briefly, mouse skin was homogenized with a polytron homogenizer in calcium reticulocyte buffer (10mM Tris pH 7.6, 1.5 mM $CaCl_2$, 10 mM NaCl) and mixed with 2ml of ice-cold mannitol-sucrose buffer (210 mM mannitol, 70 mM sucrose, 5 mM EDTA, 5 mM Tris, pH 7.6). Two hundred microlitres of whole skin homogenate was stored at -20°C for further use. The remainder of the whole skin homogenate was centrifuged thrice at 1000 x g for 5 min at 4°C to clear nuclear, cytosolic and intact skin cell fraction. The mitochondria were isolated by discontinuous sucrose gradient centrifugation.

2.3.7   Co-Immunoprecipitation

Immunoprecipitation was performed as previously described (Bonifacino et al 2001). Briefly, the protein A/G-agarose beads (40 μL) were conjugated overnight to Polγ, MnSOD, p53 (DO-1), and 3-nitrotyrosine antibodies (3 μg) at 4°C in 0.5 mL ice-cold PBS. Appropriate control antibody was used as negative control. The mitochondrial pellets were lysed in denaturing buffer (1% w/v sodium dodecyl sulfate (SDS), 50 mM Tris-HCl, pH 7.4, 10 mM dithiothreitol, 5 mM EDTA, 15 U/ml DNase I, and 1 μL/mL Protease inhibitior) by heat at 95ºC for 5 min and the DNA was sheared. After denaturation and shearing, 250-500 μg of precleared mitochondrial protein were immunoprecipitated with antibody conjugated protein A/G-agarose beads with 10 μL of 10% BSA incubated overnight at 4ºC in a tube rotator. The immunoprecipitates were analyzed with 4-10% gradient gel.

2.3.8   mtDNA immunoprecipitation

The ChIP-IT system (Active Motif, Carlsbad, CA) was used to investigate the interaction of Polγ, MnSOD, p53 (DO-1) and mtDNA. Briefly, skin mtDNA exposed to UVB was immunoprecipitated with p53 and Polγ antibodies, and the mtDNA D-loop region was quantified by real-time PCR (LightCycler 480 Real-Time PCR System, Roche). The following primer sets were designed and used to amplify the mtDNA D-loop region: 5′-ACT ATC CCC TTC CCC ATT TG-3′ and 5′-TGT TGG TCA TGG GCT GAT TA-3′. Equal amounts of mtDNA from each treatment were used as input loading control, and mtDNA pulled down by IgG served as the negative antibody control.

2.3.9   Polγ reverse transcriptase activity assay

The RNA-dependent DNA polymerase activity of Polγ was measured as described previously (Longley and Copeland 2002, Taanman et al 2010). Briefly, the mitochondrial lysates prepared in extraction buffer (100 mM NaCl, 25 mM HEPES-KOH pH 8.0, 1% v/v Triton-X 100) were assayed at 37ºC for 10 min in 50 μL reaction mixture with 10 μg of the mitochondrial protein, 25 mM HEPES-KOH pH 8.0, 0.5 mM $MnCl_2$, 100 mM NaCl, 2.5 mM β-mercaptoethanol, 50 μg/mL

poly(rA).oligo(dT)$_{12-18}$, 100 μg/mL acetylated bovine serum albumin (Ac-BSA), 0.1 mM aphidicolin, 500 μg/mL RNasin® RNase inhibitor (Promega, Madison, WI) and 5 μM [α-^{32}P]thymidine 5′-triphosphate (dTTP; specific activity: 5 Ci/mmol) (Amersham Corp., Piscataway, NJ). The reaction was stopped with 1.0 ml of stop solution (500 mM NaOH, 100 mM sodium pyro-phosphate, 0.1 mg/mL sonicated calf thymus DNA, 0.5 mg/ml BSA). The DNA precipitated with 20% TCA was filtered through GF/C filters and washed thrice with 1N HCl, rinsed with 95% ethanol and dried. The TCA-insoluble radioactivity was measured by liquid scintillation counting.

2.3.10 Treatment with Mn-based porphyrin

The Mn(III) meso-tetrakis(*N*-ethylpyridinium-2-yl) porphyrin (Mn^{III}TE-2-PyP^{5+}) was synthesized as previously described (Batinic-Haberle et al 1999, Ferrer-Sueta et al 1999). The mice were injected intraperitoneally with 5 mg/kg of Mn^{III}TE-2-PyP^{5+} in saline twice daily for 2 days before UVB treatment.

2.3.11 Data analysis

The data are represented as mean ± SEM from replicate samples (n = 3), and were analyzed by one-way and two-way analyses of variance using Prism software (GraphPad, San Diego, CA). An α level of $P < 0.05$ was considered significant.

2.4 Results

2.4.1 UVB induces mtDNA damage in mouse skin

To assess mtDNA damage by UVB, we performed a time course study in which wild-type C57BL/6 mice were exposed to 5kJ/m^2 of UVB radiation. mtDNA isolated from skin at 1 and 24 h after exposure to UVB was subjected to quantitative PCR analysis. The mtDNA damage was analyzed based on the difference in amplification due to blockage of the recombinant *Thermus thermophilus* (rTth) DNA polymerase by UVB-induced lesions. PCR negative control was used as a blank reference to eliminate background fluorescence. The relative amplification plot in Figure1 shows a significant decrease in amplification of 10 kb mtDNA at 1 h and 24 h after UVB treatment compared to undamaged control template, indicating an increase in mtDNA damage. A quantitative analysis of lesions induced by UVB treatment in the 10 kb mtDNA is shown in Table 1. We normalized mtDNA copy number variation using fluorescence values from amplified short mtDNA fragments (117 bp), as there is a very low probability that UVB treatment will introduce a lesion in small mtDNA segments. This analysis indicates a significant increase in lesions at 1 h and 24 h after UVB treatment, suggesting mtDNA is highly prone to damage by UVB treatment.

A
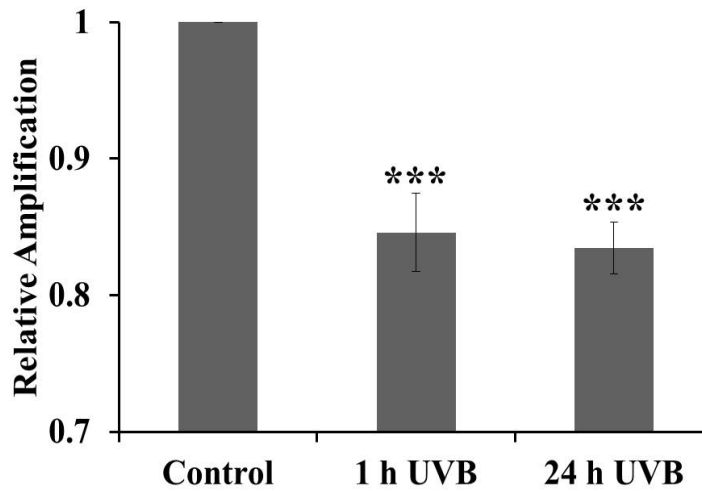
Figure 2.1. Quantification of mtDNA damage in mice skin induced by UVB radiation

(A) Wild-type C57BL/6 mice were exposed to $5kJ/m^2$ of UVB radiation. mtDNA was isolated and analyzed with Q-PCR using primers specific for mouse mtDNA. The 10 kb mtDNA fragment was amplified and the blockage of rTth DNA polymerase amplification by damage in mtDNA was quantified in PCR products with Pico-Green dye. The relative amplification levels at 1 h and 24 h after UVB treatment were normalized with untreated control. ***$P < 0.001$ compared with control.

Table 1	Control	1 h UVB	24 h UVB
Lesions/10kb	0	0.17±0.03**	0.18±0.02***

The 10-kb mDNA fragment was normalized with 117-bp mtDNA fragment

Table 2.1 The number of lesions per 10kb mtDNA by UVB treatment was quantified after normalizing with mitochondrial copy number

2.4.2   UVB induces p53 translocation to mitochondria in mice epidermal cells

We have previously observed p53 translocation to mitochondria in a multistage skin cancer model using a known mutagenic chemical initiator, 7,12-dimethyl-benz(a)-anthracene (DMBA), followed by repetitive treatment with the known tumor promoter 12-*O*-tetradecanoylphorbol-13-acetate (TPA) (Zhao et al 2002). It has also been shown that p53 translocates into mitochondria after exposure to a stress inducing agent, including ionizing radiation (Vaseva and Moll 2009). To determine whether UVB-induced mtDNA damage triggers p53 translocation to mitochondria *in vivo*, skin mitochondrial fractions devoid of cytosolic and nuclear contamination were prepared from mouse skin by a sucrose density gradient ultracentrifugation process after UVB treatment and subjected to immunoblot analysis. As shown in Figures 2A & 2B, the p53 level increased significantly in both whole skin lysates and mitochondrial fractions at 1 h and at 24 h after UVB treatment. The absence of cytosolic and nuclear contamination was confirmed by immunoblotting of the mitochondrial fractions with antibodies against cytosolic and nuclear marker proteins IκBα and PCNA, respectively.

A
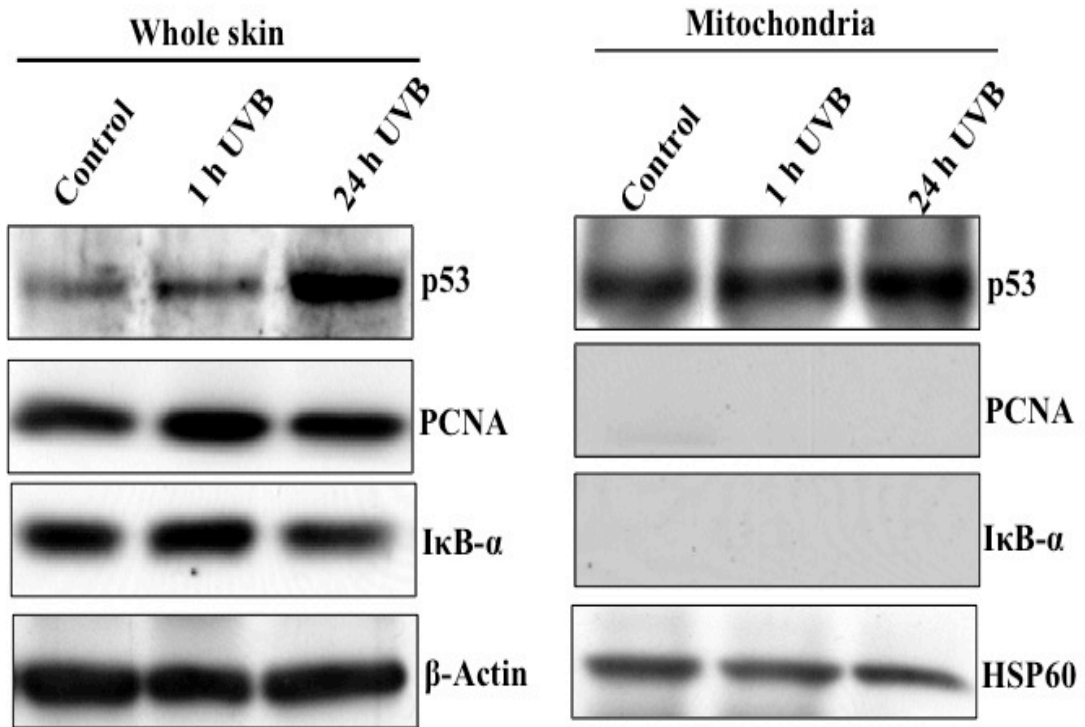
B
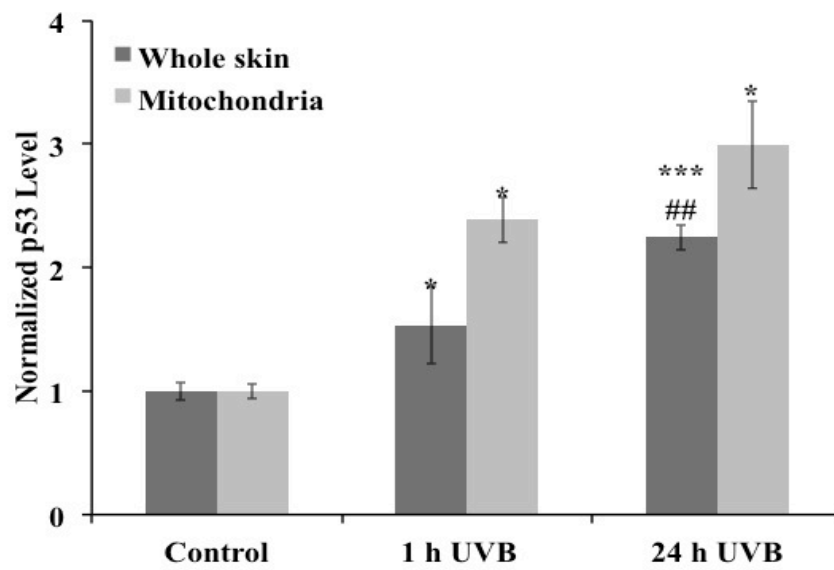
Figure 2.2 UVB enhances p53 mitochondrial translocation

(A) C57BL/6 mice were exposed to 5kJ/m^2 of UVB radiation. Whole skin tissue lysates and fractionated mitochondrial lysates were immunoblotted with p53 antibody (DO-1). Ponceau staining was used to confirm equal loading and uniform transfer of protein. Monoclonal anti-β-actin and anti-HSP60 antibodies were used as internal loading control. (B) The p53 accumulations in whole skin lysates and mitochondrial lysates at 1 h and 24 h after UVB exposure were quantified. Results were averaged from 3 sets of independent experiments. *P < 0.05, ***P < 0.001, compared with control, ##P < 0.01, comparison of 1 h and 24 h UVB treatment.

2.4.3 UVB enhances physical interaction of p53 with Polγ and mtDNA, and the role of p53 in Polγ and mtDNA interaction

Previous studies have shown that p53 can directly interact with Polγ and mtDNA and enhance Polγ repair efficiency (Achanta et al 2005, Bakhanashvili et al 2008, Heyne et al 2004). Here, we tested whether UVB could enhance p53 interaction with Polγ and mtDNA. Mitochondria were isolated from the skin of wild-type C57BL/6 mice exposed to $5kJ/m^2$ of UVB radiation and the interaction between p53 and Polγ was assessed by co-immunoprecipitation with an antibody specific for p53 with subsequent detection of p53 or Polγ by Western analysis. As shown in Figure 3A, Polγ and p53 proteins pulled down from the mitochondrial lysates by both p53 and Polγ antibodies increased at 1 h and 24 h after UVB treatment. We also determined UVB-induced p53 and mtDNA interaction by isolating mtDNA from the skin of C57BL/6 wild-type mice exposed to $5kJ/m^2$ of UVB radiation. The mtDNA immunoprecipitated with p53 antibody were purified and amplified by real-time PCR with primers specific for mtDNA D-loop region to probe the relationship between mtDNA and Polγ function. As shown in Figure 3B, the amplification of the D-loop region of mtDNA immunoprecipitated by p53 antibody increased significantly at 1 h and 24 h after UVB treatment. To verify the role of p53 in mtDNA repair by Polγ after UVB treatment, mtDNA immunoprecipitation was performed on p53$^{+/+}$ and p53$^{-/-}$ mice at 1 h and 24 h after UVB treatment. As shown in Figure 3C, the amplification of the D-loop region of mtDNA immunoprecipitated by Polγ antibody in p53$^{+/+}$ mice increased significantly at 1 h and 24 h after UVB treatment. The amplification level of the D-loop in p53$^{-/-}$ mice was lower than that in the p53$^{+/+}$ mice and did not change significantly in response to UVB treatment. Thus, the significant increase in amplification of the D-loop region after UVB treatment was limited to the p53$^{+/+}$ genotypes, suggesting a role for p53 in the interaction of Polγ with mtDNA.

A
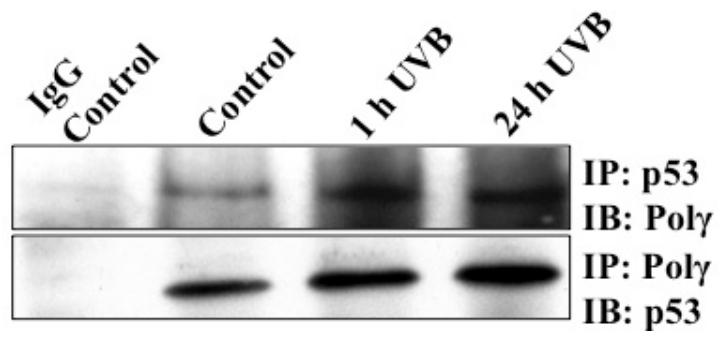
B
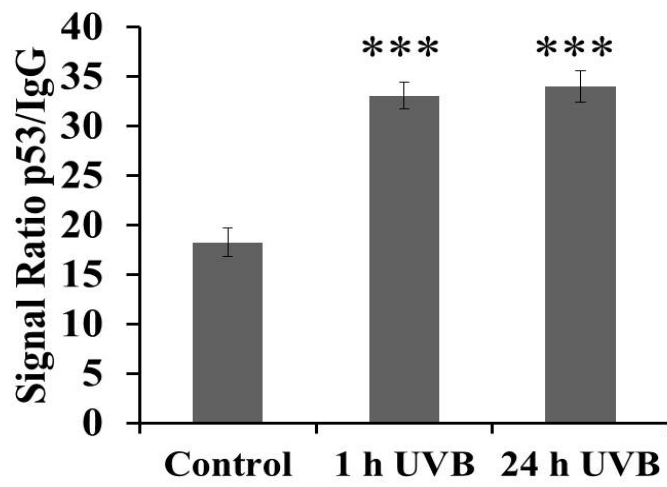
C
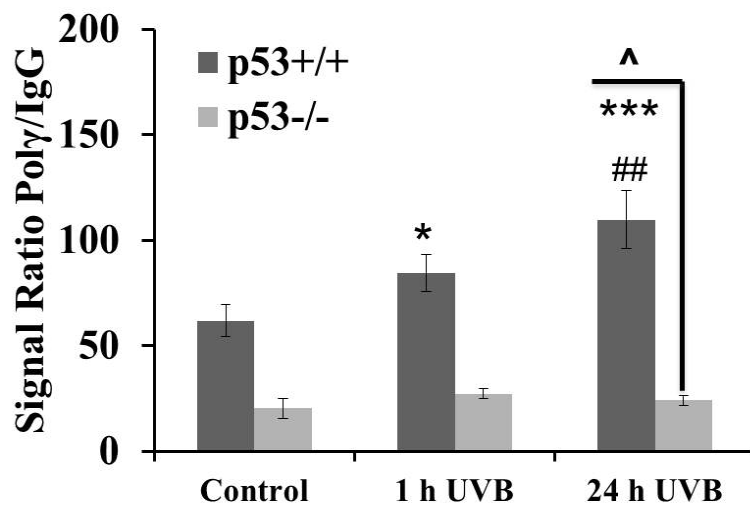
Figure 2.3 UVB-induced physical interaction of p53-Polγ-mtDNA

(A) Skin mitochondrial lysates from wild-type C57BL/6 mice exposed to 5kJ/m^2 of UVB radiation were immunoprecipitated with p53 (DO-1), Polγ antibodies, and control IgG. **(B)** mtDNA isolated from wild-type C57BL/6 mice skin exposed or sham exposed to 5 kJ/m^2 of UVB radiation was immunoprecipitated with p53 antibody (DO-1) and control IgG. The input mtDNA from control at 1 h and 24 h after UVB treatment was used as internal control. Real-Time PCR was used to amplify mtDNA D-loop region from input and immunoprecipitated mtDNA. *****P** < 0.001**. (C)** mtDNA isolated from p53$^{+/+}$ and p53$^{-/-}$ mice skin exposed or not exposed to 5kJ/m^2 of UVB radiation was immunoprecipitated with Polγ antibody. Real-time PCR was used to amplify the immunoprecipitated mtDNA D-loop. *P < 0.05, ***P < 0.001, compared with control; ##P < 0.01, compared at 1 h and 24 h after UVB treatment; ^P<0.05, compared between p53$^{+/+}$ and p53$^{-/-}$ genotypes.

2.4.4 UVB induces physical interaction of MnSOD with p53 and Polγ and the effect of MnSOD on Polγ and mtDNA

We have previously observed an interaction between p53 and MnSOD in the mitochondria of epidermal cells exposed to DMBA and TPA (Zhao et al 2002, Zhao et al 2005b). To determine whether UVB causes p53 and MnSOD to interact in mitochondria, skin mitochondrial lysates from UVB-treated wild-type C57BL/6 mice were immunoprecipitated with p53 and MnSOD antibodies, respectively. As shown in Figure 4A, the amount of MnSOD and p53 proteins pulled down from mitochondrial lysates by p53 and MnSOD antibodies increased at 1 h and 24 h after UVB treatment. Previous studies have demonstrated that MnSOD is an integral part of the nucleoid complex (Kienhofer et al 2009). Hence, we tested whether UVB induces MnSOD and Polγ interaction using co-immunoprecipitation. As shown in Figure 4B, the amount of MnSOD and Polγ proteins pulled down from mitochondrial lysates by Polγ and MnSOD antibodies increased at 1 h and 24 h after UVB treatment. We further used $p53^{+/+}$ and $p53^{-/-}$ mice to perform a co-immunoprecipitation study to determine whether UVB induces interaction between MnSOD and Polγ and whether it is dependent on p53. As shown in Figure 4C, the amount of MnSOD and Polγ proteins pulled down from mitochondrial lysates by Polγ and MnSOD antibodies increased at 1 h and 24 h after UVB treatment in both genotypes. To assess the role of MnSOD in mtDNA and Polγ interaction after UVB treatment, mtDNA immunoprecipitation was performed on $MnSOD^{+/+}$ and $MnSOD^{+/-}$ mice. As shown in Figure 4D, amplification of the D-loop region of mtDNA immunoprecipitated by the Polγ antibody resulted in more than 1.5 fold increase at 1 h after UVB treatment in both genotypes, and when compared between the genotypes. Although the increase was less than 1.5 fold at 24 h after UVB treatment in both genotypes, the increase was significant in the $MnSOD^{+/+}$ genotype at 24 h after UVB treatment. The results suggest that MnSOD interacts with both p53 and Polγ, but the interaction between MnSOD and Polγ appears to be independent of p53. The results also show that MnSOD enhances the Polγ/mtDNA interaction 24 h after UVB-irradiation, implying a role for MnSOD in maintaining Polγ activity.

A

IP: p53
IB: MnSOD

IP: MnSOD
IB: p53

B

IP: Polγ
IB: MnSOD

IP: MnSOD
IB: Polγ

C

IP: MnSOD
IB: Polγ

IP: Polγ
IB: MnSOD
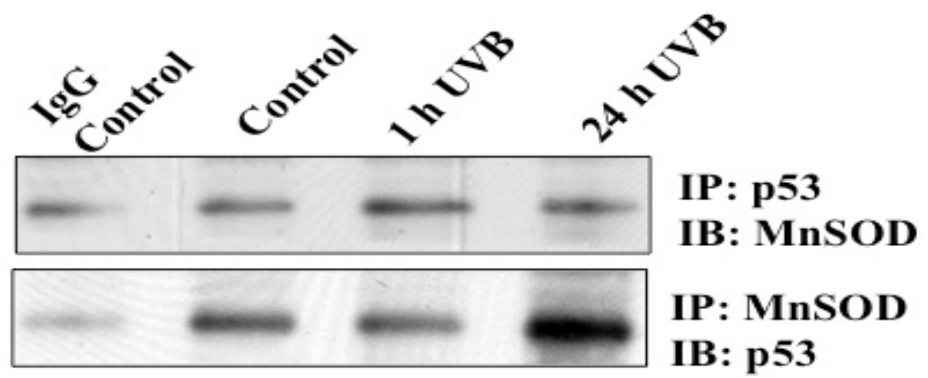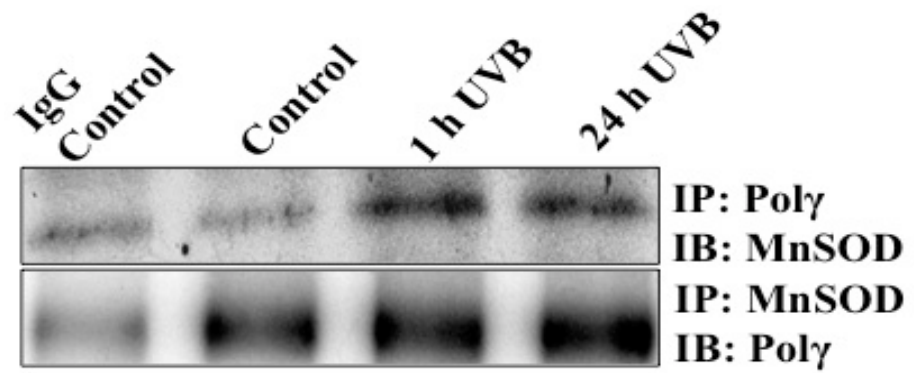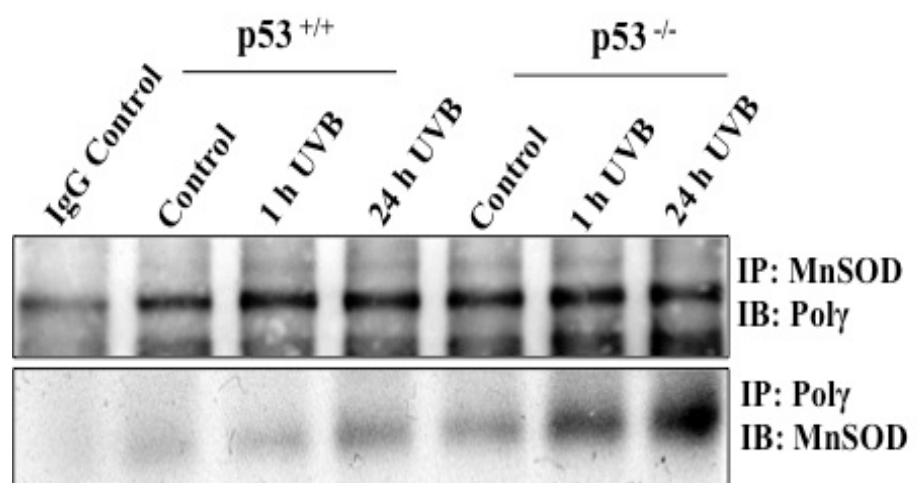
D
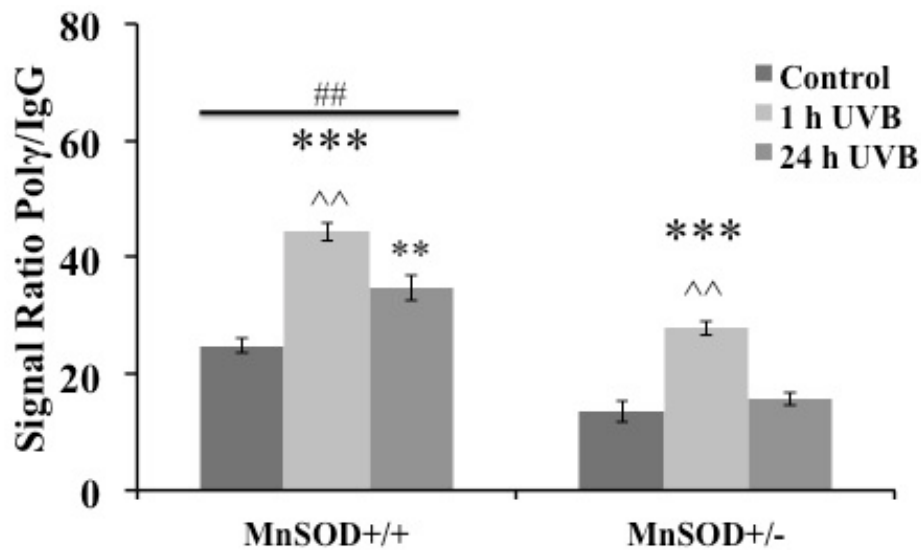
Figure 2.4 UVB-induced physical interaction of MnSOD-p53-Polγ

(A) Skin mitochondrial lysates from wild-type C57BL/6 mice exposed to $5kJ/m^2$ of UVB radiation were immunoprecipitated with p53 (DO-1), MnSOD antibodies, and control IgG. Co-immunoprecipitated MnSOD and p53 were quantified by immunoblotting with specific antibodies. **(B)** Co-immunoprecipitation of Polγ and MnSOD. Mitochondrial lysates from mice skin exposed to UVB at 1 h and 24 h were immunoprecipitated with Polγ and MnSOD antibodies, and control IgG. Co-immunoprecipitated Polγ and MnSOD were quantified by immunoblotting with specific antibodies. **(C)** Mitochondrial lysates from $p53^{+/+}$ and $p53^{-/-}$ mice skin exposed to UVB were immunoprecipitated with Polγ, MnSOD antibodies and control IgG. Co-immunoprecipitated Polγ and MnSOD were quantified by immunoblotting with specific antibodies. **(D)** mtDNA isolated from $MnSOD^{+/+}$ and $MnSOD^{+/-}$ mice skin exposed to $5kJ/m^2$ of UVB radiation was immunoprecipitated with Polγ antibody. Real-time PCR was used to amplify the precipitated mtDNA D-loop. ***$P < 0.001$, **$P < 0.01$, compared with control; ^^$P < 0.01$ compared at 1 h and 24 h after UVB treatment; ##$P < 0.01$ compared between $MnSOD^{+/+}$ and $MnSOD^{+/-}$ mice.

2.4.5 MnSOD deficiency enhances UVB-mediated Polγ inactivation

To determine whether UVB treatment induces an alteration in Polγ protein level in the mitochondria of MnSOD$^{+/+}$ and MnSOD$^{+/-}$ mice, Western blotting for Polγ protein was performed using skin mitochondrial lysates from UVB- treated wild-type C57BL/6 mice. As shown in Figure 5A, there was no apparent change in the Polγ protein level at 1 h and 24 h after UVB treatment in either genotype. UVB induces OONO$^-$ production in skin by the reaction of NO$^{\bullet}$ with O$_2^{-\bullet}$ and nitrates proteins, further Polγ protein undergoes oxidative damage-induced inactivation (Graziewicz et al 2002, Wu et al 2010). A Polγ reverse transcriptase activity assay was performed using the skin mitochondrial lysates from UVB-treated MnSOD$^{+/+}$ and MnSOD$^{+/-}$ mice to determine whether UVB treatment results in a change in Polγ activity in the mitochondria. As shown in Figure 5B, Polγ reverse transcriptase activity decreased significantly in MnSOD$^{+/-}$ genotype at 1 h and 24 h after UVB treatment compared to MnSOD$^{+/+}$ mice, where a significant decrease in activity was observed only at 24 h after UVB treatment. To determine whether UVB-induced Polγ inactivation is associated with nitration, we performed a co-immunoprecipitation study using 3-nitrotyrosine antibody. As shown in Figures 5C & 5D, the amount of Polγ protein pulled down from the mitochondrial lysates by 3-nitrotyrosine antibody significantly increased at 1 h and 24 h after UVB treatment in MnSOD$^{+/-}$ mice. There was a significant difference between the genotypes at 24 h after UVB treatment, as shown in Figure 5D. These results suggest that MnSOD may be important in preventing nitration and subsequent inactivation of Polγ after UV exposure.

A
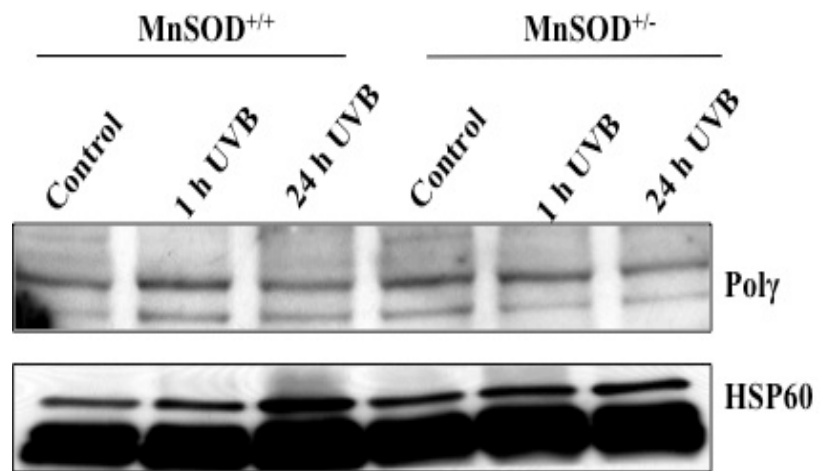
B
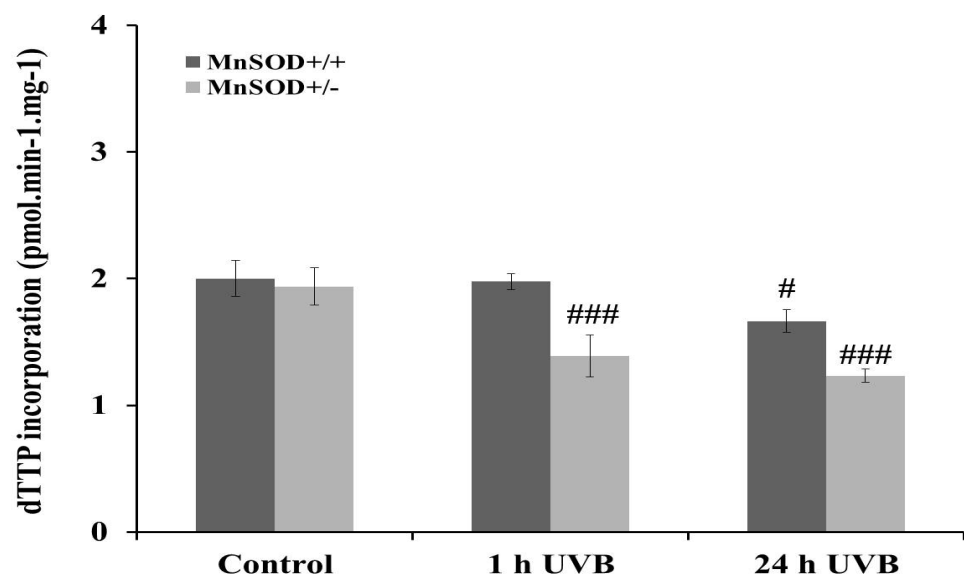
C
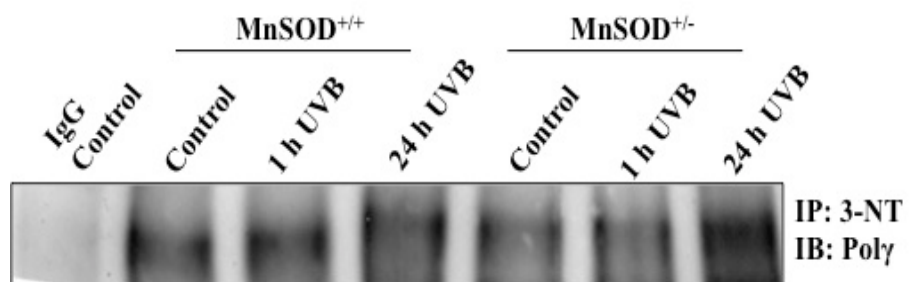
D
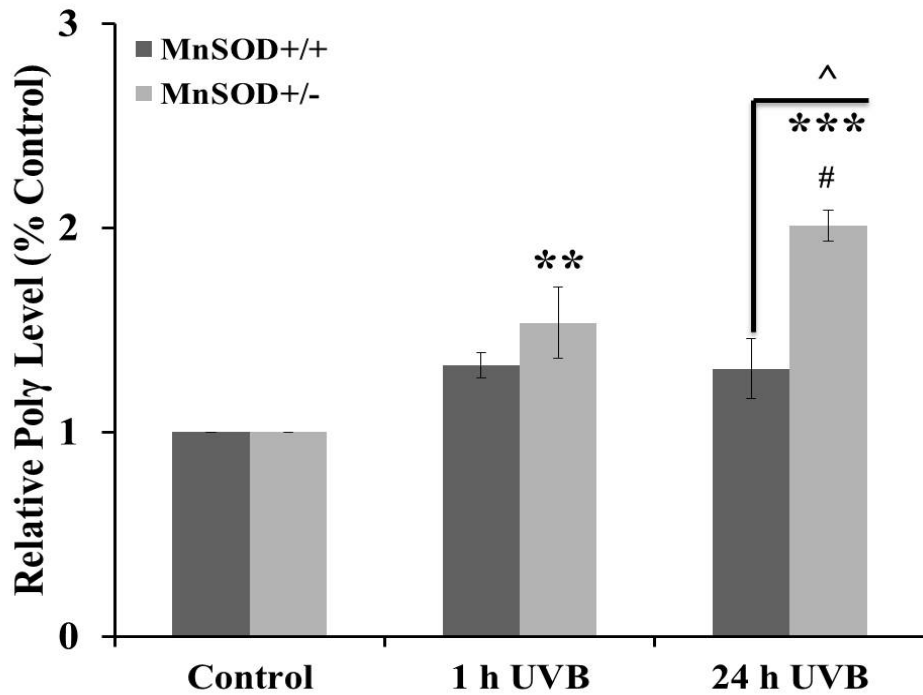
Figure 2.5 UVB induced Polγ inactivation by nitration

(A) Immunoblot analysis of Polγ protein levels in MnSOD$^{+/+}$ and MnSOD$^{+/-}$ mice skin mitochondria exposed to 5kJ/m^2 of UVB radiation. **(B)** Polγ reverse transcriptase activity assay in MnSOD$^{+/+}$ and MnSOD$^{+/-}$ mice skin mitochondria exposed or not exposed to 5 kJ/m^2 of UVB radiation #P < 0.05, ###P < 0.001 compared with control. **(C)** MnSOD$^{+/+}$ and MnSOD$^{+/-}$ mouse skin exposed to 5 kJ/m^2 of UVB radiation was co-immunoprecipitated with 3-nitrotyrosine antibody. Co-immunoprecipitates were immunoblotted with Polγ antibody. **(D)** Quantification of Polγ co-immunoprecipitation by 3-nitrotyrosine antibody. **P < 0.01, ***P<0.001 compared with control; #P < 0.05 compared between 1 h and 24 h after UVB treatment; ^P < 0.05 compared between MnSOD$^{+/+}$ and MnSOD$^{+/-}$ mice.

2.4.6 Mn^{III}TE-2-PyP^{5+} rescues Polγ from inactivation by UVB-mediated nitration

Previous studies have clearly established Mn^{III}TE-2-PyP^{5+} as a potent $O_2^{-\bullet}$ and $OONO^-$ scavenger (Batinic-Haberle et al 2010, Batinic-Haberle 2010). To test if Polγ could be rescued from UV-induced inactivation, MnSOD$^{+/-}$ mice were pre-treated twice daily with Mn^{III}TE-2-PyP^{5+} at 5mg/kg body weight in 250 μl volume before UVB exposure. Polγ reverse transcriptase activity assay was performed in skin mitochondrial lysates from saline and Mn^{III}TE-2-PyP^{5+} treated MnSOD$^{+/-}$ mice after UVB exposure. As shown in Figure 6A, Polγ reverse transcriptase activity in Mn^{III}TE-2-PyP^{5+} pre-treated MnSOD$^{+/-}$ mice increased significantly at 24 h after UVB treatment and compared with saline pre-treated MnSOD$^{+/-}$ mice. There was a significant decrease in activity in saline pre-treated MnSOD$^{+/-}$ mice at 24 h after UVB treatment. To determine whether Mn^{III}TE-2-PyP^{5+} pre-treatment reduce UVB-mediated Polγ inactivation by nitration, co-immunoprecipitation was performed using 3-nitrotyrosine antibody. As shown in Figure 6B, the amount of Polγ protein pulled down from the mitochondrial lysates by 3-nitrotyrosine antibody in saline pre-treated MnSOD$^{+/-}$ mice increased significantly at 1 h and 24 h after UVB treatment. There was no significant change in nitration levels in Mn^{III}TE-2-PyP^{5+} pre-treated MnSOD$^{+/-}$ mice. When compared with saline pre-treated MnSOD$^{+/-}$ mice, the decrease in nitration in Mn^{III}TE-2-PyP^{5+} pre-treatment was significant at 24 h after UVB treatment, as shown in Figure 6C.

A
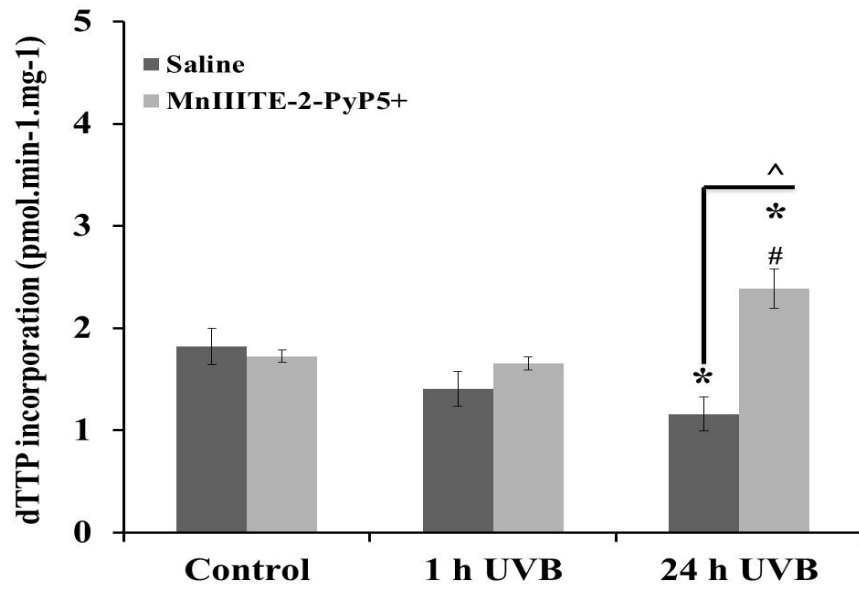
B
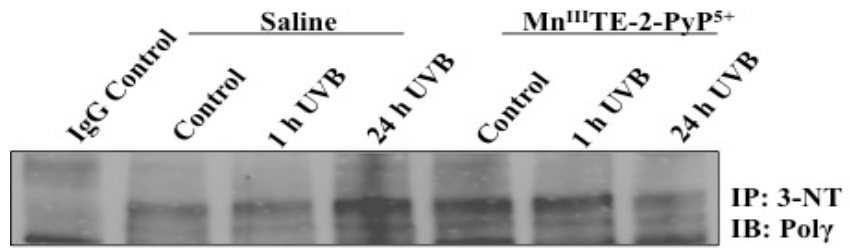
C
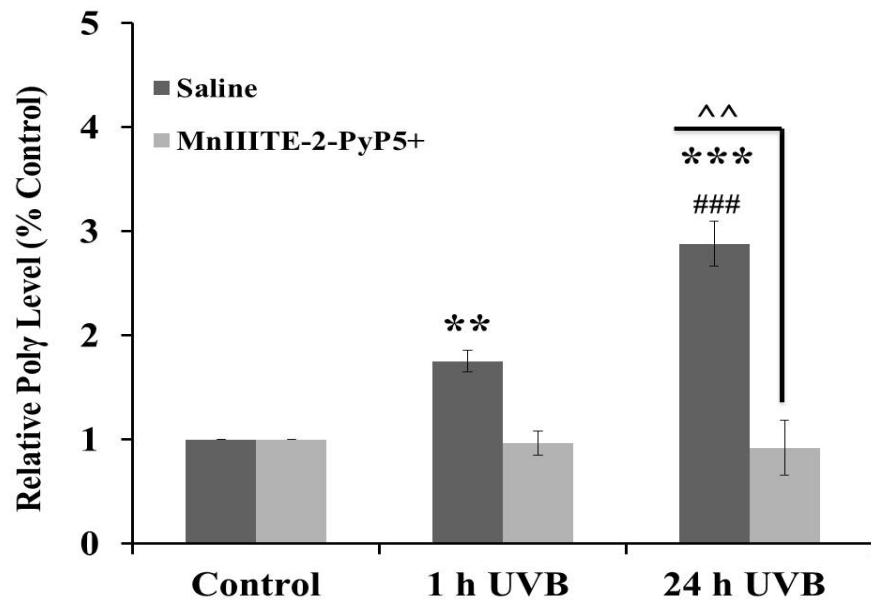
Figure 2.6 Mn^{III}TE-2-PyP^{5+} protects UVB induced Polγ inactivation by nitration in MnSOD$^{+/-}$ mice

(A) Polγ reverse transcriptase activity assay in Mn^{III}TE-2-PyP^{5+} and saline pre-treated MnSOD$^{+/-}$ mice skin mitochondria exposed to 5 kJ/m^2 of UVB radiation *$P < 0.05$ compared with control; #$P < 0.05$ compared between 1 h and 24 h after UVB treatment; ^$P < 0.05$ compared between Mn^{III}TE-2-PyP^{5+} and saline pre-treatment. (B) Mn^{III}TE-2-PyP^{5+} and saline pre-treated MnSOD$^{+/-}$ mice skin exposed to 5 kJ/m^2 of UVB radiation were co-immunoprecipated with 3-nitrotyrosine antibody and immunoblotted with Polγ antibody. (C) Quantification of Polγ co-immunoprecipitation by anti-3-nitrotyrosine antibody in Mn^{III}TE-2-PyP^{5+} and saline pre-treated MnSOD$^{+/-}$ mice skin exposed to 5 kJ/m^2 of UVB radiation. **$P < 0.01$, ***$P < 0.001$ compared with control; ###$P < 0.001$ compared between 1 h and 24 h after UVB treatment; ^^$P < 0.01$ compared between Mn^{III}TE-2-PyP^{5+} and saline pre-treatment.

2.5   Discussion

The present study demonstrates that UVB-induced mtDNA damage triggers p53 accumulation of mitochondria, that mitochondrial p53 interacts with both mtDNA and Polγ after UVB exposure, and that the mtDNA/Polγ association is dependent on the availability of p53. These results support a previous report on the role of p53 in the mtDNA repair process (Achanta et al 2005, Bakhanashvili et al 2008).   We have previously shown that oxidative stress induces p53 translocation to mitochondria and its subsequent interaction with MnSOD in a multistage chemical carcinogenesis model (Zhao et al 2002, Zhao et al 2005b). The present study confirms these findings using UVB treatment to cause DNA damage, and extends to demonstrate that UVB treatment leads to increased interaction between MnSOD and Polγ and that the interaction between MnSOD and Polγ is p53 independent. These results suggest that MnSOD participates in mtDNA repair processes by acting as a fidelity protein protecting the function of the major DNA repair enzyme in the mitochondria. This conclusion is supported by the findings that 1) MnSOD deficiency leads to a decrease in mtDNA-Polγ interaction and 2) inactivation of Polγ by nitration is prevented by treatment with $Mn^{III}TE-2-PyP^{5+}$, a potent peroxynitrite inhibitor. The findings of this study verify that MnSOD is an integral part of the nucleoid complex and extend to demonstrate that the antioxidant property of MnSOD serves to enhance the fidelity of mtDNA repair by salvaging the DNA polymerase (Polγ) in mitochondria from UV-induced peroxynitrite mediated inactivation.

Skin is the primary target of UVB radiation. UVB exposure has wide-ranging effects in skin, such as erythema and epidermal hyperplasia, which can eventually lead to photocarcinogenesis or photoaging. The underlying cellular processes for these conditions include DNA damage, apoptosis and oxidative stress. Both nuclear and mitochondrial DNA can be damaged by UVB radiation. Owing to its uniqueness, mtDNA has been used as a reliable biomarker for UV induced DNA damage (Birch-machin et al 1998, Harbottle and Birch-Machin 2006, Krishnan et al 2004). Our Q-PCR analysis of the mitochondrial genome indicates that UVB causes damage to mtDNA in mouse skin. The relative amplification ratio of the 10 kb mtDNA fragment at 1 h and 24 h after UVB treatment was significantly less than that of the reference control, which indicates the presence of DNA damage that blocks the amplification

process. There were ~0.15 lesions per 10 kb per strand at both the 1 h and 24 h treatments compared to the reference control. An earlier report that used Q-PCR to analyze UVB-exposed epidermal mtDNA from human skin shows deletions ranging from 4 to 10.5 kb in a 11.1 kb PCR fragment (Ray et al 2000). Thus, in our model UVB-induced mtDNA damage is being repaired.

UVB-induced oxidative stress and DNA damage stabilize p53 protein in the skin, leading to DNA repair in proliferating basal keratinocytes but cell cycle arrest and apoptosis in differentiated keratinocytes (Berg et al 1996, Li et al 1997, Ouhtit et al 2000, Renzing et al 1996, Tron et al 1998). UVB signature mutations in the p53 gene may lead to dysregulation of apoptosis and DNA repair, resulting in skin carcinogenesis (Li et al 1995). Our results demonstrating p53-dependent UVB-induced mtDNA repair are consistent with these findings. The increased physical interaction of p53 with mtDNA and Polγ might be a p53 response to mtDNA damage after UVB treatment. A basal level of interaction between mtDNA and Polγ has been observed in both $p53^{+/+}$ and $p53^{-/-}$ genotypes. This interaction can be attributed to a p53-independent mtDNA replication process, since the very same basal level interaction between mtDNA and Polγ was observed 1 h and 24 h after UVB treatment in the $p53^{-/-}$ phenotype. In contrast, increased interaction between mtDNA and Polγ was observed 1 h and 24 h after UVB treatment in $p53^{+/+}$ mice. This increase from basal level can be attributed to mtDNA repair and indicates that the interaction requires p53. The presence of p53 enhances the accuracy of mtDNA repair by proof reading and by reducing the misincorporation of dNTP into mtDNA by Polγ (Bakhanashvili et al 2008). Recent studies have identified p53-regulated p53R2 as a subunit of ribonucleotide reductase (RNR), a rate-limiting enzyme in the de novo synthesis of deoxyribonucleotides (dNTPs) (Bourdon et al 2007, Kulawiec et al 2009, Lebedeva et al 2009). The UVB induced p53 stabilization triggers transcriptional up-regulation of p53R2, and increases output of dNTPs required for the UVB induced mtDNA repair process. This may be attributed to the increase in amplification of the D-loop region after UVB treatment observed in Figure 3B.

The diverse functions of mitochondrial p53, which range from maintaining mtDNA integrity to apoptosis, led us to further explore our previous finding concerning MnSOD and p53 interaction in mitochondria. The physical interaction between p53 and MnSOD is observed with UVB treatment as was seen in chemical carcinogenesis

studies. In light of new evidence that establishes MnSOD as an integral component of nucleoids (Kienhofer et al 2009), and our findings that a physical interaction occurs between MnSOD and Polγ after UVB treatment and that this interaction is p53-independent, these results suggest that MnSOD may enhance mtDNA stability by serving as a fidelity protein protecting the function of the key mitochondrial DNA repair enzyme. The interaction between MnSOD and Polγ and subsequent protection of Polγ from UVB-induced inactivation support a new role for mitochondrial antioxidant enzyme MnSOD in maintaining mtDNA fidelity. Our previous studies with MnSOD over-expressing and knockdown mice treated with DMBA/TPA have clearly established that MnSOD prevents protein oxidation in mitochondria (Zhao et al 2001, Zhao et al 2002). The decrease in the interaction between mtDNA and Polγ after UVB treatment in MnSOD$^{+/-}$ mice might be attributed to increased oxidative modification of Polγ. Oxidative stress in yeast due to a lack of MnSOD leads to oxidation of various mitochondrial proteins such as aconitase, pyruvate, keto-acid dehydrogenase, α-ketoglutarate dehydrogenase, HSP60, glyceraldheyde-3-phosphate, and cytosolic fatty acid synthase (Cabiscol et al 2000, O'Brien et al 2004). The Polγ protein is known to be sensitive to oxidative modification when exposed to H_2O_2 (Graziewicz et al 2002). The Polγ exonuclease proof reading transgenic mice have increased point mutations, mtDNA deletions, and increased apoptosis that leads to accelerated aging (Kujoth et al 2005, Trifunovic et al 2004, Vermulst et al 2008). NO$^{\bullet}$ and $O_2^{-\bullet}$ generated by UVB can result in OONO^{-} production in skin, leading to nitration of proteins (Wu et al 2010). In this study we provide evidence for the first time that Polγ nitration and the consequent inactivation after UVB exposure are enhanced when MnSOD is deficient, and that pre-treatment of MnSOD$^{+/-}$ with Mn^{III}TE-2-PyP^{5+} results in decreased nitration and inactivation of Polγ.

In summary, our study shows that MnSOD plays an important role in protecting the fidelity of mtDNA against UVB-induced mtDNA damage in keratinocytes. We propose a model in Figure 7 to illustrate a novel dual-step strategy adapted by keratinocytes in response to UVB insult that enhances the repair of mtDNA and protects the mtDNA repair enzyme from being inactivated. On one hand, UVB-induced mtDNA damage triggers p53 translocation to mitochondria. The mitochondrial p53 interacts with mtDNA and enhances the polymerase and exonuclease activities of Polγ, which plays a major role in the mtDNA repair process

with its proof reading ability. On the other hand, mitochondrial antioxidant MnSOD plays a novel role by interacting with Polγ and protecting it from peroxynitrite-mediated inactivation. Circumstances that lead to increased oxidative stress by depleting MnSOD level and/or decrease MnSOD activity by acetylation can result in Polγ inactivation. Increasing MnSOD levels and/or activity by Sirt3 deacetylation enhances mitochondrial $O_2^{\cdot-}$ scavenging and reduces ROS-mediated insult on vital mitochondrial proteins such as Polγ. Additional studies aimed at the identification of the specific tyrosine residues of Polγ that are nitrated after UVB exposure and are responsible for reduced activity and/or protection by MnSOD will provide further biochemical insight into the mechanisms by which the nuclear encoded, mitochondrial localized protein, MnSOD, serves to maintain the fidelity of the mtDNA and will establish a nuclear mitochondrial feed forward loop in cellular adaptive responses against oxidative stress-mediated mitochondrial DNA instability.
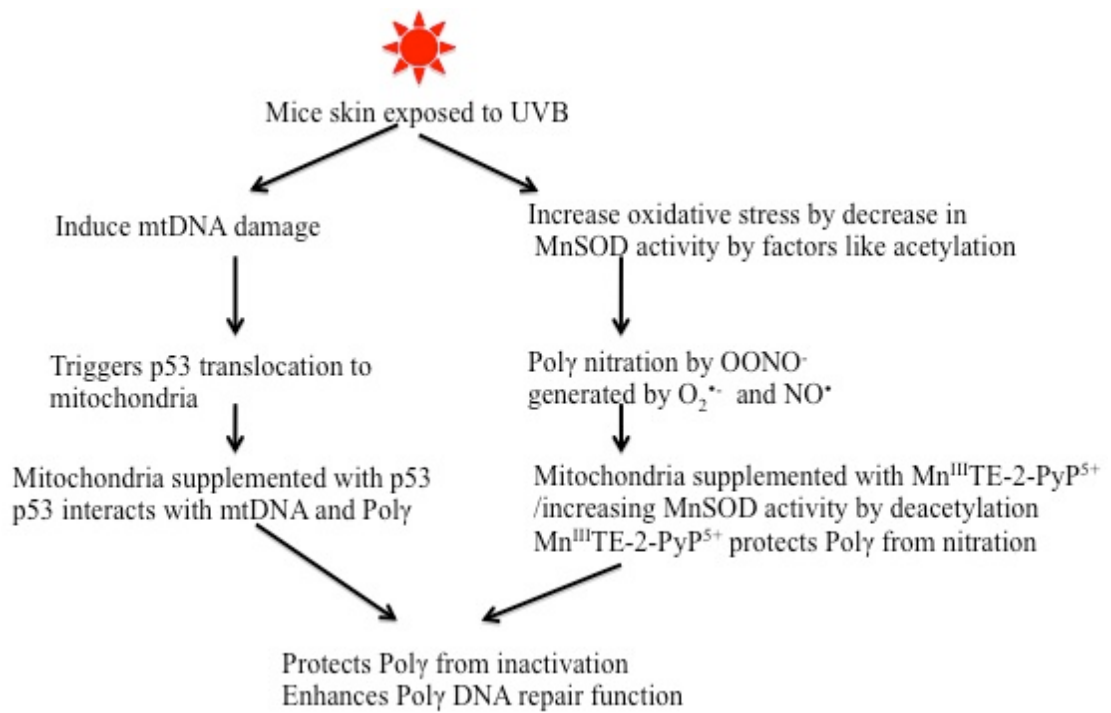
Figure 2.7 Schematic illustration of novel dual step strategy adapted by keratinocytes to survive UVB insult

3   Chapter Three

Autophagy activation by UV in murine skin model

3.1   Highlights

Acute exposure to UVB radiation causes increased DNA damage and ROS generation. Depending on the severity of the insult and keratinocyte differentiation status, a cascade of signaling events culminates in cell survival or apoptosis. Recent studies have demonstrated the diverse role of autophagy in cellular stress, metabolic homeostasis, and cell death. Our recent studies have demonstrated that 1) UVB induces an increase in ROS-mediated damage in mitochondria; 2) MnSOD protects Polγ from oxidative inactivation in mitochondria. As the primary source and target of ROS, damaged mitochondria and mitochondrial components such as mtDNA and cytochrome c are capable of triggering severe inflammatory response and cell death processes. Autophagy mediated scavenging of damaged mitochondria and mitochondrial components play a critical role in regulating inflammatory and cell death processes. Thus, it is possible that exposure to UVB radiation may lead to activation of autophagy as an adaptive response to mitochondrial injury. The present study used mouse keratinocytes (JB6 cells) and C57/BL6 mice as *in vitro* and *in vivo* models to study the effects of UVB radiation. Keratinocytes and whole skin were collected 1 h and 24 h post UVB irradiation. Immunoblotting reveals a decrease in phosphorylated AKT and mTOR levels in both *in vitro* and *in vivo* models. A significant increase in autophagy markers such as LC3-II and Beclin-1 were observed in the *in vivo* model. Taken together, the results suggest that exposure to UVB leads to activation of autophagy associated with inhibition of AKT-mTOR pathways.

3.2   Introduction

Skin is the primary target of UV radiation, a known environmental carcinogen implicated in skin cancer and aging (Yaar and Gilchrest 2001). The carcinogenic effect of UV is mainly due to the UVB spectrum, which primarily affects the epidermis of the skin. Based on the optics of skin, stratum corneum and epidermis form an optical barrier to the UVB spectrum by absorbing and scattering UVB radiation. Absorption of UVB by chromophores such as melanin (Kobayashi et al 1998) and urocanic acid results in a photo-protective effect. UVB radiation increases ROS and absorption of UVB by aromatic amino acids and nucleic acids causes damage to DNA, RNA and proteins in keratinocytes of the epidermal layer (Anderson and Parrish 1981, Takeuchi et al 2004).

The UVB-induced response in keratinocytes depends on the differentiation status of the keratinocytes and UVB dosage. The epidermis is composed of a heterogeneous population of keratinocytes that differ in proliferation potential and differential status. The basal layer is composed of undifferentiated cells with unlimited proliferation potential. The suprabasal and granular layers are composed of differentiated cells with limited or no proliferation potential that terminally differentiate keratinocytes to form an outer keratinized layer (Candi et al 2005, Nemes and Steinert 1999). p53 enhances DNA repair by a nucleotide excision repair system in the basal layer of the epidermis (Li et al 1997). In the differentiated layers, p53 induces apoptosis, which eliminates damaged cells (Baba et al 1996, Tron et al 1998). However, the induction of DNA repair occurs mostly at low doses of UVB while apoptosis is strictly induced at high doses; both events are dependent on wild-type p53 function (Li and Ho 1998).

On the molecular level, protection against UVB insult to keratinocytes is conferred by formation of sunburn cells (apoptotic cells). When the DNA damage inflicted by UVB is extensive and beyond repair, the affected keratinocytes undergo apoptosis to prevent malignant transformation. UVB up-regulates both extrinsic and intrinsic apoptotic pathways in response to DNA damage and ROS production (Kulms and Schwarz 2002, Takasawa et al 2005).

Keratinocytes undergo apoptosis at 3 h and 24 h after UVB exposure by early and late apoptotic pathways. However, the presence of the exogenous growth factor (EGF)

activates the AKT pro-survival signaling pathway that inhibits the mitochondria mediated "early-activated apoptotic pathway" in keratinocytes exposed to UVB radiation. This inhibition in turn assists the nucleotide excision repair pathway in removing additional thymidine dimers from DNA (Decraene et al 2002, Kuhn et al 1999). Furthermore, in malignant keratinocytes, the induction of the early apoptotic pathway is inhibited by dysregulation of the AKT pathway (Decraene et al 2004b).

Recent advances in understanding the signaling pathway have helped to elucidate different and somewhat unique cell death and cell survival pathways of epidermis. Based on the dosage, UVB induces differentiation-based cornification/keratinization, apoptosis, necrosis and autophagy in keratinocytes (Mammone et al 2000). Recent studies have established that activation of AKT not only inhibits apoptosis but also inhibits autophagy in keratinocytes (Claerhout et al 2010). AKT is a serine/threonine kinase that belongs to the protein kinase B family and is encoded by a proto-oncogene. AKT activation is a multistep process that involves membrane translocation and phosphorylation induced conformational change. The T-loop, αB and αC helices, and hydrophobic motif of the C-terminal tail of an inactive AKT are in complete disarray. AKT is phosphorylated on serine 473 in the hydrophobic motif by PI3K-related, DNA-dependent protein kinase (PDK1). PI3K-generated PIP3 and PIP2 recruit phosphorylated AKT and PDK1 to the plasma membrane. The phosphorylated hydrophobic motif of AKT activates and stabilizes PDK1. Phosphorylation of AKT on threonine 308 by activated PDK1 and stabilization of the kinase domain by the phosphorylated hydrophobic motif lead to orderly arrangement of the T-loop and αB and αC helices, resulting in activation of AKT (Bellacosa et al 2005, Manning and Cantley 2007). The AKT-mTOR pathway plays a critical role in regulating autophagy. The mammalian target of rapamycin (mTOR) is a member of the phosphoinositide kinase-related kinase (PIKK) family that phosphorylates serine and threonine residues of its target proteins. mTOR is a complex comprised of mTOR complex 1 (mTORC1) and mTOR complex 2 (mTORC2). mTOR regulates an array of cellular functions such as translation, transcription, protein stability, mRNA turn-over, actin cytoskeletal organization and autophagy (Jacinto and Hall 2003). mTOR is a major downstream target of the AKT signaling pathway that regulates cellular growth, proliferation, and metabolism by integrating cell growth factors such as insulin with cellular nutrients such as glucose and/or amino acids. AKT disrupts

the interaction between tumor suppressor proteins TSC1 and TSC2 by phosphorylating TSC2, resulting in increased accumulation of Rheb (Ras family small GTPase). Accumulation of Rheb results in activation of the mTOR complex. Activation of mTOR regulates its downstream targets, such as eukaryotic initiation factor 4E-binding protein (4E-BPs), p70 ribosomal S6 kinase, and HIF-1. As mTOR is an important down-regulator of autophagy, activators of the mTOR pathway such as AKT, suppress autophagy (He and Klionsky 2009, Ravikumar et al 2010). Recent studies show that mTORC1 phosphorylates the autophagy regulatory complex [composed of mammalian Atg13 protein (mAtg13), unc-51-like kinase 1(ULK1), and focal adhesion kinase interacting protein 200 kDa (FIP 200)] at ULK1 serine residue 757, resulting in inhibition of autophagy (Chan 2009, Egan et al 2011a). Inhibition of mTOR causes dephosphorylation of ULK1/mAtg13/FIP200 complex resulting in activation of autophagy. Further, mAtg13 and FIP200 are critical for ULK1 membrane translocation and stability (Ganley et al 2009, Jung et al 2009). Nutrient sensing kinases such as adenosine monophosphate-activated kinase induces autophagy and mitophagy by phosphorylation of ULK1 and inactivation of mTOR (Egan et al 2011a, Egan et al 2011b, Lee et al 2010).

Autophagy is defined as a programmed cell death (type II) or a pro-survival pathway in different physiological and pathological contexts (Ferraro and Cecconi 2007). Autophagy is a catabolic pathway involved in degradation and recycling of cellular components such as long-lived and damaged organelles and proteins. Organelles such as mitochondria are the source and primary target of ROS. In our previous study, we showed that UVB causes direct mtDNA damage and generates ROS that inactivates Polγ by nitration, thereby impairing its mtDNA repair function. Recent studies have shown evidence for efficient removal of defective mitochondria that generate more ROS and less ATP with high levels of mtDNA mutations by autophagy. Such an effective mechanism of mitochondrial turnover by autophagy ensures cell survivability by maintaining mtDNA integrity and thereby mitochondrial function (Gu et al 2004, Kroemer et al 2010, Yen and Klionsky 2008). Recent studies show that mitochondrial ROS generates lipid peroxidation products induce autophagy (Scherz-Shouval and Elazar 2007). Our studies previously demonstrated that nitration of mitochondrial proteins such as Polγ may lead to activation of autophagy in UVB-exposed epidermal keratinocytes. Furthermore, mitochondria are considered to be a

67

potential source of damage associated with molecular patterns (DAMPs) such as mtDNA, cytochrome C, ATP, and formyl peptides (Zitvogel et al 2010). Intracytoplasmic release of DAMPs and/or exposure to UVB trigger formation of the NLR (nucleotide-binding domain, leucine-rich-repeat-containing) family and pyrin domain containing 3 (NRLP3) inflammasome, which in turn leads to caspase-1 mediated activation of such pro-inflammatory cytokines (Feldmeyer et al 2007, Keller et al 2008, Nestle et al 2009). Leakage of DAMPs into the extracellular milieu can trigger severe inflammatory response such as systemic inflammatory response syndrome (SIRS) (Krysko et al 2011, Zhang et al 2010). Autophagic clearance of mitochondria with compromised integrity inhibits NRLP3 inflammasome formation and activation of pro-inflammatory mediators (Nakahira et al 2011, Zhou et al 2011). Although UVB induces immunosuppression, UVB-induced inflammation plays an important role in enhancement of tumor growth (Sluyter and Halliday 2000, Sluyter and Halliday 2001). UVB radiation regulates signaling pathways that stimulate production of inflammatory mediators. Further, inhibition of inflammation with anti-inflammatory agents inhibits skin carcinogenesis especially during the tumor promotion and progression stages (Halliday and Lyons 2008).

In the previous study, we showed the importance of UVB-induced mtDNA damage in triggering p53 translocation to mitochondria to aid Polγ in mtDNA repair and the role of MnSOD in protecting Polγ from ROS-induced inactivation by nitration. In this study, we hypothesize that UVB-induced AKT inhibition triggers activation of autophagy and play a significant role in removal of damaged mitochondria that prevent activation of inflammasomes.

3.3   Materials and Methods

3.3.1   Materials

All chemicals and reagents were purchased from Sigma-Aldrich (St. Louis, MO) with exception of the following: protease inhibitor set III from Calbiochem (La Jolla, CA); Propidium iodide from Molecular Probes, Inc. (Eugene, OR); rabbit poly-clonal anti-MnSOD from Upstate Technology (Lake Placid, NY); rabbit polyclonal anti-LC3, Beclin-1, PI3kinase P110a, AKT, phospho-AKT (Ser473), mTOR, and phosphor-mTOR (Ser2448) from Cell Signaling Technology Inc. (Danvers, MA); rabbit polyclonal anti-HSP60 from Santa Cruz Biotechnology (Santa Cruz, CA).

3.3.2   Cell Culture

The JB6 Cl41.5a cells derived from primary cultures of neonatal Balb/C epithelial cells were established and maintained as previously described (Colburn et al 1979). The cells were grown in MEM (Minimum Essential Medium, Earle's, Invitrogen), supplemented with 4% fetal bovine serum (Hyclone), and 2 mmol/L of L-glutamine (Gibco, Life Technologies Inc., USA). A day after plating, the MEM media was discarded and culture dishes were washed and replenished with 1 ml of sterile PBS. The JB^ cells were exposed or not exposed to 50 mJ/cm^2 UVB radiation.

3.3.3   Animals Studies

Six- to eight-week-old, wild-type, female C57BL/6 mice were purchased from Jackson Laboratory (Indianapolis, IN) and maintained at the University of Kentucky animal facility. Dorsal hairs were initially trimmed using an electrical surgical trimmer in conjunction with topical depilatory cream (Nair, Church & Dwight Co., Inc.) 3 days prior to UVB irradiation. The experimental protocol used in this study was approved by IACUC (The Institutional Animal Care and Use Committee of the University of Kentucky).

3.3.4   UV exposure

Depilated mice in the resting phase of the hair cycle were anaesthetized with ketamine and xylazine as described earlier (Xu et al 2007a) and exposed to a single dose of 5 kJ/m^2 UVB radiation. JB6 cells covered with 1 ml of sterile PBS were

exposed to 50 mJ/cm^2 UVB radiation. All the UVB exposures were carried out in a Plexiglass Lucite chamber (Plastic Design Corporation, Chelmsford, MA) delivered by UVB lamps (Black light blue lamp, Sankyo Denkco Ltd., Japan). The UV emittance was measured by UVB photometer radiometer (International Light Technologies, Peabody, MA) equipped with UVB measuring head.

3.3.5 Immunocytochemistry

JB6 cells were plated (1x10^4) in an eight-well Lab-Tek Chamber Slide w/Cover (BD, Biosciences) in 350 μl antibiotic-free medium (Minimum essential medium, Earle's, Invitrogen, Carlsbad, CA). One hour and 24 h after UVB treatment, the cells were washed and fixed with 4% paraformaldehyde for 30 min at room temperature. The cells were permeabilized with permeabilizing solution (0.1% Na citrate / 0.1% Triton X-100) on ice for 15 min and washed thrice with ice-cold blocking buffer. LC3 antibody was added at a dilution of 1:100 in blocking buffer and cells were incubated overnight at 4°C followed by incubation with anti-rabbit IgG-FITC (Jackson ImmunoResearch Laboratories, West Grove, PA) at a dilution of 1:200 for 1 h at room temperature. The cells were then washed three times with blocking buffer and counter-stained with 1 mg/ml of Propidium iodide. Laser scanning confocal images were acquired with Leica TCS confocal system at the University of Kentucky Imaging facility.

3.3.6 Western blot analysis

Equal amounts of skin mitochondrial proteins, and whole skin and cell lysate proteins were resuspended in 2X sample buffer with or without 2-Mercaptoethanol and separated on 6%, 10%, and 4-20% gradient polyacrylamide gels. After the separation, the proteins were transferred electrophoretically to nitrocellulose membrane and blocked with 5% nonfat dried milk in TBST buffer containing 50 mmol/L Tris, pH 7.9, 150 mmol/L NaCl and 0.05% (v/v) Tween-20. The blots were incubated overnight at 4°C with respective primary antibody at 1:2500 dilution, followed by incubation with horseradish peroxidase conjugated secondary antibody appropriate for the primary antibody species. The membranes were washed thrice with TBST

buffer, and the proteins were detected using enhanced chemiluminescence (Amersham Corp, Piscataway, NJ.)

3.3.7 Immunohistochemistry

The mouse skin tissue was fixed in 4% paraformaldehyde in PBS at 4°C on a rotator overnight. The skin tissue was incubated in 10%, 20%, and 30% serial PBS-sucrose solution for 1 h each at 4°C in a rotator. The skin tissue was embedded in cryo-O.C.T. compound (Sakura Finetek Inc., Torrance, CA), frozen on dry ice and stored at -80°C. Immunostaining was performed on 7-10 μm frozen sections as described using the TSA amplification system (NEN Life Sciences, Cambridge, MA). Heat-induced target retrieval was performed for 30 min with Target retrieval solution as described (DAKO Carpinteria, CA). Endogenous peroxidase activity was quenched with 1.5-3% H_2O_2, and then washed 3 times with phosphate buffered saline for 5 minutes each. The sections were incubated with MnSOD antibody diluted to 1:1000 in blocking buffer for 1 h at room temperature. Following washes with wash buffer, the sections were incubated with horseradish peroxidase conjugated goat anti-rabbit secondary antibodies (Jackson Immuno Research, West Grove, PA) diluted to 1:2000 in blocking buffer for 1 h at room temperature. Following three washes with wash buffer 5 min each, tyramide signal amplification (TSA, Perkin-Elmer Life Science Products, Boston, MA) was used according to the manufacturer's instructions. Laser scanning confocal images were acquired with Leica TCS confocal system at the University of Kentucky Imaging facility.

3.3.8 Data analysis

The data are represented as mean ± SEM from replicate samples (n = 3), and were analyzed by one-way and two-way analyses of variance using Prism software (GraphPad, San Diego, CA). An α level of $P<0.05$ was considered significant.

3.4 Results

3.4.1 UVB- induced modulation in mitochondrial antioxidant MnSOD

UVB is known to generate $O_2^{-\bullet}$ radicals in the skin. MnSOD is the major antioxidant enzyme that dismutates $O_2^{-\bullet}$ radicals in mitochondria. Increase in MnSOD is indicative of an increase in the mitochondrial $O_2^{-\bullet}$ level. Recent studies have indicated that $O_2^{-\bullet}$ is the major ROS that regulates autophagy (Chen et al 2009, Kim et al 2007). Hence, MnSOD levels were analyzed in JB6 cells and mice skin exposed to UVB radiation by immunoblotting. As shown in Figure 1A, in JB6 cells exposed to 50mJ/cm^2 of UVB radiation, MnSOD levels increased at 1 h and 24 h after UVB exposure. A similar increase in MnSOD level in mouse whole skin lysate and mitochondrial fraction at 1 h and 24 h after UVB exposure was further confirmed by immunoblotting, as shown in Figure 1B. β-Actin and HSP60 were used as loading control. As shownin Figure 1C the increase in MnSOD levels after UVB treatments were significant. The *in vitro* and *in vivo* increases in MnSOD level suggest an increased mitochondrial $O_2^{-\bullet}$ level. Since MnSOD is known to induce cell differentiation and increased cell turnover ratio, we performed immunohistochemistry to determine MnSOD localization in different layers of the epidermis. Immunohistochemical studies with mouse skin exposed to 5 kJ/m^2 UVB suggest increased MnSOD immunostaining in keratinocytes that line the basement membrane (basal layer of epidermis) and in the dermal fibroblasts at 1 h after UVB treatment, as shown in Figure 1D. However, by 24 h after UVB treatment, there is increased MnSOD immunostaining in the basal and suprabasal layers of the epidermis, and in the papillary layer of the dermis, as shown Figure 1D.

A
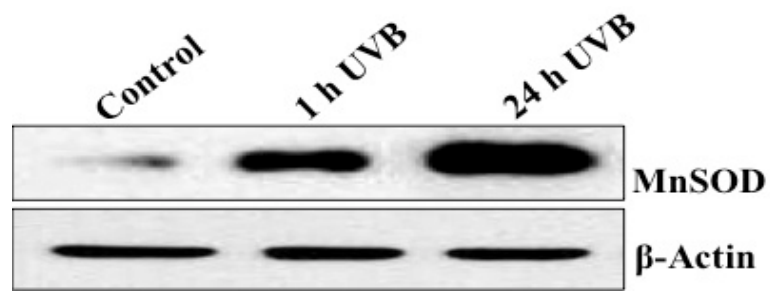
B
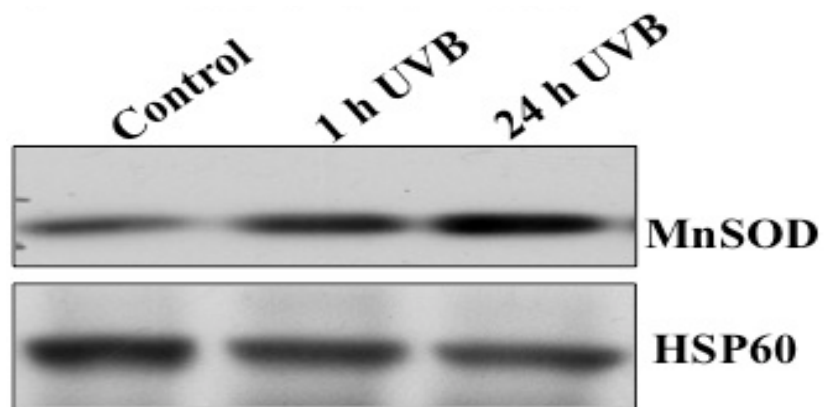
C
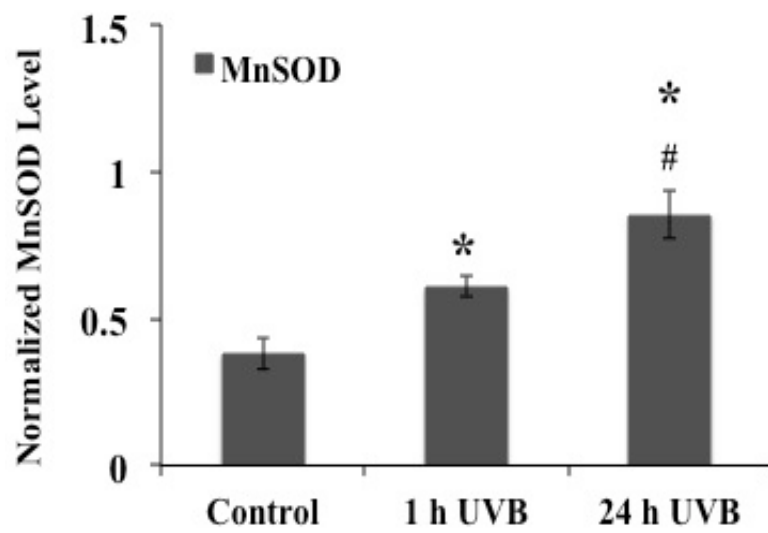
D
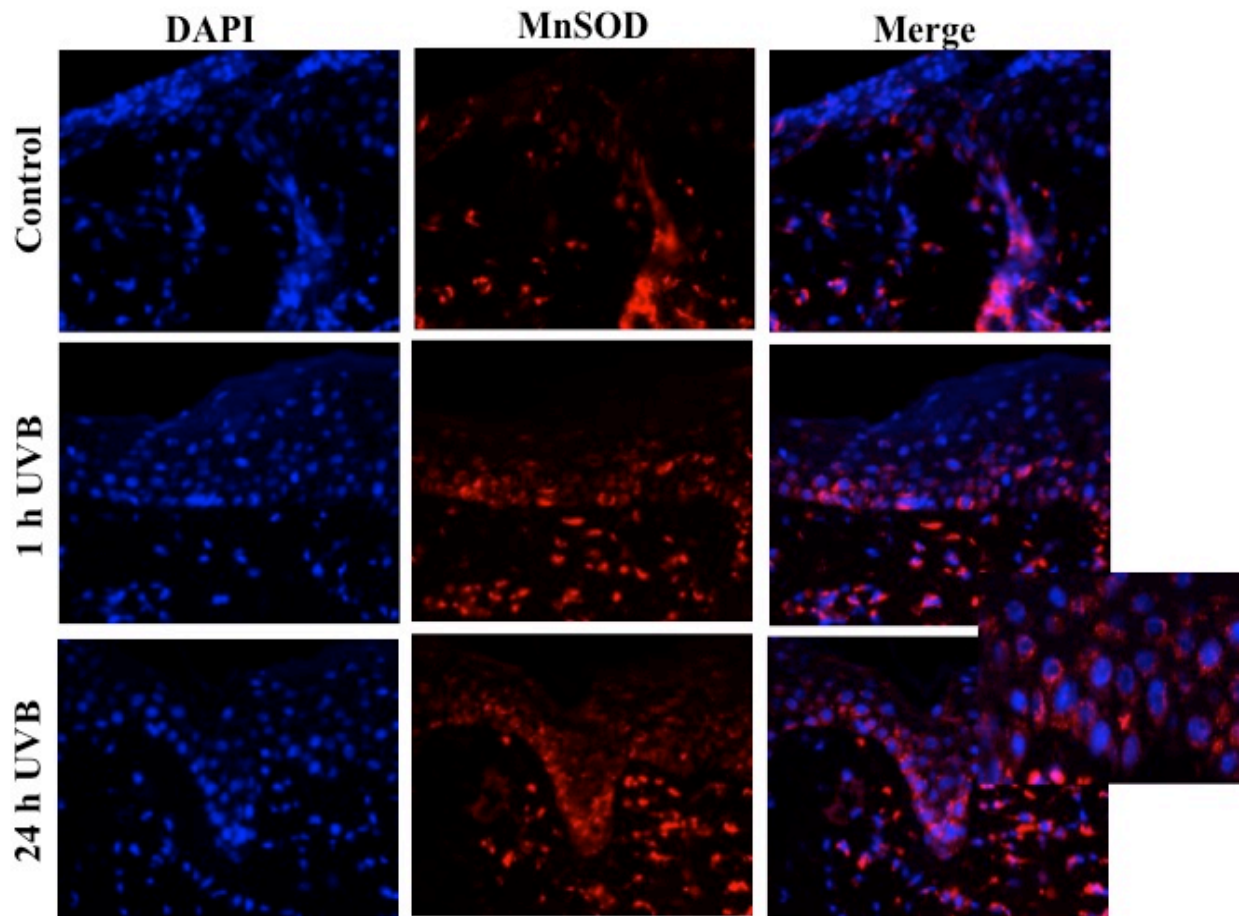
Figure 3.1 UVB-induced modulation in mitochondrial antioxidant MnSOD level in keratinocytes and murine skin tissue

(A) JB6 cells were exposed or unexposed to $50mJ/cm^2$ of UVB radiation. Whole cell lysates were immunoblotted for MnSOD antibody. β-actin was used as internal loading control. **(B)** C57BL/6 mice were exposed to 5 kJ/m^2 of UVB radiation. Whole skin mitochondrial fraction was immunoblotted for MnSOD antibody. HSP-60 was used as internal loading control. **(C)** MnSOD levels in skin mitochondrial lysate at 1 h and 24 h after UVB exposure were quantified. *P<0.05, compared with control, #P<0.05, compared between 1 h and 24 h UVB treatment. Results were averaged from 3 sets of independent experiments. **(D)** C57BL/6 mice were exposed to 5 kJ/m^2 of UVB radiation. Approximately 7-10 μm thick skin cryosections were immunostained with anti-MnSOD followed by cyanine 3 (Cy3) tagged goat anti-rabbit using tyramide signal amplification system and then counterstained with DAPI (nucleus).

3.4.2 UVB- induced modulations in AKT status

Recent studies have shown that activation of the AKT signaling pathway through various growth factors and oxidative stress offers transient protective effect to keratinocytes from UVB-induced apoptosis (Decraene et al 2002, Lotti et al 2007, Martindale and Holbrook 2002). To verify UVB-induced modulation of the AKT signaling pathway, cell lysates from cultured JB6 cells and skin lysates from C57BL/6 mice exposed to $50mJ/cm^2$ and $5kJ/m^2$ UVB radiation, respectively, were subjected to immunoblot analysis. AKT activation was measured by detection of AKT Thr-308 phosphorylation. As shown in Figures 2A, 2B, 2C, and 2D, UVB induced a significant increase in AKT Thr-308 phosphorylation which peaked at 1 h post irradiation and decreased to basal level at 24 h post- irradiation in both *in vitro* and *in vivo* models. β-Actin was used as loading control. These results indicate that the significant increase in AKT phosphorylation at 1 h post- irradiation was transient, since it reaches the basal level at 24 h post-UVB radiation and there was no significant change observed with PI3K levels at 1 h and 24 h post-UVB radiation compared to the controls in both in vitro and in vivo models.

A
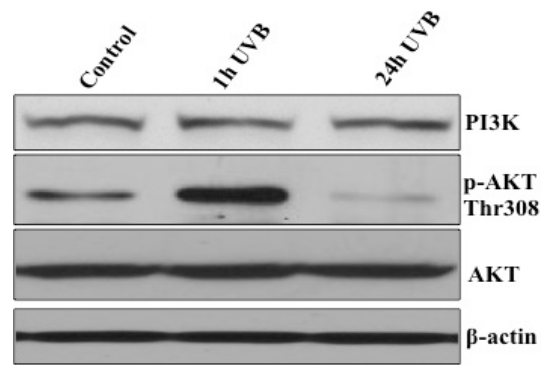
B
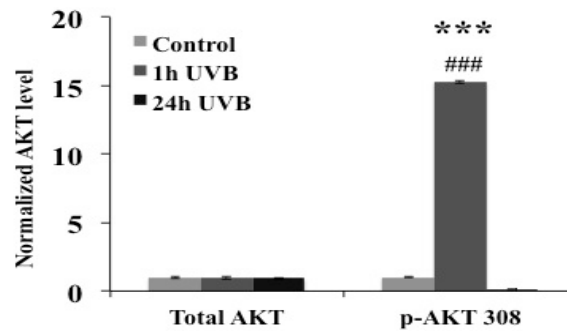
C
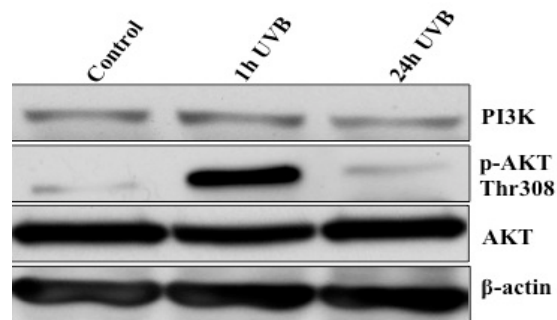
D
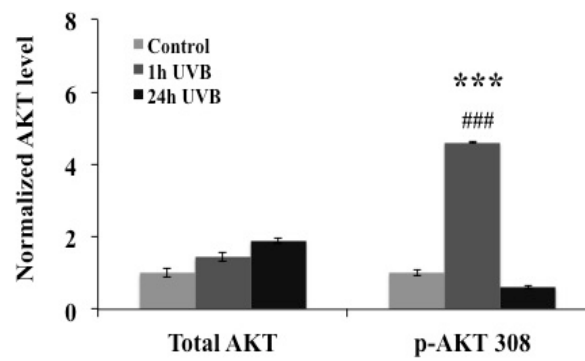
Figure 3.2 UVB-induced suppression of PI3K-AKT pathway in cultured keratinocytes and murine skin tissue

(A) JB6 cells were exposed or unexposed to 50 mJ/cm^2 of UVB radiation. Fifty micrograms of whole cell lysate was immunoblotted for PI3K, AKT and phosphorylated AKT (Thr 308). β-actin was used as internal loading control. **(B)** The total AKT and phosphorylated AKT levels in whole cell lysate at 1h and 24h after UVB exposure were quantified. ***P<0.001, compared with control, ###P<0.001, compared between 1 h and 24 h UVB treatment. **(C)** C57BL/6 mice were exposed or unexposed to 5kJ/m^2 of UVB radiation. Fifty micrograms of whole skin tissue lysate was immunoblotted for PI3K, AKT and phosphorylated AKT (Thr 308). The Ponceau staining was used to confirm equal loading and uniform transfer of protein. Monoclonal anti-β-actin antibody was used as internal loading control. **(D)** The total AKT and phosphorylated AKT levels in skin lysate at 1 h and 24 h after UVB exposure were quantified. ***P<0.001, compared with control, ###P<0.001, compared between 1 h and 24 h UVB treatment.

3.4.3 UVB- induced modulations in AKT downstream target m-TOR

Previous studies have shown that mTOR is a downstream target of the AKT signaling pathway. mTOR phosphorylation at ser-2448 residue indicates activation of mTOR via the AKT signaling pathway (Altomare et al 2004). To verify whether UVB modulates the mTOR complex, cell lysates from cultured JB6 mouse keratinocytes and skin lysates from C57BL/6 mice exposed to 50mJ/cm^2 and 5kJ/m^2 UVB radiation, respectively, were subjected to immunoblot analysis. mTOR activation was measured by detection of ser-2448 residue phosphorylation. As shown in Figures 3A, 3B, 3C, and 3D, UVB induced a significant increase in mTOR ser-2448 phosphorylation which peaked at 1 h post-irradiation and decreased to basal level at 24 h post-irradiation in both *in vitro* and *in vivo* models. These results indicate that the activation of mTOR closely followed the activation of AKT since a similar pattern of changes was seen with mTOR activation. This suggests that mTOR is a downstream target of AKT that is activated in keratinocytes acutely exposed to UVB radiation.

A
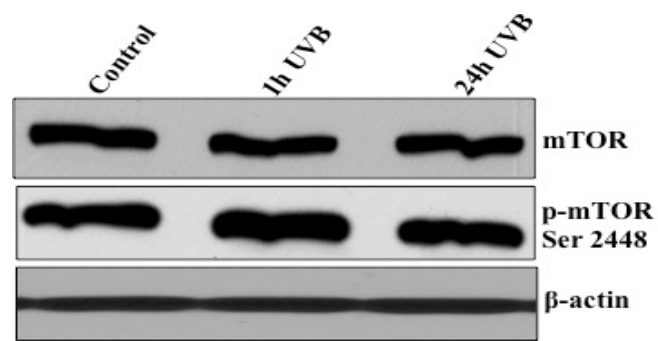
B
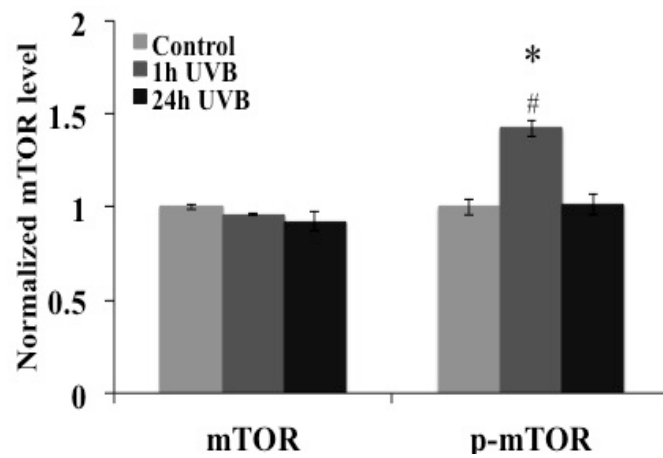
C
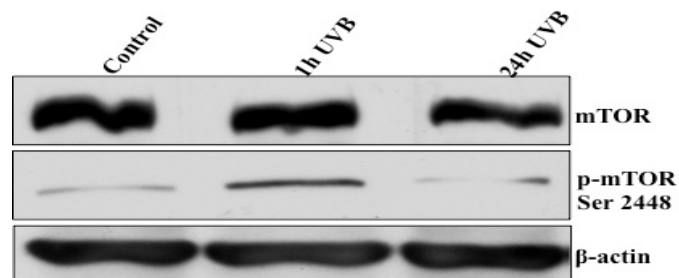
D
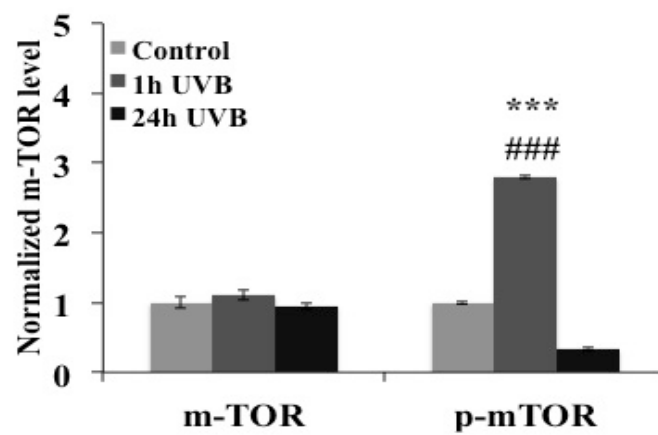
Figure 3.3 UVB-induced suppression of mTOR pathway in cultured keratinocytes and murine skin tissue

(A) JB6 cells were exposed or not exposed to 50 mJ/cm^2 of UVB radiation. Fifty micrograms of whole cell lysate was immunoblotted for mTOR and phosphorylated mTOR (Ser 2448). β-actin was used as internal loading control. **(B)** The total mTOR and phosphorylated mTOR levels in whole cell lysate at 1 h and 24 h after UVB exposure were quantified. *P<0.05, compared 1 h UVB treatment and control, #P<0.05, compared between 1 h and 24 h UVB treatment. **(C)** C57BL/6 mice were exposed or unexposed to 5kJ/m^2 of UVB radiation. Fifty micrograms of whole skin tissue lysate was immunoblotted for mTOR and phosphorylated mTOR (Ser 2448). β-actin was used as internal loading control. **(D)** The mTOR and phosphorylated mTOR (Ser 2448) in skin lysate at 1 h and 24 h after UVB exposure were quantified. ***P<0.001, compared with control, ###P<0.001, compared between 1 h and 24 h UVB treatment.

3.4.4 UVB- induced AKT inhibition activates autophagy in mouse epidermis

Previous studies have identified autophagy as a pro-survival mechanism activated by AKT-mTOR axis inhibition in skin squamous cells carcinoma cell lines (Claerhout et al 2010). Activation of autophagy by UVB was assessed in JB6 cells exposed to 50mJ/cm^2 UVB radiation and immunostained for LC3. The JB6 cells were counterstained with propidium iodide. As shown in Figure 4A, punctate LC3 immunostaining slightly increased at 1 h and 24 h after UVB treatment compared to the control. Increase in punctate staining compared to diffuse staining by LC3 antibody is indicative of activation of autophagy. The change in the staining pattern suggests that LC3-I is processed to phospholipid conjugated LC3-II (lipidated form) with subsequent targeting to autophagosomal membranes. Hence, we performed immunoblotting with whole cell lysate obtained from JB6 cells treated with 50mJ/cm^2 UVB radiation to assess the modulations in LC3-II after UVB treatment. As shown in Figures 4B and 4C, in contrast to immunostaining, there was a significant decrease in LC3-II level at 24 h after UVB treatment compared to the control and 1 h UVB treatment group. However, there was no significant difference in the LC3-II level when compared between the control and 1 h UVB treatment groups. Furthermore, there was a significant decrease in Beclin-1 protein levels at 24 h after UVB treatment compared to control and 1 h UVB treatment group, as shown in Figures 4B and 4D.

Surprisingly immunoblot analysis of whole skin lysates from C57Bl/6 mice exposed to 5kJ/m^2 UVB radiation confirmed a significant increase in LC3-II and Beclin-1 levels at 24 h after UVB treatment compared to the control and 1 h UVB treatment group as shown in Figures 5A, 5B, and 5C.

A
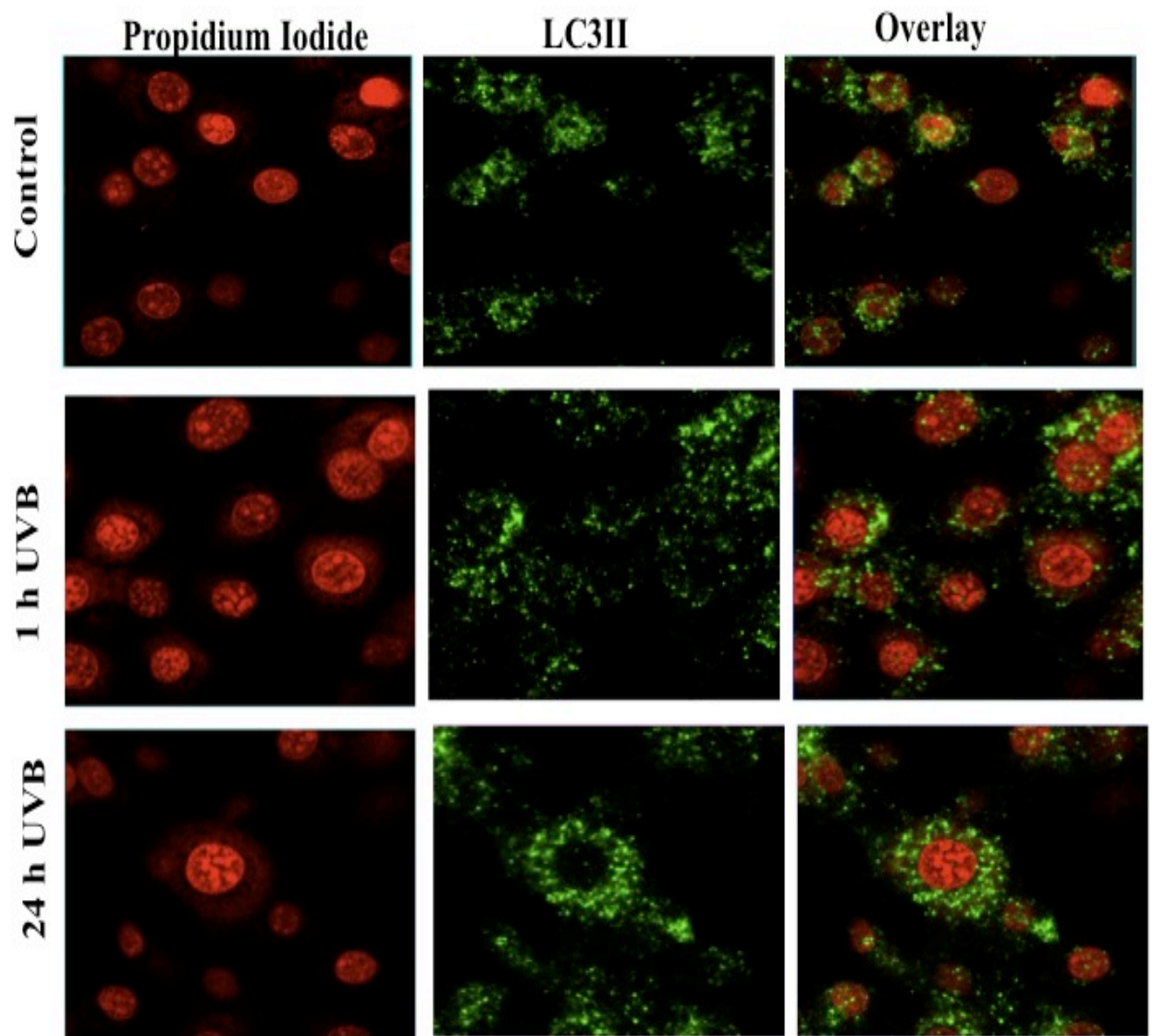
B
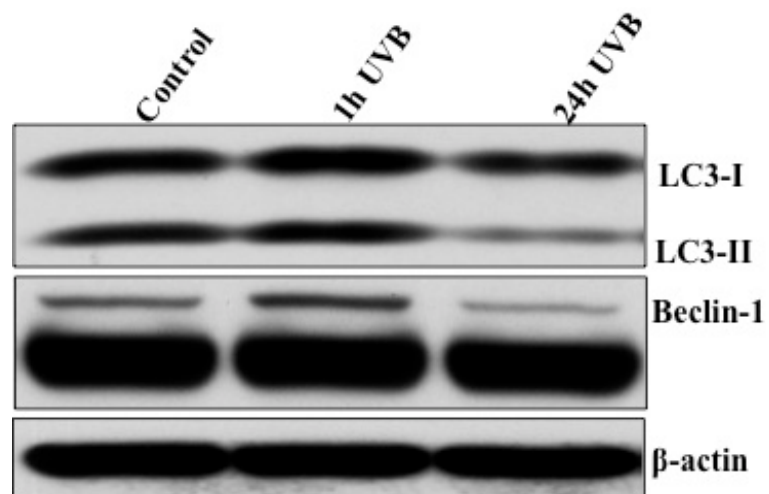
C
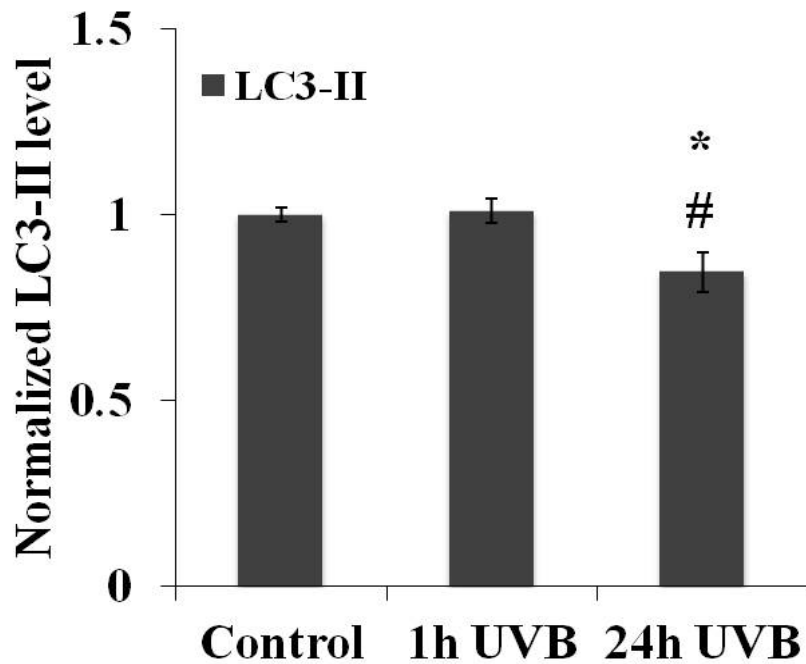
D
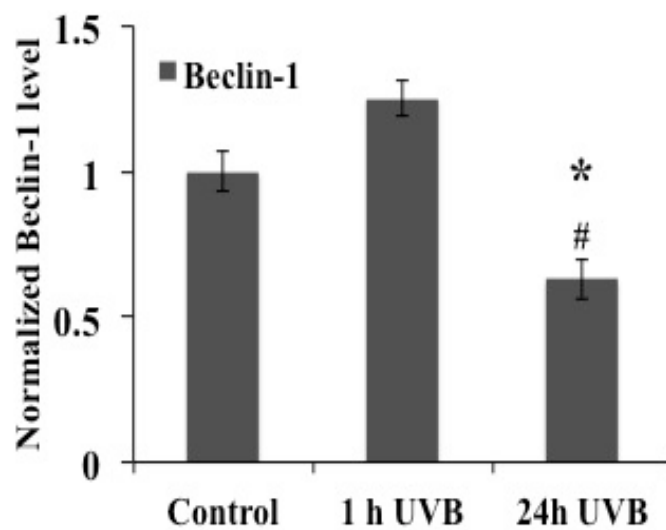
Figure 3.4 UVB-induced modulation of autophagy in murine cell culture system

(A) JB6 cells were unexposed or exposed to 50mJ/cm^2 of UVB radiation. Cells were immunostained anti-LC3 antibody followed by FITC-goat anti-rabbit antibody and counterstained with propidium iodide (nucleus). An increase in punctate LC3 staining was observed at 1 h and 24 h after UVB exposure compared with control. **(B)** JB6 cells were unexposed or exposed to 50 mJ/cm^2 of UVB radiation. One hundred micrograms of whole cell lysate was immunoblotted for LC3 and Beclin-1. β-actin

was used as internal loading control. **(C)** The LC3-II levels in whole cell lysate at 1 h and 24 h after UVB exposure were quantified. *P<0.05, compared between control and 24 h UVB treatment, #P<0.05, compared between 1 h and 24 h UVB treatment. **(D)** The Beclin-1 levels in whole cell lysate at 1 h and 24 h after UVB exposure were quantified. *P<0.05, compared between control and 24 h UVB treatment, #P<0.05, compared between 1 h and 24 h UVB treatment.

A
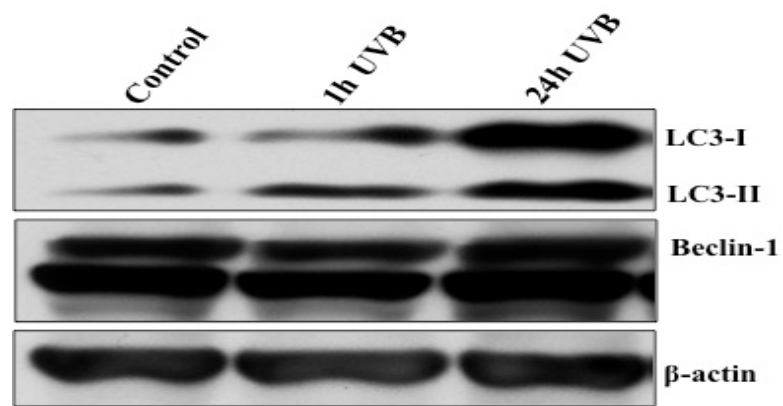
B
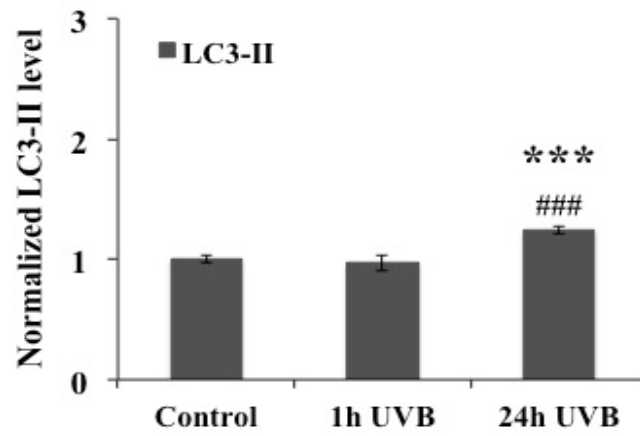
C
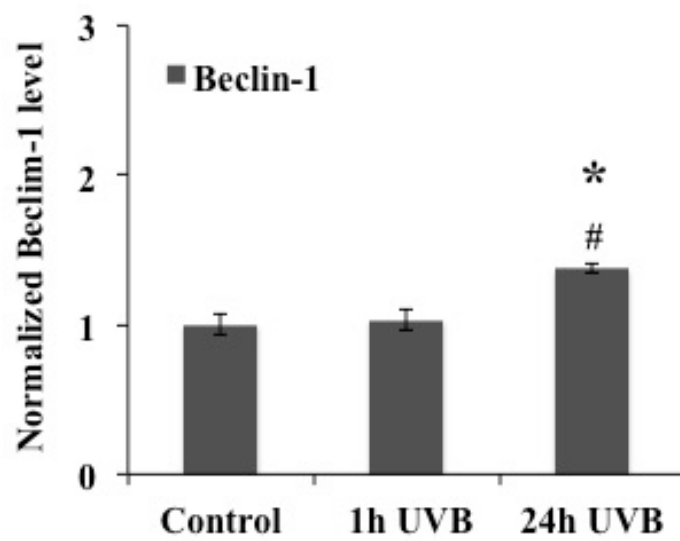
Figure 3.5 UVB-induced activation of autophagy in murine skin tissue

(A) C57BL/6 mice were unexposed or exposed to 5kJ/m^2 of UVB radiation. One hundred micrograms of whole skin lysate was immunoblotted for LC3 and Beclin-1. β-actin was used as internal loading control. **(B)** The LC3-II levels in skin tissue lysate at 1 h and 24 h after UVB exposure were quantified. ***P<0.05, compared between control and 24 h UVB treatment, ###P<0.05, compared between 1 h and 24 h UVB treatment. Results were averaged from 3 sets of independent experiments. **(C)** The Beclin-1 levels in skin tissue lysate at 1 h and 24 h after UVB exposure were quantified. *P<0.05, compared between control and 24 h UVB treatment, #P<0.05, compared between 1 h and 24 h UVB treatment.

3.5 Discussion

Skin is constantly exposed to oxygen, the main source of $O_2^{-\bullet}$ radical, which is aggravated by exposure to extrinsic factors such as UVB radiation. This enormous burden is overcome by dynamic compartmentalization of the skin into the highly cellular epidermis and the collagen-rich dermis. Within the epidermal milieu, keratinocytes are in a constant state of flux through a programmed cell death process called terminal differentiation (Lippens et al 2005), in which UVB is known to induce apoptosis and necrosis depending on the dose and duration of exposure. For the first time, this study shows evidence for activation of macroautophagy (autophagy) in keratinocytes exposed to UVB radiation.

In this study, both *in vivo* and *in vitro* models showed an initial transient but significant increase in phosphorylated AKT (Thr-308) at 1 h after UVB treatment and a significant decrease to basal levels in phosphorylated AKT (Thr-308) 24 h after UVB treatment. mTOR, a downstream target of AKT, followed a similar trend to that of AKT. This observation concurs with a previous study that shows that growth factor-mediated activation of the AKT pro-survival pathway. AKT activation leads to inhibition of early UVB-induced apoptosis by disrupting Bax translocation to mitochondria to enhance DNA repair (Claerhout et al 2007, Decraene et al 2002). UVB exposure causes a transient activation of the AKT pathway that delays early onset of the mitochondrial apoptotic pathway. The increase in the apoptotic initiation threshold is mediated by IGF-1 (Decraene et al 2002). This delay in apoptosis onset provides more time for keratinocytes to initiate the DNA repair process. This temporal pause is particularly more relevant in basal layers of keratinocytes. This is due to the fact that the IGF-1 binding protein-3 that modulates the IGF-1 mediated AKT pathway is expressed only in basal keratinocytes of skin (Batch et al 1994). Activation of apoptosis and autophagy were observed when AKT inhibitors were used to treat squamous cell carcinoma. (Claerhout et al 2010). In addition, recent studies indicate that increased ROS generation leads to inhibition of the AKT pathway (Hussain et al 2011). This prompted us to investigate the possibility of autophagy activation by UVB-mediated inhibition of the AKT pathway in murine epidermal cells. The time-dependent increase in lipidation of LC3 protein and increase in Beclin-1 levels confirm induction of autophagy in murine skin exposed to

UVB radiation. In the *in vitro*, study we observed a significant decrease in lipidation of LC3 protein and Beclin-1 levels at 1 and 24 h post-UV radiation. This suggests that autophagy is not a major mechanism in JB6 cells exposed to 50 mJ/cm^2 of UVB. However, in the *in vivo* study we observed a significant increase in lipidation of LC3 protein and Beclin-1 levels at 24 h post-UV radiation. This discrepancy in autophagy induction in *in vivo* and *in vitro* models can be attributed to the difference in UVB dosage. Further, within murine skin epidermis, keratinocytes with various differentiation potentials are compartmentalized. The supporting dermis contains fibroblasts that secrete several growth factors and cytokines essential for keratinocytes. These cytokines are also involved in proliferation, apoptosis, and inflammation. After UVB exposure, presence of melanocytes and dendritic cells activity will further influence the outcome in murine epidermis. A simple monolayer of JB6 cells is less complicated and devoid of the above-mentioned factors that are critical in determining the outcome with respect to any insult. The cause for the activation of autophagy is poorly understood. Recent studies have shown autophagic clearance of ROS generating and/or oxidatively damaged mitochondria as key a mechanism to prevent activation of inflammasome by intracytoplasmic and extracellular release of mtDNA and mitochondrial protein (Nakahira et al 2011, Zhou et al 2011).

In the previous chapter, we opined UVB-induced mtDNA damage and inactivation of mitochondrial DNA proteins such as Polγ by ROS -mediated nitration. The damaged DNA in mitochondria can be a major contributor to the formation of ROS-generating mitochondria. Our immunohistochemistry and immunoblotting studies suggest an increase in MnSOD expression in basal, suprabasal and dermal fibroblasts after UVB exposure. Previous studies have demonstrated the ROS-dependent pleiotropic ability of MnSOD to induce cell differentiation and cell turnover by induction of apoptosis and mitosis through regulation of AP-1 and p53 levels in nucleus (Oberley et al 2004, St Clair et al 1994). Recent studies have implicated MnSOD in regulating ROS-mediated autophagy of oxidatively damaged mitochondria and nucleus in keratinocytes (Deruy et al 2010). Acute exposure to UVB radiation induces IL-1α, Il-1β and TNF-α in human keratinocytes that stimulate UVB-exposed dermal fibroblasts to upregulate MnSOD (Naderi-Hachtroudi et al 2002). Hence, an increase in MnSOD level in basal and suprabasal layers and in dermal fibroblasts may be

attributed to ROS-mediated cell differentiation processes or cytokine-mediated paracrine signaling pathways. In these scenarios activation of autophagy after UVB exposure might help in the clearance of damaged mitochondria by cells. This might be particularly relevant in the basal compartment of the epidermis that comprises the undifferentiated proliferating cells. Any intracellular spillage of damaged mitochondrial proteins or mtDNA might trigger apoptosis resulting in loss of cells in the proliferating compartment. Previous studies have demonstrated "temporo-spatial" differences in keratinocytes response to UVB exposure based on their differentiation status. Well-differentiated keratinocytes of the epidermis with a minimal capacity for DNA repair are destined to apoptosis. Keratinocytes in the undifferentiated compartment reveal predominant activation of DNA repair process rather than apoptosis (Li et al 1996, Li et al 1997, Tron et al 1998). Thus, it can be hypothesized that keratinocytes exposed to UVB initiate apoptosis in well-differentiated keratinocytes that have limited proliferative potential. However, autophagy initiated in undifferentiated layers of keratinocytes protects epidermal integrity by protecting its stem cell population, which is responsible for replenishing the epidermis with keratinocytes. Autophagy may serve as a survival pathway by eliminating ROS producing mitochondria and damaged proteins. However increased damage leading to increased elimination of damaged organelles and protein by autophagy itself could threaten the very survivability of the cells. This may result in autophagy acting as a cell death pathway (Tsujimoto and Shimizu 2005).

Taken altogether, our results support the hypothesis (summarized schematically in Figure 6 that UVB-induced ROS-mediated inhibition of AKT-mTOR triggers activation of autophagy and may prevent activation of the NRLP3 inflammasomes that can contribute to the development of skin cancer.
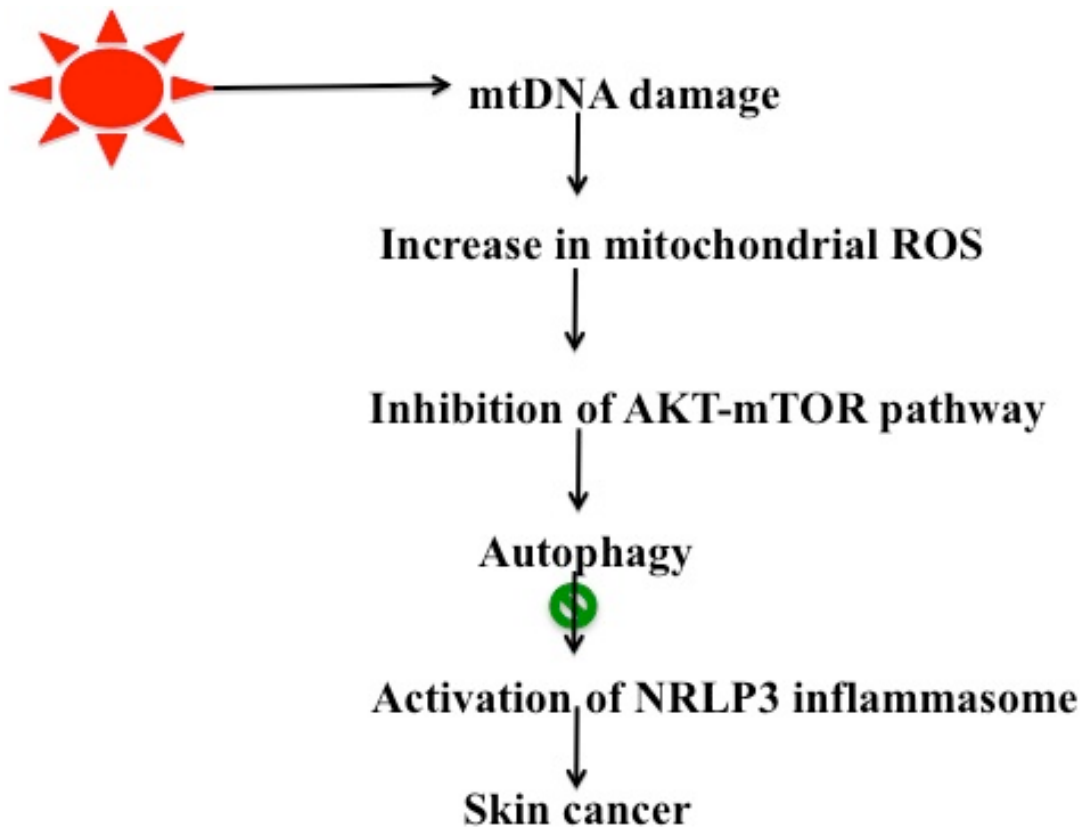
Figure 3.6. Schematic representation of autophagy's potential role in prevention of carcinogenesis

4   Chapter Four

4.1   Summary and future studies

Skin, an important organ is constantly exposed to environmental toxicants such as UVB radiation. Skin exposed to UVB is under pronounced oxidative stress. Mitochondria are the major source and target of ROS. Any damage to vital mitochondrial proteins such as Polγ may exacerbate mitochondrial damage in UVB-exposed skin tissue. The data presented in this dissertation strongly suggest that inactivation of Polγ contributes to mitochondrial dysfunction and subsequent leakage of damaged mitochondrial constituents. Although the role of MnSOD as an antioxidant has been well recognized, to my knowledge the data presented here are the first to support the novel role of MnSOD as a mitochondrial fidelity protein that influences the mtDNA repair process by protecting Polγ inactivation by nitration and activation of autophagy by UVB in murine skin tissue. The data obtained in the study addresses the following hypotheses:

1. Manganese superoxide dismutase is a mitochondrial fidelity protein that protects Polγ against UV-induced inactivation

2. Activation of autophagy by UVB in murine skin model

UVB-induced mtDNA damage and inactivation of Polγ by nitration were studied using p53 and MnSOD transgenic mice in the C57BL/6 strain. Polγ was nitrated with an associated decrease in its reverse transcriptase activity in skin mitochondria after acute exposure to UVB radiation. The time dependent increase in nitration and inactivation of Polγ showed a strong inverse correlation to MnSOD level in the mitochondria based on studies with MnSOD transgenic mice. However, there was no change in the Polγ protein levels after UVB treatment. Amino acid sequence analysis of Polγ catalytic subunit reveals the presence of 31 tyrosine residues, of which 2 tyrosine residues are present in the catalytic active site of the polymerase motif. These 2 tyrosine residues are responsible for the uptake of incoming nucleotide. This in turn is further supported by the findings that Polγ has increased sensitivity to oxidation induced by H_2O_2 and the oxidizing environment (Graziewicz et al 2002).

91

Furthermore, studies show that inactivation of tyrosine residue in the catalytic site, by antiretroviral nucleoside drugs leads to unwanted side effects such as muscle wasting.

UVB-induced translocation of p53 to mitochondria is consistent with previous studies (Achanta et al 2005, Erster et al 2004, Zhao et al 2005b). In addition, our data from C57BL/6 wild-type mice acutely exposed to UVB radiation reveal increased mtDNA lesions in skin. Mitochondrially translocated p53 interacts with mtDNA, Polγ and MnSOD, which is consistent with previous studies (Achanta et al 2005, Zhao et al 2005b). The significance of p53 in UVB-induced mtDNA-Polγ interaction was assessed using p53 transgenic mice. Consistent with previous findings, UVB-induced Polγ-mtDNA interaction is enhanced by p53. This observation suggests a critical role for p53 in the enhancement of the Polγ-mediated mtDNA repair process after UVB exposure (Achanta et al 2005, Bakhanashvili et al 2008).

Previous findings from chemical carcinogenesis study from our lab suggest that oxidative stress induces p53 accumulation in mitochondria. Mitochondrial p53 interact with MnSOD (Zhao et al 2005b). Recent studies suggest that MnSOD is an integral constituent of the nucleoid macromolecular complex composed of mtDNA and its associated proteins such as Polγ (Kienhofer et al 2009). The UVB-induced increase in interaction between MnSOD and Polγ supports the possibility of MnSOD-mediated modulation in Polγ-mtDNA interaction in skin mitochondria after UVB exposure. Acute UVB exposure studies with MnSOD transgenic mice reveal that modulations in the interaction between Polγ and mtDNA are MnSOD-dependent. However, there was no significant increase in Polγ protein level with respect to MnSOD level in the mitochondria. Recent studies suggest a considerable increase in $NO^\bullet$ and $O_2^{-\bullet}$ generation within murine skin mitochondria acutely exposed to UVB radiation (Maglio et al 2005). This suggests an increased possibility that the above-mentioned free radicals react instantaneously and generate the powerful oxidant, peroxynitrite anions. Tyrosine residues within the protein are potential targets of peroxynitrite for nitration and thereby inactivation of the protein functions. UVB induces increased nitration and inactivation of Polγ, which is assessed by a decrease in reverse transcriptase activity.

The role of MnSOD in Polγ nitration was analyzed using MnSOD transgenic mice. For the first time, the results from this study demonstrate protection of Polγ protein from UVB-mediated nitration by MnSOD. To further confirm the novel role of MnSOD in protecting Polγ, MnSOD deficient mice were treated with Mn-based porphyrin, $Mn^{III}TE$-2-PyP^{5+}. The decrease in Polγ nitration and increase in reverse transcriptase activity after $Mn^{III}TE$-2-PyP^{5+} treatment suggest that Polγ is rescued from UVB-mediated nitration and inactivation by $Mn^{III}TE$-2-PyP^{5+}. The results from this study are the first to suggest that the classical antioxidant function of MnSOD extends to a novel mitochondrial fidelity protein that protects Polγ from inactivation by UVB-mediated nitration. Based on this study, we propose that skin tissue exposed to acute UVB radiation may adapt a novel dual-step strategy to protect itself against the damaging effects of UVB radiation. This involves p53 translocation to mitochondria in response to increased mtDNA damage and oxidative stress. Mitochondrially translocated p53 interacts with mtDNA and Polγ, and mediates UVB-induced Polγ-mtDNA interaction. This enhances the UVB-induced mtDNA repair process by Polγ. Concomitantly, MnSOD protects Polγ from inactivation due to nitration. Peroxynitrite is a powerful oxidant and is known to nitrate and inactivate MnSOD and other mitochondrial proteins involved in oxidative phosphorylation and Kerb's cycle. Hence, the effect of peroxynitrite on the activity of these proteins after UVB exposure needs to be further investigated. Since Polγ has 31 tyrosine residues in the catalytic subunit that are potential targets for peroxynitrite, further studies are required to identify the specific tyrosine residues that are nitrated after UVB exposure in skin mitochondria. The significance of the nitrated tyrosine residue with respect to Polγ polymerase and exonuclease activity and structural integrity needs to be further explored. Polγ holoenzyme is a heterotrimer composed of a catalytic unit and 2 accessory subunits. Recent studies have shown that in holoenzyme form, the accessory subunit provides sufficient protection to the catalytic unit against H_2O_2 and N-ethylmaleimide (NEM) mediated damage. Although our *in vivo* study has taken into account the holoenzyme complex of Polγ, further studies are required to analyze the effects of UVB radiation on the accessory subunit. Studies to assess effect of UVB radiation on the catalytic unit in the absence of accessory subunits might also provide some useful information.

Recent studies have revealed that any ROS-mediated mitochondrial dysfunction culminates in the development of various diseases. Mitochondria with "compromised integrity" are a potential source for DAMPs such as mtDNA, cyt c, and other mitochondrial proteins. Formation of inflammasomes is triggered by leakage or intracytoplasmic release of these mitochondrial DAMPs. Activation of autophagy is implicated in scavenging damaged mitochondria, thereby preventing activation of inflammasomes. We have already presented data from our study confirming damage to mtDNA and mitochondrial proteins such as Polγ by UVB radiation in murine skin tissue.

Autophagy is a catabolic pathway involved in the degradation and recycling of cellular components such as proteins and damaged cellular organelles. AKT-mTOR pathway tightly regulates autophagy activation. In this study, activation of autophagy was examined after acute exposure to UVB radiation in both cultured keratinocytes (JB6 cells) and wild-type C57BL/6 mice skin tissue. Our results demonstrate activation of AKT by an increase in AKT (Thr-308) phosphorylation at 1 h after UVB radiation in both *in vitro* and *in vivo* models. A transient but significant increase in AKT phosphorylation at 1 h post-UVB radiation was followed by a decrease to basal level at 24 h post-UVB radiation. Activation of the AKT pathway immediately after acute UVB exposure has been implicated in protection against early transcription independent mitochondrial apoptotic pathway (Claerhout et al 2010, Decraene et al 2004b). Previous studies have shown that mTOR is a downstream target of the AKT signaling pathway. mTOR phosphorylation at ser-2448 residue is due to activation of mTOR via the AKT signaling pathway (Altomare et al 2004). Activation of mTOR by AKT was measured by the increase in the levels of phosphorylated mTOR (ser-2448), which peaks at 1 h post-UVB irradiation and decreases to basal level at 24 h post-UVB irradiation. These results indicate that the activation of mTOR closely followed the activation of AKT since a similar pattern of changes was seen with mTOR phosphorylation. This suggests that mTOR is a downstream target of AKT that is transiently activated in keratinocytes exposed to acute UVB radiation. Previous studies have identified autophagy as a pro-survival mechanism in conditions where AKT-mTOR axis is inhibited (Claerhout et al 2010). Based on the AKT-mTOR phosphorylation, activation of autophagy was measured by assessing the processing

of LC3-I to phospholipid conjugated LC3-II (lipidated form) and change in Beclin-1 levels.

Our study for the first time demonstrates that murine skin tissue exposed to UVB radiation has increased LC3-II and Beclin-1 levels consistent with activation of autophagy. Future studies should be aimed at understanding the mechanism involved in scavenging mitochondria by autophagy. Autophagy is triggered by release of mitochondrial DAMPs. We have already established damage to mtDNA and Polγ by UVB. Now, we need to understand whether and how leakage of mtDNA and Polγ from the mitochondrial matrix into cytoplasm activates signaling events that can eventually result in retrograde signaling by mitochondria.

5   Appendix

The findings presented in the appendix have been published in the journal entitled "Carcinogenesis" 2008. 29(10): 1920-29. This study was designed to test the carcinogenic potential of alumina nanoparticle. Nanoparticles have an increased surface area to volume ratio that increases their reactivity, which differs from bulk materials of the same compositions. Significant contributions have been made in understanding the uptake of nanoparticles by keratinocytes. This was achieved by standardization and analysis of the uptake of alumina nanoparticle by JB6 cells. Further, alumina is considered to be a pro-oxidant similar to UVB and other well-known chemical tumor promoters like TPA that can cause increased oxidative damage to the skin. Assays to measure ROS level in the cells were standardized using DCFH dyes. This helped to determine the cellular oxidative status after alumina nanoparticle exposure. Assays to measure MnSOD activity were standardized to measure the adaptive response mounted by the cells to counteract the increased ROS generated by alumina nanoparticles.

Interaction between SIRT1 and AP-1 reveal a mechanistic insight into the growth promoting properties of Alumina (Al$_2$O$_3$) nanoparticles in mouse skin epithelial cells

5.1 Highlights

The physicochemical properties of nanomaterials differ from those of the bulk material of the same composition. However, little is known about the underlying effects of these particles in carcinogenesis. The purpose of this study was to determine the mechanisms involved in the carcinogenic properties of nanoparticles using aluminum oxide (Al$_2$O$_3$/alumina) nanoparticles as the prototype. Well-established mouse epithelial JB6 cells, sensitive to neoplastic transformation, were used as the experimental model. We demonstrate that alumina was internalized and maintained its physicochemical composition inside the cells. Alumina increased cell proliferation (53%), proliferative cell nuclear antigen (PCNA) levels, cell viability, and growth in soft agar. The level of manganese superoxide dismutase (MnSOD), a key mitochondrial-antioxidant enzyme, was elevated, suggesting a redox signaling event. In addition, the levels of reactive oxygen species (ROS) and the activities of the redox sensitive transcription factor AP-1 and a longevity-related protein, (sirtuin-1) SIRT1, were increased. SIRT1 knock-down reduces DNA synthesis, cell viability, PCNA levels, AP-1 transcriptional activity, and protein levels of its targets, JunD, c-Jun, and Bcl-xL, relative to controls. Immunoprecipitation studies revealed that SIRT1 interacts with the AP-1 components c-Jun and JunD, but not with c-Fos. The results identify SIRT1 as an AP-1 modulator and suggest a novel mechanism by which alumina nanoparticles may function as a potential carcinogen.

5.2 Introduction

The rapidly evolving field of nanotechnology has increased human exposure to engineered nanoparticles (diameter < 100 nm) via inhalation, oral, dermal and injection routes. Despite the wide application of nanoparticles and highly publicized benefits of industrial and medical applications, sufficient knowledge of potential toxicity and human health risk is lacking. The unique physicochemical properties of nanoparticles are attributable to their particle size, distribution, chemical composition, surface area, surface chemistry and surface charge, which differ from bulk materials of the same compositions (Oberdorster et al 2005a, Xia et al 2006). Some of the nanomaterials used are primarily of metals and metal oxides of Al, Fe, Au, Si, Pd, Ce, Zn and Ti. To date, the majority of studies show that inhalation of toxic metals and metal oxides leads to lung cancer and implicate ROS in oxidative stress-related inflammatory functions, cardiovascular injury and lung cytotoxicity (Borm et al 2006, Donaldson and Tran 2002, Donaldson et al 2004, Elder et al 2006, Oberdorster et al 2005b, Warheit et al 2005, Xia et al 2006).

Little is known about the effect of these particles on skin carcinogenesis, particularly the effect of oxides of non-transition metals such as aluminum oxide (Al_2O_3). Aluminum has a very strong oxide film on its surface that generally inhibits corrosion and chemical attack. Aluminum flake is commonly used in metallic paints, cosmetics, and medical devices. Aluminum is known to be toxic (Exley 1998, Yokel and McNamara 2001). The International Agency for Research on Cancer (IARC), the National Toxicology Program (NTP), and others have classified alumina fibers, commonly known as ceramic fibers, as possible human carcinogens (Group 2B) (Siemiatycki et al 2004). Aluminum used in antiperspirants has the potential to cause breast cancer by entering the lymphatic system (Darbre 2006, Exley et al 2007). In addition, epidemiological studies of drinking water and food have implicated aluminum as a potential risk factor in cognitive impairment in the elderly, and in Alzheimer's Disease (Flaten 2001). However, the potential skin carcinogenic effect of aluminum is unknown.

To explore the carcinogenic potential for aluminum oxide nanoparticles, we used mouse epithelial cells JB6 (cl41-5a) as an *in vitro* model of skin carcinogenesis. JB6 cells are sensitive to neoplastic transformation by tumor promoter phorbol esters, such as 12-*O*-tetradecanoylphorbol-13-acetate (TPA) (Colburn et al 1978). In this model, activation of the activator protein-1 (AP-1) is a well-established event associated with tumor promotion (Zhao et al 2002).

SIRT1 (sirtuin-1), a type III nicotinamide adenine dinucleotide (NAD)-dependent histone/protein deacetylase, is of particular interest because of its pleiotropic nature (Blander and Guarente 2004). SIRT1 regulates a variety of stress-response cellular and molecular processes such as survival, neuronal protection, aging, calorie restriction, glucose metabolism, and longevity (Brunet et al 2004, Lim 2006, Luo et al 2001). Interaction between SIRT1 and transcriptional coactivator Peroxisome proliferator-activated receptor-γ coactivator 1α (PGC-1α), a key regulator of metabolism and mitochondrial biogenesis, has been demonstrated (Nemoto et al 2005). In response to oxidative stress, mammalian SIRT1 physiologically interacts with Forkhead transcription factor (FOXO) and increases the transcription of FOXO target genes, including the primary antioxidant enzyme manganese containing superoxide dismutase (MnSOD) (Kops et al 2002), suggesting that SIRT1 may play an important role in cell survival under oxidative stress conditions. Furthermore, in response to an increase in ROS concentration, there is an increase in MnSOD expression level in JB6 cells (Zhao et al 2005b). In this study, we investigated the carcinogenesis potential of alumina and identified a novel mechanism by which alumina may enhance cell proliferation by a SIRT1 mediated event.

5.3 Materials and Methods

5.3.1 Preparation and characterization of alumina nanoparticles

Metal oxide-nanoparticles prepared by gas-phase synthesis are often aggregated into much larger secondary particles. While commercial "nanoparticle" products may have primary particles with the advertised diameters, the aggregates are often much larger than 1 μm, and may not physically pass through biological structures. In addition, metal oxides often have surface charges and tend to coagulate into agglomerates through their interactions with salts, buffers, proteins, and/or themselves. We used the following procedure to produce nanoparticles with known particle size distributions from a commercial nanoparticle sample that formed a relatively stable suspension in polar solvents. Aluminum oxide nanoparticles (alumina) were purchased from Alfa Aesar Ward Hill, MA, 01835, USA (item # 10459, CAS Reg. #1344-28-1, γ-α mixture, 99.98% purity, 10 to 20 nanometer diameter, surface area ~ 100 m^2/g). Transmission electron microscopic images (TEM, Jeol 2010F) (Figure1A) verify that the purchased nanoparticles were aggregated with average diameters in the range of 500 nm on a vol % basis. X-ray diffraction shows that the sample was the gamma phase (not shown). Aggregates were dispersed by ultrasonication. Alumina (2.5 g) was added into 47.5 g (5 wt %) of deionized, ultrafiltered water and sonicated at a power level of 50 W for one hour using a Hielscher UP400s sonicater. The suspension was cooled continuously to prevent water evaporation. The product had 75 vol % particles less than 200 nm and 70 vol % less than 100 nm as determined by light scattering. The particles greater than 100 nm were removed via centrifugation (1500 g for 10 minutes, bowl radius = 6 cm, tube length = 5 cm). The larger particles accumulated at the bottom of the tube, and the top 1 cm of liquid in the tube was siphoned off as the product. The volume-fraction particle size distribution is shown in Figure 1B. Ninety-five vol % of the sample was between 8 to 12 nm in diameter, with the remainder about 65 nm in diameter. The concentration of alumina in the supernatant fraction was 0.6 wt % as confirmed by atomic absorption spectrometry. The material shown in Figure 1B, was relatively stable and did not coagulate much more when allowed to settle overnight. In such preparations, the particle size distribution could be recovered by brief sonication (30 s) at the same power level prior to use.

5.3.2   Uptake of alumina-nanoparticles in mouse skin epithelial cells

Cells were treated with non-sonicated (alumina aggregates ~ 500 nm) and sonicated alumina nanoparticles (diameter < 20 nm). The amount of particle used was based on the surface area of 9.8 cm^2 of the tissue culture dish and the mean particle diameter from each preparation to cover the entire surface area of the dish as monolayer. Alumina-treated cells were washed three times in PBS and scraped, and cell suspension was centrifuged at low speed. The resulting cell pellets were fixed in 4% formalin and examined using a combination of light and electron microscopy. At the light microscopy level, Toluidine blue staining revealed that there were visibly fewer cells containing internalized alumina in cells subjected to non-sonicated (aggregated) alumina (Figure 1C) than in cells exposed to sonicated alumina (Figure 1D). In addition, a large number of mitotic cells were observed in the alumina treated cells (Figure 1D). To validate the composition of alumina-nanoparticles as Al_2O_3, high-resolution transmission electron microscopy and scanning transmission electron microscopy (HRTEM/STEM) were performed on unstained samples. The elemental profile identified in each sample matches that of alumina (Figure 1E).

A

0.2 μm
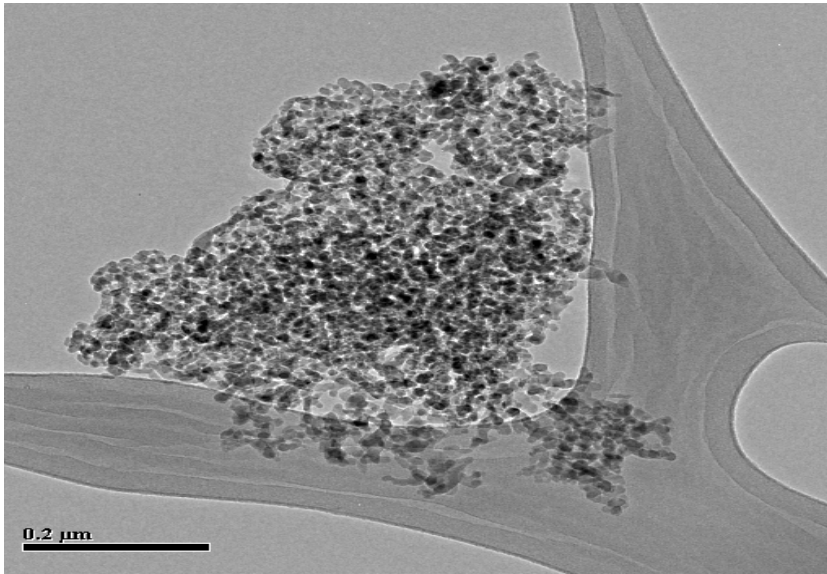
B
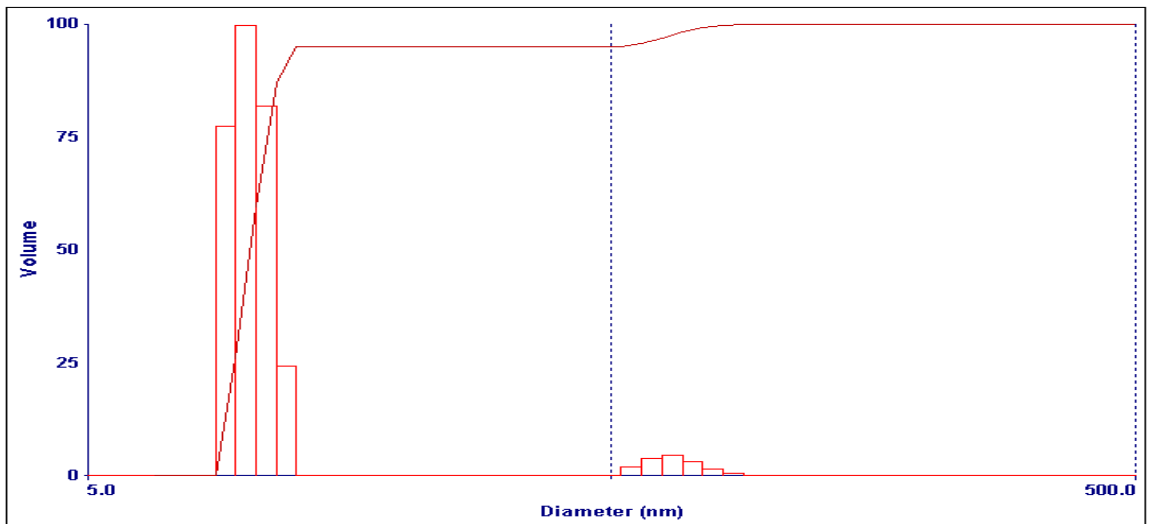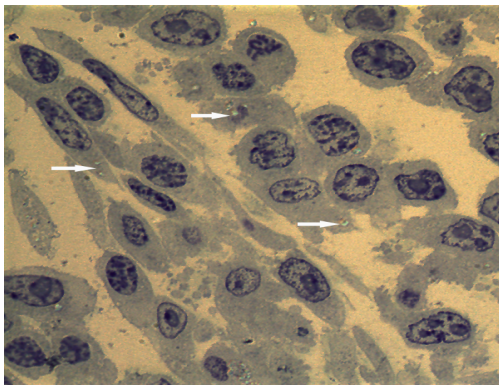
C   **D**
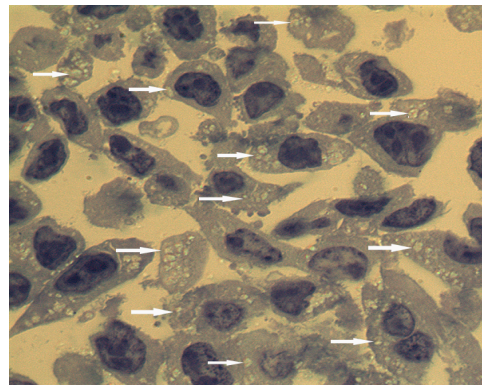
E
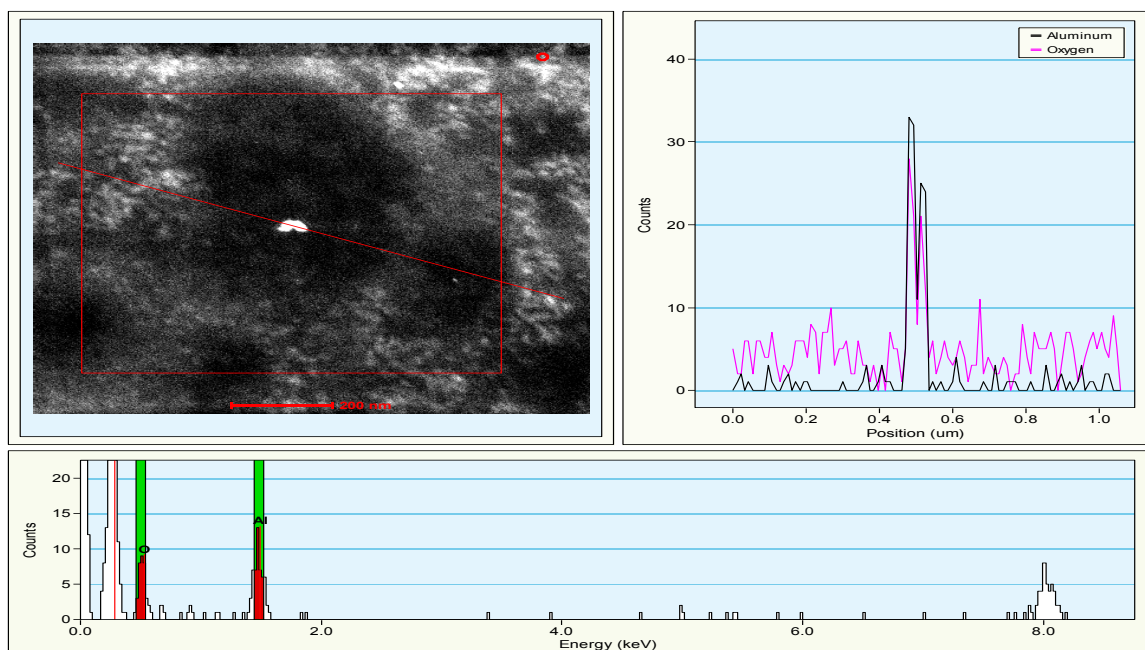
Figure 5.1 Characterization of alumina nanoparticles

A Transmission electron microscopy image of aggregated alumina nanoparticles.

B Light scattering particle size distribution for supernatant of ultrasonicated, centrifuged material.

Detection of intracellular nanoparticles of alumina (Al$_2$O$_3$)

C JB6 cells treated with non-sonicated particles showing uptake of particles in some cells. Arrows point to the refractory inclusions in the affected cells.

D JB6 cells treated with sonicated/dispersed particles. Virtually, all cells contain refractory inclusions, and presence of a large number of mitotic cells is evident. Toluidine blue-stained plastic section, magnification x 1000.

Characterization of alumina nanoparticle (Al$_2$O$_3$) by HRSTEM and scanning transmission electron microscopy

E The image with a red line passing through a bright spot (top/left) indicates the area of X- ray elemental analysis. The elemental profile shown on the top/right panel shows both aluminum and oxygen that are highlighted in the bottom frame.

103

5.3.3 Characterization of cell growth

Cells were cultured at a density of (1×10^4) in triplicate in a 6-well plate. The cells were mixed with Trypan blue stain to mark dead cells and counted daily for 5 days to determine the number of live cells per well. Growth rate was determined by calculating the doubling time from the initial slope of the growth curve before saturation occurred.

5.3.4 Cell viability assay

The effect of alumina on JB6 cell viability/metabolic activity was determined using the colorimetric MTT assay–(3-[4,5-dimethythiazol-2yl]-2,5 diphenyl tetrazolium bromide, Roche Applied Science, Indianapolis, IN). Cells were cultured at a density of (1×10^5) in triplicate in a 48- well plate.

5.3.5 Manganese superoxide dismutase (MnSOD) activity assay

The MnSOD activity was measured using modified NBT (nitro blue tetrazolium) method as described previously (Spitz and Oberley 1989). This assay is based on the competition between superoxide dismutase in the cell homogenate and NBT, an indicator molecule for the $O_2^{-\cdot}$. The xanthine-xanthine oxidase system was used for the generation of constant flux of $O_2^{-\cdot}$. The cells were cultured at a density of $(1 \times 10^6$ cells) in triplicate in P-150 plates. The amount of alumina nanoparticles used to treat the cells was calculated based on the surface area of the P-150 plate and the mean diameter of the alumina nanoparticle. The cells were washed three times in PBS and stored at -80°C overnight. The cell were thawed, scraped and homogenized in 0.25 ml of 50 mM potassium phosphate buffer (pH 7.8, with diethylenetriaminepentaacetic acid) per plate. The homogenate was sonicated on ice with three 15 sec bursts with 400-W microtip sonicater at 70% output. The reduction of NBT to blue formazan by $O_2^{-\cdot}$ with/without cell homogenate was measured spectrophotometrically at 560 nm at 25°C. The rate of NBT reduction in the absence of cell homogenate was used as the reference rate (0.02±0.005 absorbance/min). The data were plotted as percent inhibition of NBT reduction versus protein concentration and fitted with a curve using GraphPad Prism 4 (Enzyme kinetics) software program. One unit of activity was

defined as the amount of protein necessary to reduce the rate of NBT reduction to 50% of maximum inhibition. All the data were expressed in units of SOD activity per milligram of protein.

5.3.6   Detection of ROS

The intracellular ROS production was assayed using 2',7'-dichlorofluorescein diacetate (DCFH) (Molecular Probes, Eugene, OR) as described previously (Smith et al 2007). The cell permeant DCFH dye was cleaved of its acetate moiety by cellular esterase producing 2',7'-dichlorofluorescein (DCF) that fluoresces upon ROS oxidation in the cells. The carboxy-DCFH (C-369) (Molecular Probes, Eugene, OR) dye is a non-oxidizable fluorescent dye that does not change its fluorescence in the presence of ROS in the cells. The cells were cultured at a density of (1×10^4 cells) in triplicate in 48-well plates. After 24 hours the cells were treated with alumina per the working surface area of the cell culture plate and the size of the alumina nanoparticle. The cells were incubated for 24 hours after alumina nanoparticle treatment. After the 24 hour incubation the cells were washed with PBS (pH 7.4) and incubated for 45 min with 0.25ml of PBS containing 10 µM of DCFH or with 1 µM of C-369, which served as a negative control. The cells were washed twice with PBS (pH 7.4) and 0.25 ml of fresh PBS was added. The fluorescence was read at excitation/emission of 488/525 nm with a Spectra Max Gemini plate reader from Molecular Devices. The background fluorescence from wells with cells only (no DCFH/ C-369 dye added) was subtracted from those with DCFH/ C-369 dye added.

5.3.7   Anchorage-independent cell transformation assay in soft agar

Anchorage-independent cell transformation is one of the best *in vitro* indicators of neoplastic growth potential. The cells were treated with TPA as the positive control. Agar plates were prepared which contained a bottom layer of 0.5% agar, overlaid with a layer of 0.33% soft agar inclusive of cells and test compounds. Cultured untreated JB6 cells were trypsinized and diluted in culture media to obtain single cell suspensions. Aliquots of cell suspensions (5000 cells) left untreated, or treated with alumina or TPA - positive control, were mixed with the 0.5% agar media and layered gently over the solidified bottom agar. The top layer was allowed to set for 30 min at

room temperature. Excess culture media was added over the set-soft agar layer and incubated at 37°C in a 5% CO_2-air humidified incubator for 14 days. Colonies comprising more than 50 cells were counted under a dissecting microscope.

5.3.8 Transient transfection and Luciferase assay for detecting AP-1 activity

JB6 cells (2×10^5) were cultured at 70% confluency in culture plates in antibiotic-free culture media (Minimum Essential Medium, Earle's, Invitrogen), supplemented with 4% FBS. A lipofectamine transfection protocol was used as described by the manufacturer (Invitrogen, Carlsbad, CA). Cells were transfected with 2 µg of empty vector alone (pGL3-Luc), or empty vector containing a tandem of four AP-1 consensus binding sites in the promoter (AP-1-pGL3-Luc), and co-transfected with pRL-TK (0.22 µM), which contains the *Renilla* cDNA, driven by the thymidine kinase promoter, as the internal control. The samples were analyzed for luciferase activity using the Dual-Luc Reporter Assay System (Promega, Madison, WI), according to the manufacturer's instructions, in a TD-20/20 luminometer (Turner Designs, Sunnyvale, CA).

5.3.9 SIRT1 activity assay

The lysyl deacetylase activity of SIRT-1 was measured using the *fluor de Lys*-SIRT1 substrate (a peptide comprised of amino acids 379-382 of human p53 [Arg-His-Lys-Lys(Ac)], Biomol, Plymouth Meeting, PA). Briefly, JB6 (cl41-5a) cells were left untreated or treated with alumina for 72 hours. Following treatment, cells were harvested in lysis buffer (described above; see Western blot). Crude cell lysates were frozen/thawed three times and centrifuged at 12,000g for 10 min. The supernatants (cell lysates) were normalized for protein content and incubated in assay buffer supplemented with 50 µM of SIRT1 substrate at 37°C in 96-well plates for 1 hour. The reaction was subsequently quenched with the quenching buffer containing the developer and SIRT1 inhibitor, NAD, for 45 min at room temperature (23°C). The enzyme-catalyzed release of the fluorophore triggered by the NAD^+-dependent deacetylation of the substrate by SIRT1 was quantified by a SpectraMax Gemini Fluorimeter (Molecular Device, Sunnyvale, CA) using 360 nm excitation and 460 nm emission wavelengths. SIRT1 activity was expressed as units per microgram of total

protein. Changes in alumina-induced SIRT1 activity were compared with the control cells (no treatment). Mean values were obtained from three replicates (n = 3). Protein concentrations were determined using the Bradford method (Biorad, Hercules, CA).

5.3.10 Immunoprecipitation

Whole cell lysates from JB6 cells left untreated or treated with alumina were used for immunoprecipitation studies. Cell lysates (200 µg) were mixed with 2 µg of anti-c-Jun polyclonal antibody or anti-JunD polyclonal antibody or anti-c-Fos polyclonal antibody, and incubated overnight at 4°C with continuous mixing. Subsequently, 20 µl of protein A/G agarose beads were added to the reaction mixture of lysate and antibody and incubated overnight at 4°C with continuous mixing. Immunoprecipitates were collected by centrifugation at 2500 rpm for 5 mins at 4°C, followed by washing 4 times with radioimmune precipitation assay (RIPA) buffer (9.1 mM Na_2HPO_4, 1.7 mM NaH_2PO_4, 150 mM NaCl 0.5 %, Sodium deoxycholate, 1 % Nonidet P-40, 0.1 % SDS, 10 µg/ml phenylmethylsulphonyl fluoride [PMSF], and 1 µg/ml aprotinin [Sigma-Aldrich, St. Louis, MO 63178, USA]).   Subsequently, the supernatant was carefully removed and the pellets were resuspended in 1X electrophoresis sample buffer. The samples were boiled for 5 mins and immunoprecipitated proteins were detected by Western blot.

5.3.11 SIRT1 knockdown by siRNA approach

JB6 (cl41-5a) cells were transfected using small interfering RNA (siRNA) to SIRT1 (a cocktail of 5'-AUC UUG CCU GAU UUG UAA TT-3'; 5'- GUA CCA CCA AAU CGU UAC ATT-3'; and 5'-GCA UAG AUC UUC ACC ACA ATT-3', Santa Cruz Biotechnology, Santa Cruz, CA). Cells (2 x 10^{5}) were grown in 6-well culture plates in antibiotic-free culture media (Minimum Essential Medium, Earle's, Invitrogen, Carlsbad, CA), supplemented with 4% FBS at 37°C in a 5% CO_2-air humidified incubator until the cells were 70 - 80% confluent. Cells were transfected using a lipofectamine transfection reagent as directed by the manufacturer (Santa Cruz Biotechnology, Santa Cruz, CA). For each transfection, 0.8 µg of siRNA duplex for SIRT1 and control siRNA were mixed with transfection reagent and medium. The transfection media was removed after 7 hours and replenished with fresh culture

media. After 24 hours, cells were left untreated or treated with alumina. Seventy-two hours after treatment, cells were washed with PBS and lysed in lysis buffer (described above; see Western blot) and centrifuged for 10 mins to pellet cellular debris. The samples were analyzed for SIRT1, JunD, c-Jun, c-Fos, Bcl-xL and Bax protein expressions using Western blot analysis. Mean values were obtained from three replicates (n = 3).

5.3.12 Detection of cell proliferation

Cell proliferation was determined by detecting the incorporation of bromodeoxyuridine (BrdU), a thymidine analog, using anti-BrdU specific antibodies (BD Biosciences, San Jose, CA). To study the function of SIRT1 in proliferation, the cells were transfected with siRNA for SIRT1 and control siRNA (as described above). Twenty-four hours after transfection, the cells were labeled with BrdU solution followed by treatment with alumina, or by no treatment. Seventy-two hours after treatment, cells were fixed with Zamboni's fixative and washed with PBS, permeabilized and incubated with biotin anti-BrdU monoclonal antibody. The slides were visualized using the streptavidin-HRP enzyme complex and the signal was detected by DAB substrate. The number of BrdU positive cells was counted from 10 randomly selected fields and the percentage of proliferating cells was calculated as (number of BrdU cells/number of total cells x 100). Mean values were calculated from three replicates (n = 3).

5.3.13 Data Analysis

Data are represented as mean $\pm$ SEM from replicate samples obtained from at least 3 separate experiments. Overall differences between experimental groups were analyzed using ANOVA (JMP IN statistical software, release version 5.1, SAS Institute Inc., Belmont, CA). When significant differences were found between experimental groups, paired group differences were analyzed *post hoc* using Dunnett's (d) test. An α level of $p < 0.05$ was considered significant for all statistical tests employed.

5.4 Results

5.4.1 Alumina nanoparticle-induced cell proliferation and transformation

As an initial step to determine the effects of alumina on cell proliferation we determined the growth characteristics of cells over time. TPA, a well-established tumor promoter, was used as the positive control. Cells were left untreated, or treated with alumina (diameter < 20 nm) or TPA (10 ng/ml). The amount of particles to be applied was calculated to provide uniform coverage of monolayer cells. Alumina and TPA treated cells showed a 53% and 124% increase in growth, respectively, compared to untreated controls (Figure 2A). Western blot analysis revealed increases in PCNA levels in alumina and TPA treated cells, compared to controls, at 72 hours ($p < 0.001$) and 120 hours ($p < 0.006$), which further validates the increase in cell proliferation (Figures 2B, C). Consistent with these findings, a large number of mitotic cells were observed in the toluidine-stained, alumina-treated JB6 cells (Figure. 1D). Changes in viability and metabolic activity of cells exposed to alumina were measured using the MTT assay. The results indicate a significant increase in cell viability after 72 hours, compared to untreated controls (*$p < 0.001$) (Figure 2D). Alumina also induced anchorage-independent transformation of JB6 cells in soft agar. Single cells were seeded in 33% soft agar with, or without, alumina or TPA (positive control). Transformed colonies in alumina and TPA treated cells were significantly greater in number and larger in diameter compared to controls (alumina: $p < 0.05$; TPA: $p < 0.001$) (Figures. 2E, F).

Figure 1
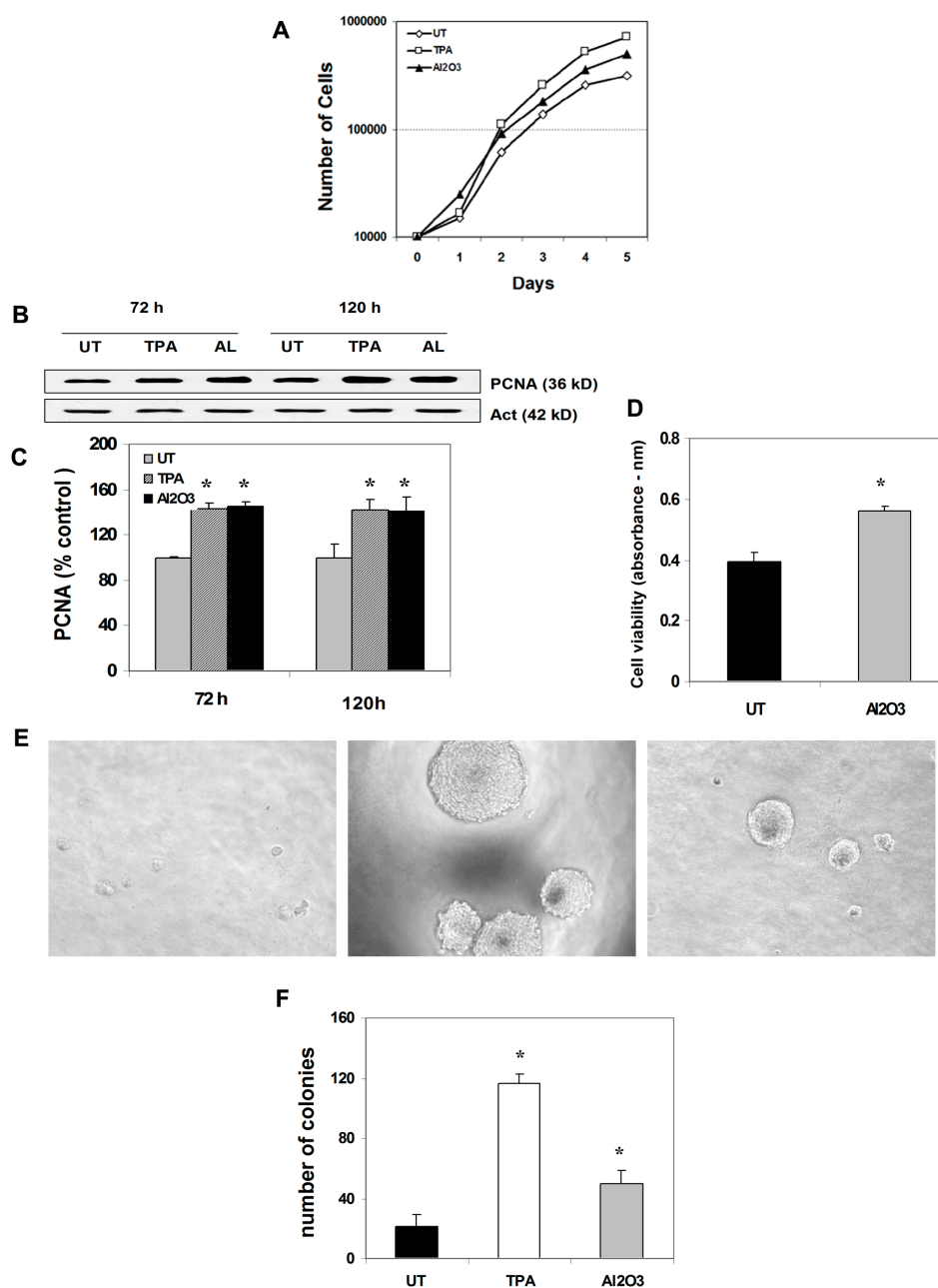
Figure 5.2 Alumina nanoparticle-induced cell proliferation and transformation

(A) Cells were left untreated or treated with alumina nanoparticles (diameter < 20 nm; dose calculated for uniform application over cell surface) or TPA (10 ng/ml; positive control) and a growth curve was established by daily counting of cell numbers. Alumina- and TPA-treated JB6 cells demonstrated increase in growth rate, compared with controls *P<0.006; **P<0.001. **(B)** Western blot analysis indicated significantly

110

increased PCNA levels in alumina- and TPA-treated cells, compared with controls, at 72 h (P<0.001) and 120 h (P<0.006). Mouse anti-actin monoclonal antibody was used as an internal loading control. **(C)** Quantitative analysis of PCNA expression was performed. Results were averaged from three sets of independent experiments. **(D)** Cell viability of JB6 cells exposed to alumina in vitro was determined using the 3-(4,5-dimethythiazol-2yl)-2,5-diphenyl tetrazolium bromide assay, a colorimetric measure of metabolic activity, which serves as an indicator of cell viability. Cells treated with alumina demonstrated an increase in cell viability (*P<0.001; n=6), compared with controls. **(E)** Phase contrast microscopy images of transformed colonies of JB6 cells seeded in soft agar, untreated or treated with nanoparticles of alumina or 10 ng/ml TPA (positive control). The number of transformed colonies was counted after 14 days. The images shown were taken at ×10 magnification. All colonies found in alumina- or TPA-treated cells contain an average of >50 cells, as determined by dissociation of the smallest colony in the alumina-treated cells with trypsin and counting with a hemocytometer. **(F)** Quantitative analysis showed that alumina-treated cells demonstrated a significant increase in transformed colonies compared with controls (alumina: P<0.05; positive control TPA: P<0.001).

5.4.2 Alumina exposure enhances MnSOD expression and activity in mouse epithelial cells

Given that manganese superoxide dismutase (MnSOD) is a well-documented indicator for oxidative stress and a TPA inducible gene, and that alumina nanoparticles have similar effects as TPA in JB6 cells, we probed the effect of alumina on cellular redox status by studying the changes in protein levels of MnSOD. Results indicate a significant increase of MnSOD at 72 h and 120 hours (72 h: $p < 0.04$; 120 h: $p = < 0.03$), compared to controls (Figures 3A, B).

To verify that changes in MnSOD protein result in corresponding changes in MnSOD activity, we measured MnSOD activity using the NBT reduction assay. The results indicate corresponding increases in MnSOD activity in alumina treated cells at 72 hours $p < 0.05$ (Figure 3C).

To further probe whether the increase in MnSOD activity is likely to reduce total cellular ROS levels, we measured intracellular ROS levels using the oxidizable probe DCFH. Alumina treated cells show significantly increased ROS levels ($p < 0.05$) (Figure 3D). The non-oxidizable probe (C-369) did not manifest any differences in fluorescence (Figure 3E).
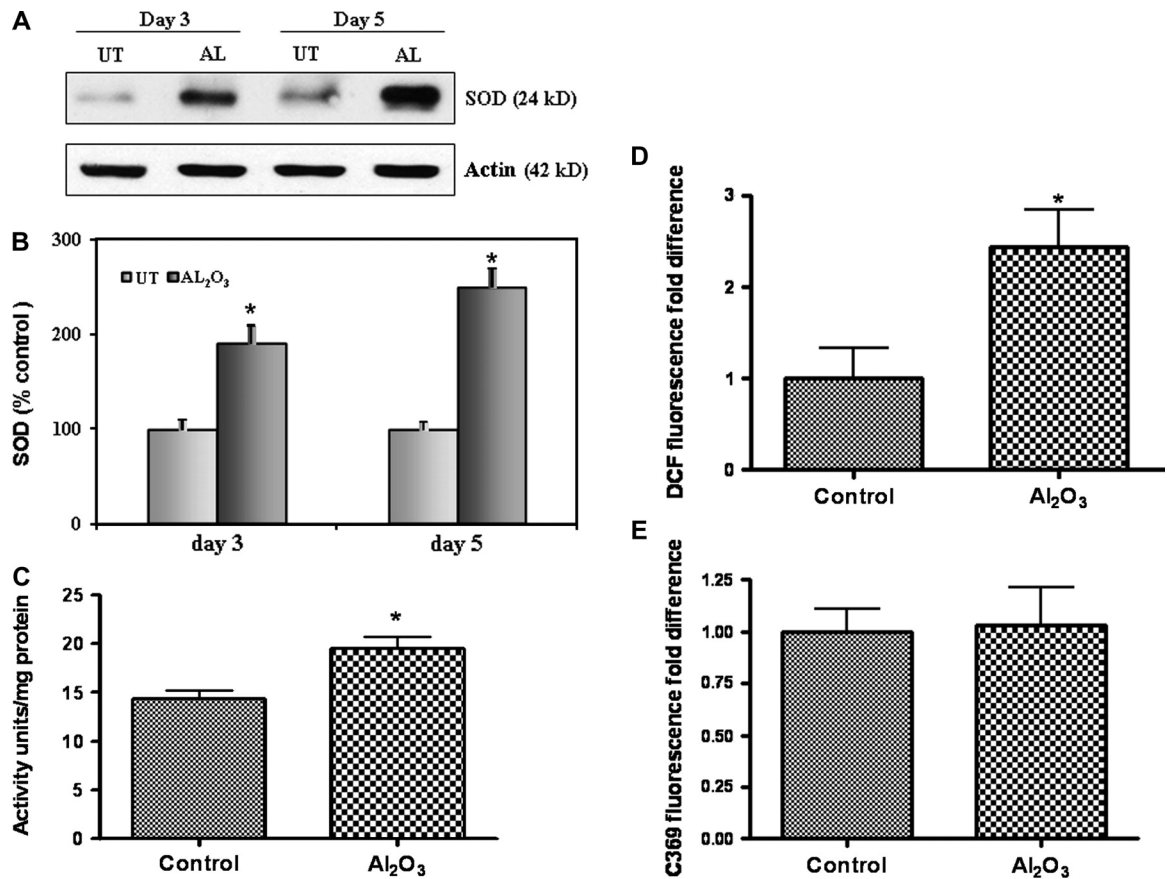
Figure 5.3 Alumina exposure enhances MnSOD and ROS levels in mouse epithelial cells

(A) Cells were left untreated or treated with alumina (diameter < 20 nm). Cell lysates were extracted for western blot analysis to detect MnSOD expression. **(B)**JB6 cells exposed to alumina showed a significant increase in MnSOD levels after 72 h (P<0.04) and 120 h (P<0.038) of treatment, compared with controls. Mouse anti-actin monoclonal antibody was used as an internal loading control. Results were averaged from three sets of independent experiments. **(C)** The MnSOD activity was measured 72 h after treatment. **(D)** Significant increase in MnSOD activity was found in alumina-treated cells (P<0.05). **(E)** The levels of total cellular ROS represented by DCF fluorescence was significantly increased (P<0.05) at 72 h, whereas the fluorescence level of the C-369 was not changed in alumina-treated cells.

5.4.3 Alumina exposure enhances AP-1 transcription activity as well as SIRT1 deacetylation activity

It has been demonstrated that activator protein-1 (AP-1) and its downstream genes induce cell proliferation in skin exposed to tumor promoter TPA (Bowden et al 1995). To determine whether increases in proliferation and transformation of JB6 cells exposed to alumina are associated with activation of AP-1, cells were transfected with the AP-1 promoter construct (API-1pGL3-Luc) or (pGL3-Luc), and transcriptional activity of AP-1 was measured using the luciferase reporter assay. A significant increase in AP-1 transcriptional activity was observed in alumina-treated cells after 24 hours, compared to the corresponding empty vector-transfected cells and untreated controls ($p < 0.001$) (Figure 4A).

Mammalian Silent information regulator 2 homolog, sirtuin (*SIRT1*), has been identified as a longevity gene and an important regulator of cell survival in the presence of stress, such as oxidative stress (Brunet et al 2004, Luo et al 2000, Luo et al 2001). Analysis of SIRT1 protein levels using Western blot showed a significant induction at 72 hours in both TPA and alumina-exposed cells ($p < 0.006$) (Figures. 4B, C). This finding was confirmed by an increase in SIRT1 activity in alumina treated cells ($p < 0.002$) (Figure 4D).

5.4.4 SIRT1 interacts with Jun members of AP-1

The AP-1 complex consists of a variety of dimers of the members of the Jun and Fos family of proteins (Raivich and Behrens 2006). Previous studies have shown that the Jun family of proteins may play a key role in TPA-induced AP-1 activity in skin (Zhao et al 2001). To explore the possibility that SRIT1 may participate in the transcription of AP-1 target genes by interacting with AP-1, we performed immunoprecipitation coupled to Western analysis of SIRT1 and AP-1 components. Immunoprecipitation studies revealed a physical interaction of SIRT1 with the AP-1 components, c-Jun and JunD, but not c-Fos, in alumina-exposed cells (Figures. 4E-G).
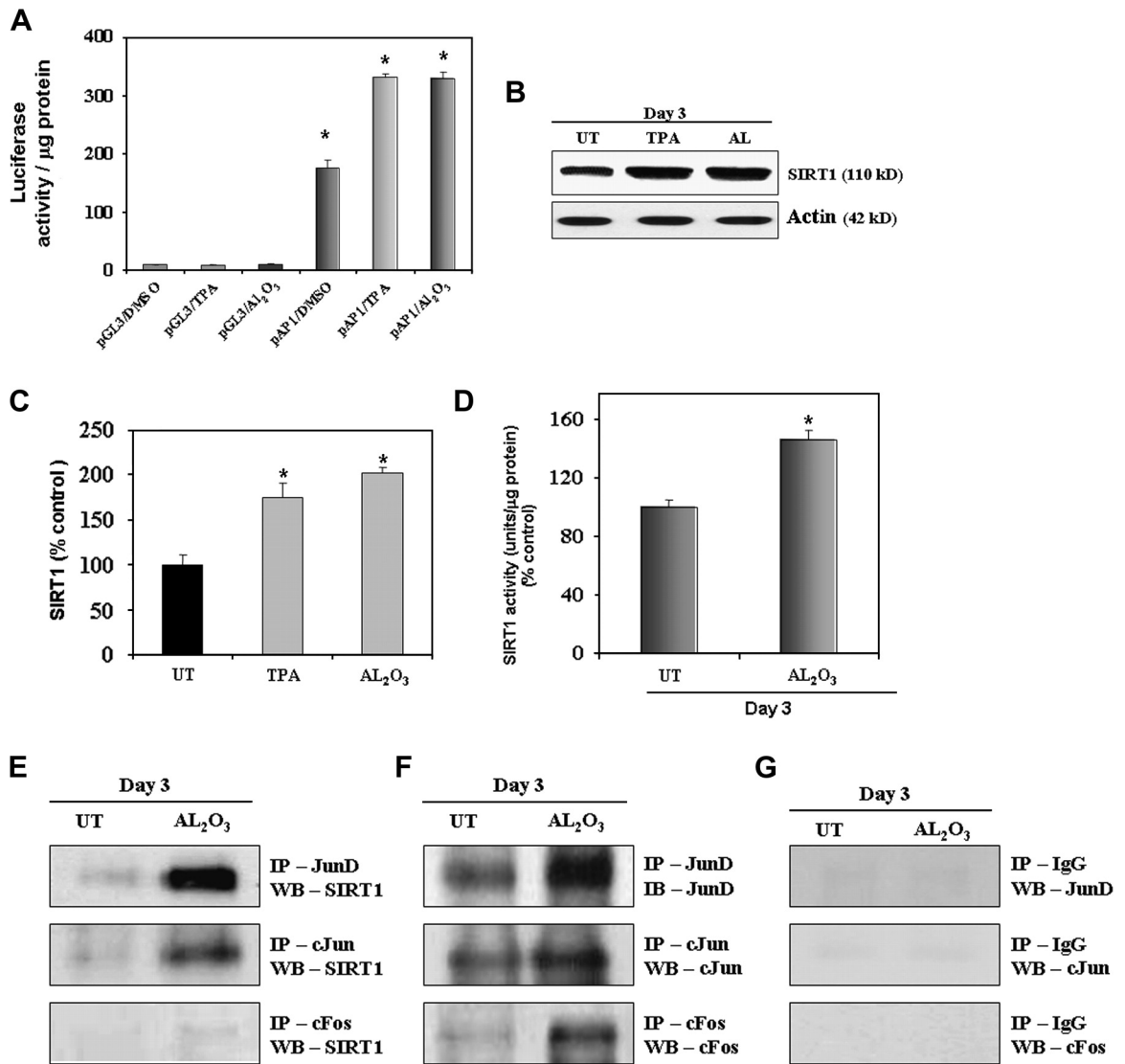
Figure 5.4 Alumina exposure enhances AP-1 transcription activity and SIRT1 deacetylation activity

(A) JB6 (cl41-5a) cells were transfected with the empty vector alone (pGL3-Luc) or empty vector containing the AP-1 promoter-driven luciferase reporter vector. Thirty-six hours after transfection, cells were divided into sets, three dishes per group, for treatment with or without alumina nanoparticles. Twenty-four hours after treatment, cells were collected for luciferase activity as a measure of AP-1 transcription activity. A significant increase in AP-1 transcriptional activity was observed in alumina-treated JB6 cells, compared with the corresponding empty vector-transfected cells and controls [pAP1/dimethyl sulfoxide (DMSO)] ($P<0.001$). **(B and C)** Western blot analysis revealed an increase in the SIRT1 protein level in alumina- and TPA-treated cells ($P<0.006$). **(D)** Increase in protein levels in alumina-exposed JB6 cells was confirmed by SIRT1 enzyme activity assay ($P<0.002$). **(E and F)** Interaction of SIRT1

and AP1 components: immunoprecipitation studies revealed physical interaction of SIRT1 with the AP-1 components, c-Jun and JunD, but not with c-Fos, in alumina-treated cells. **(G)** Immunoprecipitation with IgG was used as controls.

5.4.5 SIRT1 is essential for cell proliferation in alumina-exposed mouse epithelial cells

We used the siRNA approach to verify the role of SIRT1 in alumina-induced cell proliferation.   Cells were transfected with control siRNA and SIRT1 siRNA and 24 hours later were exposed to alumina for 72 hours. Suppression of SIRT1 reduced alumina-induced SIRT1 expression in treated cells ($^\wedge$p < 0.0001), as well as in controls ($^\wedge$p < 0.007) (Figures. 5A, B). The role of SIRT1 in cell proliferation was determined by detecting cells in S-phase using BrdU staining. Alumina exposure showed an increase in the S-phase population of cells (*p < 0.0002), which was attenuated in cells transfected with SIRT1 siRNA ($^\wedge$p < 0.0004; controls: $^\wedge$p < 0.0004) (Figures. 5C, D). The role of SIRT1 in cell proliferation was further confirmed by the increase in alumina-induced PCNA levels (*p < 0.003; [#]p < 0.02), which was reduced in the alumina-exposed SIRT1 siRNA transfected cells ($^\wedge$p < 0.001) (Figures 5E, F). Suppression of SIRT1 also reduced cell viability measured by MTT assay (*p < 0.005, [#]p < 0.02, alumina: $^\wedge$p < 0.0001; controls: $^\wedge$p < 0.0006) (Figures 5G).
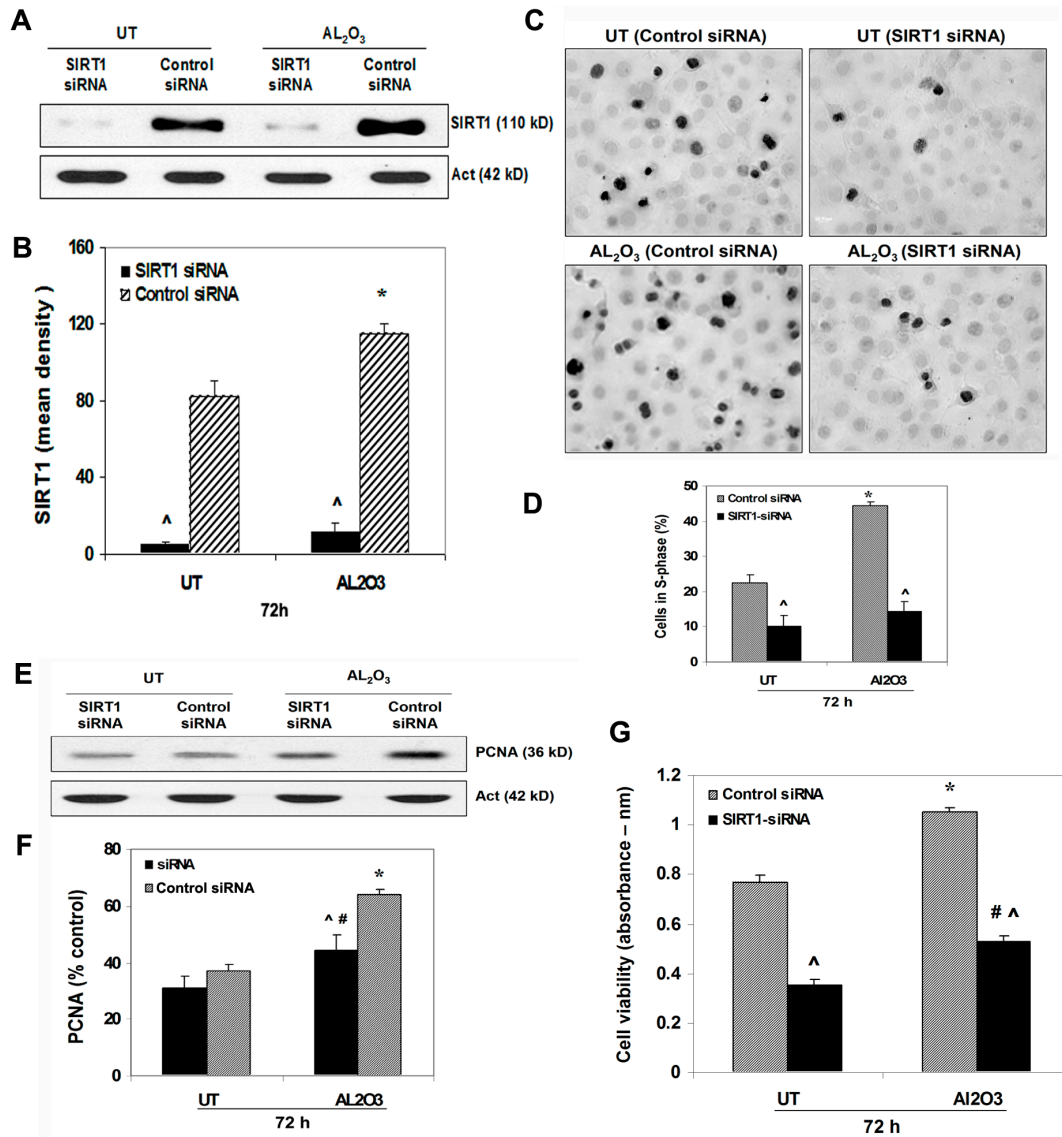
Figure 5.5 SIRT1 is essential for increased cell proliferation in alumina-exposed mouse epithelial cells

(A and B) JB6 (cl41-5a) cells were transfected with siRNA for SIRT1 and control siRNA. SIRT1 siRNA significantly suppressed basal levels and alumina-induced SIRT1 expression (*P<0.02; alumina: ^P<0.0001; controls: ^P<0.007). **(C and D)** S-phase population of cells was detected by the incorporation of BrdU, which was recognized by anti-BrdU-specific antibodies. Increase in S-phase population in alumina-treated cells (*P<0.0002) was attenuated by SIRT1 siRNA transfection (^P<0.0004; controls: ^P<0.0004). **(E and F)** Western blot analysis revealed increase in alumina-induced PCNA levels (*P<0.003; #P<0.02), which was attenuated in alumina-exposed SIRT1 knockdown cells (^P<0.001). **(G)** Cell viability was assessed

118

using 3-(4,5-dimethythiazol-2yl)-2,5-diphenyl tetrazolium bromide assay. Suppression of SIRT1 reduced cell viability in controls and alumina-treated cells (*P<0.005, #P<0.02, alumina: ^P<0.0001; controls: ^P<0.0006). *Increase in protein levels, S-phase cells and viability in cells treated with alumina and transfected with control siRNA in comparison with untreated cells. Reduction in protein levels, S-phase cells and viability in SIRT1 knockdown untreated and treated JB6 cells, compared with respective control siRNA transfected cells. #Increase in PCNA levels in alumina-exposed JB6 cells transfected with siRNA for SIRT1.

5.4.6 SIRT1 is essential for the activation of AP-1 and its target gene, Bcl-xL, in alumina-exposed mouse epithelial cells

To verify the role of SIRT1 in the activation of AP-1 and its components, JB6 cells were co-transfected with the AP-1 promoter construct (API-1pGL3-Luc) or (pGL3-Luc), and siRNA for SIRT1, or control siRNA. Transcriptional activity of AP-1 was measured using the luciferase reporter assay 72 hours after transfection. Suppression of SIRT1 reduced alumina-induced and basal levels of AP-1 transcriptional activity (alumina: *p < 0.02; ^p < 0.001, controls: ^p < 0.001) (Figures 6A). SIRT1 knock-down also reduced alumina-induced protein expression of AP-1 component, JunD (*p < 0.002; ^p < 0.0001) (Figures 6B, C), and c-Jun (*p < 0.0002; ^p < 0.001) (Figures 6B, D) but not the level of the non-AP-1 target gene, c-Fos (Figures 6B, E). Further, alumina increased pro-survival AP-1 target gene Bcl-xL, but the reverse occurred in SIRT1 knock-down cells (Figures 6F, G).
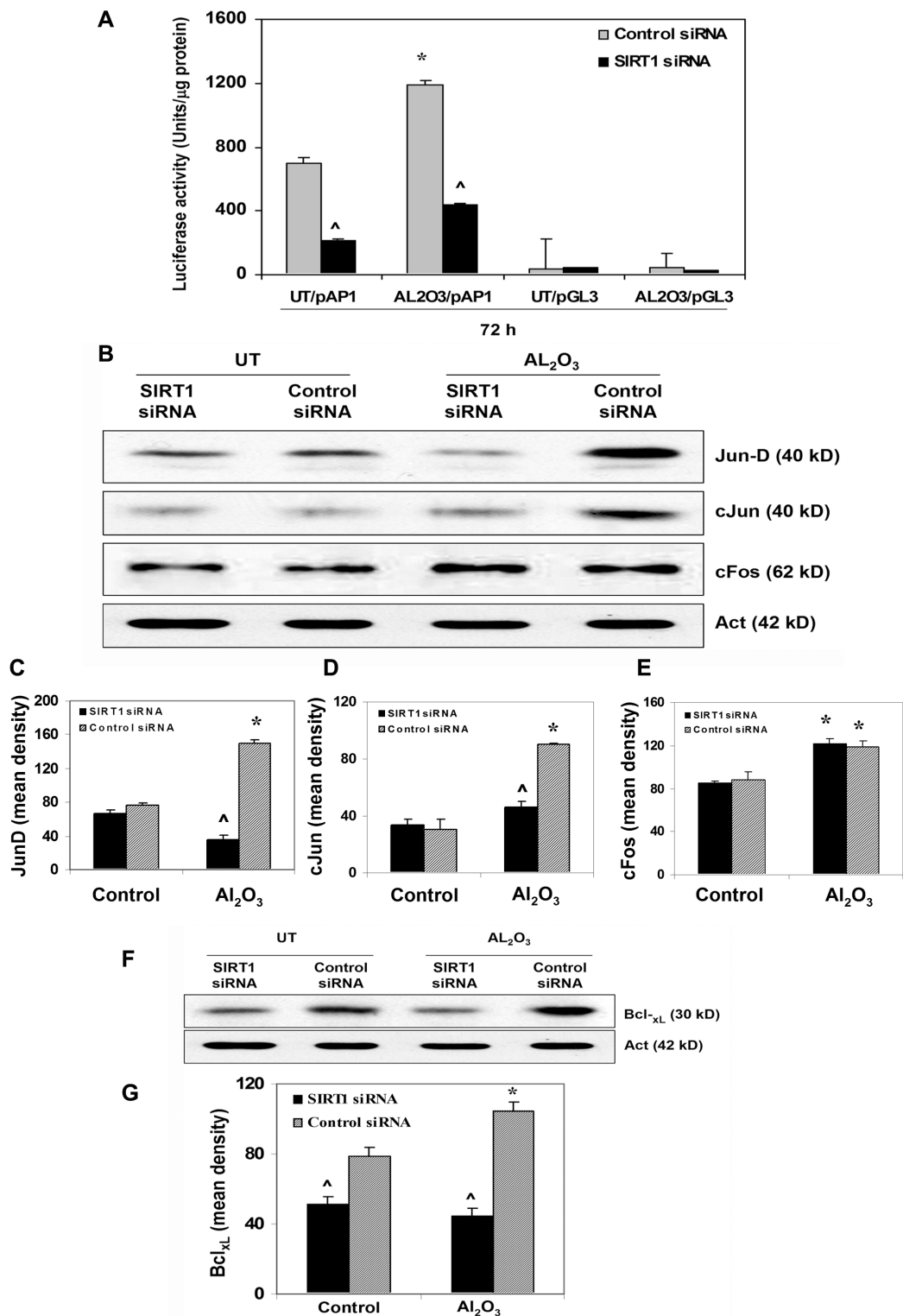
Figure 5.6 SIRT1 is essential for the activity of AP-1 and the expression of AP-1 target genes in alumina-exposed mouse epithelial cells

(A) JB6 (cl41-5a) cells were cotransfected with either the AP-1-driven luciferase reporter construct (AP-1pGL3-Luc) or empty vector (pGL3-Luc), along with siRNA for SIRT1 or control siRNA. After 24 h of cotransfection, cells were left untreated or

121

treated with alumina for 72 h. Cells were collected for luciferase activity as a measure of AP-1 transcriptional activity. AP-1 transcriptional activity was reduced in controls and alumina-exposed SIRT1 knockdown cells (alumina: *P<0.02; ^P<0.001, controls: ^P<0.001). **(B, C, D, and E)** Protein levels of AP-1 components JunD and c-Jun were attenuated in SIRT1 knockdown cells (JunD-alumina: *P<0.002; ^P<0.0001) (B and C), (c-Jun-alumina: *P<0.0002; ^P<0.001). SIRT1 suppression did not alter the alumina-induced expression levels of c-Fos (*P<0.05). **(F and G)** Prosurvival AP-1 target gene BclxL increased in alumina-exposed JB6 cells, which was reversed in SIRT1 knockdown cells (BclxL: *P<0.03; alumina: ^P<0.001, control: alumina: ^P<0.002, control: ^P<0.025). *Increase in AP-1 activity and other protein levels in cells treated with alumina and transfected with control siRNA, compared with untreated controls. Reduction in AP-1 transcriptional activity and protein expression in SIRT1 knockdown untreated and treated JB6 cells compared with respective control siRNA-treated cells.

5.5　Discussion

Ultra-microscopic nanoparticles are used to facilitate novel state-of-the-art therapeutic regimens and targeted drug delivery systems in an attempt to improve treatment efficacy (McNeil 2005). They are also used in cosmetics and other consumer products (Darbre 2005, Darbre 2006). However, the increased surface to volume ratio of the miniscule nanoparticles increases reactivity and may result in intrinsic toxicity. Despite the wide application of nanoparticles, knowledge of their adverse effects, especially on carcinogenesis, is lacking. One of the most common entry routes for nanoparticles is inhalation, and early reports indicate that workers involved in aluminum production may be at increased risk of developing lung cancer (Andersen et al 1982). *In vivo* studies have demonstrated lung inflammation due to exposure to nanoparticles (Dailey et al 2006). Systemic distribution of nanoparticles has been reported into the blood stream and lymphatic pathways (Medina et al 2007). Because aluminum distributes evenly in plasma and blood cells, aluminum concentrations in plasma and whole blood have similar value in assessing toxicity (van der Voet and de Wolff 1985). Aluminum is excreted predominantly via the kidneys and therefore accumulates in patients with renal failure (Alfrey et al 1980). Long-term exposure could lead to accumulation of aluminum, even in workers having normal renal function.

Another important route for nanoparticle entry is the skin, from accidental exposure and use of cosmetics and other topical applications. Although the outer layer of the epidermis, the stratum corneum, protects against environmental insults, TiO_2 has been shown to penetrate the stratum corneum and even hair follicles (Lademann et al 1999). Penetration of nanosized titanium dioxide (5-20 nm) into the skin and interaction with the immune system has been demonstrated (Kreilgaard 2002). Studies have also demonstrated that, in conjunction with motion, nanoparticles penetrate into the stratum corneum of human skin reaching to the epidermis and dermis (Tinkle et al 2003).

Recently, aluminum has been found to be a potential pro-oxidant in sunscreens and sunblocks (Nicholson and Exley 2007). Several studies report permeability and accumulation of aluminum salts in anti-perspirants with dispersion to systemic sites (Flarend et al 2001). In addition, aluminum has been categorized as a metalloestrogen

that can interfere with estrogen receptors and that has a potential role in breast cancer (Darbre 2005). Further, aluminum could function as a pro-oxidant increasing oxidative damage to the skin (Exley 2004). However, whether and how nanoparticles of alumina exert a carcinogenic effect on skin epithelial cells are unknown.

Our results show that alumina is internalized and significantly increases MnSOD protein levels, indicating that the effect of alumina may occur, in part, via alteration of cellular redox status. Our results also indicate that nanoparticle exposure can cause increased proliferation and anchorage-independent transformation in JB6 cells. Proliferating cell nuclear antigen (PCNA) is a well-established indicator of cell proliferation, actively involved in DNA replication and repair (Paunesku et al 2001). The increase in PCNA levels further validates the role of alumina in cell proliferation. Our results also demonstrate that treatment with alumina enhances MnSOD protein and activity as well as the levels of total cellular ROS. These results suggest that the observed increase in MnSOD levels is an adaptive response to alumina-induced oxidative stress. The finding that the total cellular ROS is also increased in the presence of higher MnSOD activity is consistent with this possibility. Further support for this possibility includes the finding that alumina activates AP-1, a redox sensitive transcription factor. The major components of AP-1 are the "Jun" (c-Jun, JunB, and JunD) and "Fos" (c-Fos, FosB, Fos related antigen-1 [Fra-1], and [Fra-2)]) family of proteins (Wisdom 1999). They are characterized by the Leucine zipper regions that allow the different components to form homodimers or heterodimers and bind to specific DNA binding elements called 12-O-tetradecanoylphorbol-13-acetate response elements (TRE) (Angel et al 1987). Unlike the Jun family of proteins, Fos proteins cannot form homodimers. They form heterodimers with the Jun family of proteins (Mason et al 2006). Activation of AP-1 is essential for the neoplastic transformation of mouse epithelial JB6 cells (Bernstein and Colburn 1989). Inhibition of c-Jun or AP-1 represses transactivation of AP-1 and transformation of JB6 cells (Dong et al 1994). Thus, AP-1 transcriptional activity instigated by alumina may result from redox-mediated events that lead to cell proliferation and neoplastic transformation.

Mammalian silent information regulator 2 homolog (SIRT1) has been recently identified as a pro-survival factor against stress-induced DNA damage (Imai et al 2000, Luo et al 2001). SIRT1 promotes cell survival by negatively regulating the

124

tumor suppressor protein p53 (Langley et al 2002, Lim 2006, Luo et al 2001, Vaziri et al 2001). Previous studies have shown that the deacetylase activity of SIRT1 is responsible for gene silencing, DNA recombination, increase in survival and longevity in response to oxidative stress and other stress factors (Bordone and Guarente 2005, Brunet et al 2004, Cohen et al 2004, Langley et al 2002, Luo et al 2001, Smith 2002, Vaziri et al 2001). Our studies indicate that alumina exposure to mouse epithelial cells increases SIRT1 protein and activity levels. Interestingly, we also observed interaction of SIRT1 with the AP-1 components c-Jun and JunD in alumina-exposed cells. This is the first study to demonstrate SIRT1 as a component of AP1-mediated transcription. Our results also show that SIRT1 is an essential modulator of AP-1 mediating cell proliferation and neoplastic transformation, as the use of siRNA to block SIRT1 attenuates AP-1 transcriptional activity, protein levels of c-Jun, JunD, and Bcl-xL, as well as PCNA levels, cells in S-phase, and cell viability.

The Bcl-2 family of proteins consists of both anti-apoptotic and pro-apoptotic members and the ratio of these proteins often determines the life/death fate of cells (Tsujimoto 1998, Tsujimoto and Shimizu 2000). The *Bcl-2* gene was originally identified as an oncogene involved in human follicular B cell lymphoma (Tsujimoto et al 1985). Bcl-2 and Bcl-xL prevent apoptosis by sequestering death-inducing pro-caspases and/or preventing release of cytochrome c and apoptosis inducing factor (AIF) into the cytoplasm (Tsujimoto 1998). In contrast, pro-apoptotic Bax and Bak trigger the release of cytochrome c that initiates the caspase signaling cascade (Grutter 2000, Jiang and Wang 2004, Tsujimoto 1998). The Bcl-xL protein is localized within the mitochondrial membrane (Gonzalez-Garcia et al 1994) and inhibits apoptosis (Boise et al 1993). An AP-1 consensus sequence was found at -267 of the promoter region of the mouse *Bcl-xL* gene (Grillot et al 1997). Our findings that alumina increases the pro-survival AP-1 target gene *Bcl-xL* and that suppression of SIRT1 reverses Bcl-xL levels further support the possibilities that AP-1 activation is a mechanism by which nanoparticles of alumina can cause transformation.

The mechanisms by which SIRT1 participates in the carcinogenesis process are unknown. Although the precise mechanism by which SIRT1 modulates AP1 activity is unclear, our study indicates that SIRT1 may contribute to the carcinogenesis potential of alumina, at least in part, by interacting with AP-1 and modulating the

expression of AP-1 target genes. These results reveal a novel mechanism involving the positive role of SIRT1 on transcription leading to enhanced proliferation in alumina-treated cells. Further study in an animal model will be needed to establish this novel observation. Our initial observations in a cellular model suggest that alteration of cellular longevity and metabolic regulator should be considered in tandem with the evolving new opportunities using engineered nanoparticles to ensure the safety of nanomaterials.

References

Achanta G, Sasaki R, Feng L, Carew JS, Lu W, Pelicano H *et al* (2005). Novel role of p53 in maintaining mitochondrial genetic stability through interaction with DNA Pol γ. *EMBO J* **24:** 3482-3492.

Aitken GR, Henderson JR, Chang SC, McNeil CJ, Birch-Machin MA (2007). Direct monitoring of UV-induced free radical generation in HaCaT keratinocytes. *Clin Exp Dermatol* **32:** 722-727.

Alfrey AC, Hegg A, Craswell P (1980). Metabolism and toxicity of aluminum in renal failure. *Am J Clin Nutr* **33:** 1509-1516.

Allen JA, Coombs MM (1980). Covalent binding of polycyclic aromatic compounds to mitochondrial and nuclear DNA. *Nature* **287:** 244-245.

Altomare DA, Wang HQ, Skele KL, De Rienzo A, Klein-Szanto AJ, Godwin AK *et al* (2004). AKT and mTOR phosphorylation is frequently detected in ovarian cancer and can be targeted to disrupt ovarian tumor cell growth. *Oncogene* **23:** 5853-5857.

Alvarez B, Radi R (2003). Peroxynitrite reactivity with amino acids and proteins. *Amino Acids* **25:** 295-311.

Alvarez MN, Piacenza L, Irigoin F, Peluffo G, Radi R (2004). Macrophage-derived peroxynitrite diffusion and toxicity to Trypanosoma cruzi. *Arch Biochem Biophys* **432:** 222-232.

Ambrosone CB, Freudenheim JL, Thompson PA, Bowman E, Vena JE, Marshall JR *et al* (1999). Manganese superoxide dismutase (MnSOD) genetic polymorphisms, dietary antioxidants, and risk of breast cancer. *Cancer Res* **59:** 602-606.

Anantharaman M, Tangpong J, Keller JN, Murphy MP, Markesbery WR, Kiningham KK *et al* (2006). Beta-amyloid mediated nitration of manganese superoxide dismutase: implication for oxidative stress in a APPNLH/NLH X PS-1P264L/P264L double knock-in mouse model of Alzheimer's disease. *Am J Pathol* **168:** 1608-1618.

Andersen A, Dahlberg BE, Magnus K, Wannag A (1982). Risk of cancer in the Norwegian aluminium industry. *Int J Cancer* **29:** 295-298.

Anderson RR, Parrish JA (1981). The optics of human skin. *J Invest Dermatol* **77:** 13-19.

Angel P, Imagawa M, Chiu R, Stein B, Imbra RJ, Rahmsdorf HJ *et al* (1987). Phorbol ester-inducible genes contain a common cis element recognized by a TPA-modulated trans-acting factor. *Cell* **49:** 729-739.

Appella E, Anderson CW (2001). Post-translational modifications and activation of p53 by genotoxic stresses. *Eur J Biochem/ FEBS* **268:** 2764-2772.

Attardi LD, Reczek EE, Cosmas C, Demicco EG, McCurrach ME, Lowe SW *et al* (2000). PERP, an apoptosis-associated target of p53, is a novel member of the PMP-22/gas3 family. *Genes Dev* **14:** 704-718.

Baba T, Hanada K, Hashimoto I (1996). The study of ultraviolet B-induced apoptosis in cultured mouse keratinocytes and in mouse skin. *J Dermatol Sci* **12:** 18-23.

Backer JM, Weinstein IB (1980). Mitochondrial DNA is a major cellular target for a dihydrodiol-epoxide derivative of benzo[a]pyrene. *Science* **209:** 297-299.

Bag A, Bag N (2008). Target sequence polymorphism of human manganese superoxide dismutase gene and its association with cancer risk: a review. *Cancer epidemiology, biomarkers & prevention : a publication of the American Association for Cancer Research, cosponsored by the American Society of Preventive Oncology* **17:** 3298-3305.

Bakhanashvili M, Grinberg S, Bonda E, Simon AJ, Moshitch-Moshkovitz S, Rahav G (2008). p53 in mitochondria enhances the accuracy of DNA synthesis. *Cell Death Differ* **15:** 1865-1874.

Batch JA, Mercuri FA, Edmondson SR, Werther GA (1994). Localization of messenger ribonucleic acid for insulin-like growth factor-binding proteins in human skin by in situ hybridization. *The Journal of clinical endocrinology and metabolism* **79:** 1444-1449.

Batinic-Haberle I, Spasojevic I, Hambright P, Benov L, Crumbliss AL, Fridovich I (1999). Relationship among Redox Potentials, Proton Dissociation Constants of Pyrrolic Nitrogens, and in Vivo and in Vitro Superoxide Dismutating Activities of Manganese(III) and Iron(III) Water-Soluble Porphyrins. *Inorg Chem* **38:** 4011-4022.

Batinic-Haberle I, Reboucas JS, Spasojevic I (2010). Superoxide dismutase mimics: chemistry, pharmacology, and therapeutic potential. *Antioxid Redox Signal* **13:** 877-918.

Batinic-Haberle I, Rajic Z, Tovmasyan A, Reboucas JS, Ye X, Leong KW *et al* (2011). Diverse functions of cationic Mn(III) N-substituted pyridylporphyrins, recognized as SOD mimics. *Free Radic Biol Med* **51:** 1035-1053.

Batinic-Haberle IR, J. S. Benov, L. Spasojevic, I (2010). Catalysis and Bio-Inspired Systems– Part 2. *In Handbook of Porphyrin Science*. World Scientific: Singapore. pp 291-393.

Batthyany C, Souza JM, Duran R, Cassina A, Cervenansky C, Radi R (2005). Time course and site(s) of cytochrome c tyrosine nitration by peroxynitrite. *Biochemistry* **44:** 8038-8046.

Bellacosa A, Kumar CC, Di Cristofano A, Testa JR (2005). Activation of AKT kinases in cancer: implications for therapeutic targeting. *Adv Cancer Res* **94:** 29-86.

Bensaad K, Tsuruta A, Selak MA, Vidal MN, Nakano K, Bartrons R *et al* (2006). TIGAR, a p53-inducible regulator of glycolysis and apoptosis. *Cell* **126:** 107-120.

Berg RJ, van Kranen HJ, Rebel HG, de Vries A, van Vloten WA, Van Kreijl CF *et al* (1996). Early p53 alterations in mouse skin carcinogenesis by UVB radiation: immunohistochemical detection of mutant p53 protein in clusters of preneoplastic epidermal cells. *Proc Natl Acad Sci U S A* **93:** 274-278.

Bernstein LR, Colburn NH (1989). AP1/jun function is differentially induced in promotion-sensitive and resistant JB6 cells. *Science* **244:** 566-569.

Bickers DR, Athar M (2006). Oxidative Stress in the Pathogenesis of Skin Disease. *J Invest Dermatol* **126:** 2565-2575.

Bienstock RJ, Copeland WC (2004). Molecular insights into NRTI inhibition and mitochondrial toxicity revealed from a structural model of the human mitochondrial DNA polymerase. *Mitochondrion* **4:** 203-213.

Birch-machin MA, Tindall M, Turner R, Haldane F, Rees JL (1998). Mitochondrial DNA Deletions in Human Skin Reflect Photo- Rather Than Chronologic Aging. *J Invest Dermatol* **110:** 149-152.

Blander G, Guarente L (2004). The Sir2 family of protein deacetylases. *Annu Rev Biochem* **73:** 417-435.

Bode AM, Dong Z (2003). Mitogen-activated protein kinase activation in UV-induced signal transduction. *Science's STKE : signal transduction knowledge environment* **2003:** RE2.

Bogenhagen DF, Pinz KG, Perez-Jannotti RM (2001). Enzymology of mitochondrial base excision repair. *Prog Nucleic Acid Res Mol Biol*. pp 257-271.

Boise LH, Gonzalez-Garcia M, Postema CE, Ding L, Lindsten T, Turka LA *et al* (1993). bcl-x, a bcl-2-related gene that functions as a dominant regulator of apoptotic cell death. *Cell* **74:** 597-608.

Bolden A, Noy GP, Weissbach A (1977). DNA polymerase of mitochondria is a gamma-polymerase. *J Biol Chem* **252:** 3351-3356.

Bonifacino JS, Dell'Angelica EC, Springer TA (2001). Immunoprecipitation. *Curr Protoc Mol Biol* **Chapter 10:** Unit 10 16.

Bordone L, Guarente L (2005). Calorie restriction, SIRT1 and metabolism: understanding longevity. *Nat Rev Mol Cell Biol* **6:** 298-305.

Borgstahl GE, Parge HE, Hickey MJ, Johnson MJ, Boissinot M, Hallewell RA *et al* (1996). Human mitochondrial manganese superoxide dismutase polymorphic variant Ile58Thr reduces activity by destabilizing the tetrameric interface. *Biochemistry* **35:** 4287-4297.

Borm PJ, Robbins D, Haubold S, Kuhlbusch T, Fissan H, Donaldson K *et al* (2006). The potential risks of nanomaterials: a review carried out for ECETOC. *Part Fibre Toxicol* **3:** 11.

Bourdon A, Minai L, Serre V, Jais JP, Sarzi E, Aubert S *et al* (2007). Mutation of RRM2B, encoding p53-controlled ribonucleotide reductase (p53R2), causes severe mitochondrial DNA depletion. *Nat Genet* **39:** 776-780.

Boveris A, Chance B (1973). The mitochondrial generation of hydrogen peroxide. General properties and effect of hyperbaric oxygen. *Biochem J* **134:** 707-716.

Bowden G, Finch J, Domann F, Krieg P (1995). Molecular mechanisms involved in skin tumor initiation, promotion and progression. Mukhtar (ed) skin cancer: mechanisms and human relevance, Boca Raton, Fl: CRC Press, Inc.**:** 99-111.

Bowden GT (2004). Prevention of non-melanoma skin cancer by targeting ultraviolet-B-light signalling. *Nature reviews Cancer* **4:** 23-35.

Brash DE, Rudolph JA, Simon JA, Lin A, McKenna GJ, Baden HP *et al* (1991). A role for sunlight in skin cancer: UV-induced p53 mutations in squamous cell carcinoma. *Proc Natl Acad Sci U S A* **88:** 10124-10128.

Brech A, Ahlquist T, Lothe RA, Stenmark H (2009). Autophagy in tumour suppression and promotion. *Mol Oncolo* **3:** 366-375.

Briganti S, Picardo M (2003). Antioxidant activity, lipid peroxidation and skin diseases. What's new. *J Eur Acad Dermatol Venereol* **17:** 663-669.

Brown WM, George M, Wilson AC (1979). Rapid Evolution of Animal Mitochondrial DNA. *Proc Natl Acad Sci U S A* **76:** 1967-1971.

Brunet A, Sweeney LB, Sturgill JF, Chua KF, Greer PL, Lin Y *et al* (2004). Stress-dependent regulation of FOXO transcription factors by the SIRT1 deacetylase. *Science* **303:** 2011-2015.

Buckbinder L, Talbott R, Velasco-Miguel S, Takenaka I, Faha B, Seizinger BR *et al* (1995). Induction of the growth inhibitor IGF-binding protein 3 by p53. *Nature* **377:** 646-649.

Burney S, Niles JC, Dedon PC, Tannenbaum SR (1999). DNA damage in deoxynucleosides and oligonucleotides treated with peroxynitrite. *Chem Res Toxicol* **12:** 513-520.

Buzek J, Latonen L, Kurki S, Peltonen K, Laiho M (2002). Redox state of tumor suppressor p53 regulates its sequence-specific DNA binding in DNA-damaged cells by cysteine 277. *Nucleic Acids Res* **30:** 2340-2348.

Cabiscol E, Piulats E, Echave P, Herrero E, Ros J (2000). Oxidative Stress Promotes Specific Protein Damage inSaccharomyces cerevisiae. *J Biol Chem* **275:** 27393-27398.

Cadet J, Douki T, Pouget JP, Ravanat JL (2000). Singlet oxygen DNA damage products: formation and measurement. *Methods Enzymol* **319:** 143-153.

Campbell C, Quinn AG, Angus B, Farr PM, Rees JL (1993). Wavelength specific patterns of p53 induction in human skin following exposure to UV radiation. *Cancer research* **53:** 2697-2699.

Candi E, Schmidt R, Melino G (2005). The cornified envelope: a model of cell death in the skin. *Nat Rev Mol Cell Biol* **6:** 328-340.

Carballal S, Radi R, Kirk MC, Barnes S, Freeman BA, Alvarez B (2003). Sulfenic acid formation in human serum albumin by hydrogen peroxide and peroxynitrite. *Biochemistry* **42:** 9906-9914.

Carrodeguas JA, Kobayashi R, Lim SE, Copeland WC, Bogenhagen DF (1999). The accessory subunit of Xenopus laevis mitochondrial DNA polymerase γ increases processivity of the catalytic subunit of human DNA polymerase γ and is related to class II aminoacyl-tRNA synthetases. *Mol Cell Biol* **19:** 4039-4046.

Cassina AM, Hodara R, Souza JM, Thomson L, Castro L, Ischiropoulos H *et al* (2000). Cytochrome c nitration by peroxynitrite. *J Biol Chem* **275:** 21409-21415.

Cerutti PA (1985). Prooxidant States and Tumor Promotion. *Science* **227:** 375-381.

Cerutti PA, Trump BF (1991). Inflammation and oxidative stress in carcinogenesis. *Cancer Cells* **3:** 1-7.

Chan DC (2006). Mitochondrial fusion and fission in mammals. *Annu Rev Cell Dev Biol* **22:** 79-99.

Chan EY (2009). mTORC1 phosphorylates the ULK1-mAtg13-FIP200 autophagy regulatory complex. *Science signaling* **2:** pe51.

Chan SS, Longley MJ, Naviaux RK, Copeland WC (2005). Mono-allelic POLG expression resulting from nonsense-mediated decay and alternative splicing in a patient with Alpers syndrome. *DNA repair* **4:** 1381-1389.

Chan SS, Longley MJ, Copeland WC (2006). Modulation of the W748S mutation in DNA polymerase γ by the E1143G polymorphismin mitochondrial disorders. *Hum Mol Genet* **15:** 3473-3483.

Chen D, Yu Z, Zhu Z, Lopez CD (2006). The p53 pathway promotes efficient mitochondrial DNA base excision repair in colorectal cancer cells. *Cancer Res* **66:** 3485-3494.

Chen XJ, Butow RA (2005). The organization and inheritance of the mitochondrial genome. *Nat Rev Genet* **6:** 815-825.

Chen Y, Azad MB, Gibson SB (2009). Superoxide is the major reactive oxygen species regulating autophagy. *Cell Death Differ* **16:** 1040-1052.

Chipuk JE, Kuwana T, Bouchier-Hayes L, Droin NM, Newmeyer DD, Schuler M *et al* (2004). Direct activation of Bax by p53 mediates mitochondrial membrane permeabilization and apoptosis. *Science* **303:** 1010-1014.

Chipuk JE, Bouchier-Hayes L, Kuwana T, Newmeyer DD, Green DR (2005). PUMA couples the nuclear and cytoplasmic proapoptotic function of p53. *Science* **309:** 1732-1735.

Chuang TC, Liu JY, Lin CT, Tang YT, Yeh MH, Chang SC *et al* (2007). Human manganese superoxide dismutase suppresses HER2/neu-mediated breast cancer malignancy. *FEBS Lett* **581:** 4443-4449.

Chuikov S, Kurash JK, Wilson JR, Xiao B, Justin N, Ivanov GS *et al* (2004). Regulation of p53 activity through lysine methylation. *Nature* **432:** 353-360.

Chung-man Ho J, Zheng S, Comhair SA, Farver C, Erzurum SC (2001). Differential expression of manganese superoxide dismutase and catalase in lung cancer. *Cancer Res* **61:** 8578-8585.

Church SL, Grant JW, Ridnour LA, Oberley LW, Swanson PE, Meltzer PS *et al* (1993). Increased manganese superoxide dismutase expression suppresses the malignant phenotype of human melanoma cells. *Proc Natl Acad Sci U S A* **90:** 3113-3117.

Ciechanover A, Orian A, Schwartz AL (2000). Ubiquitin-mediated proteolysis: biological regulation via destruction. *BioEssays : news and reviews in molecular, cellular and developmental biology* **22:** 442-451.

Claerhout S, Decraene D, Van Laethem A, Van Kelst S, Agostinis P, Garmyn M (2007). AKT delays the early-activated apoptotic pathway in UVB-irradiated keratinocytes via BAD translocation. *J Invest Dermatol* **127:** 429-438.

Claerhout S, Verschooten L, Van Kelst S, De Vos R, Proby C, Agostinis P *et al* (2010). Concomitant inhibition of AKT and autophagy is required for efficient cisplatin-induced apoptosis of metastatic skin carcinoma. *Int J Cancer* **127:** 2790-2803.

Cohen HY, Miller C, Bitterman KJ, Wall NR, Hekking B, Kessler B *et al* (2004). Calorie restriction promotes mammalian cell survival by inducing the SIRT1 deacetylase. *Science* **305:** 390-392.

Colburn NH, Bruegge WF, Bates JR, Gray RH, Rossen JD, Kelsey WH *et al* (1978). Correlation of anchorage-independent growth with tumorigenicity of chemically transformed mouse epidermal cells. *Cancer Res* **38:** 624-634.

Colburn NH, Former BF, Nelson KA, Yuspa SH (1979). Tumour promoter induces anchorage independence irreversibly. *Nature* **281:** 589-591.

Coller HA, Khrapko K, Bodyak ND, Nekhaeva E, Herrero-Jimenez P, Thilly WG (2001). High frequency of homoplasmic mitochondrial DNA mutations in human tumors can be explained without selection. *Nat Genet* **28:** 147-150.

Cooper SJ, Bowden GT (2007). Ultraviolet B regulation of transcription factor families: roles of nuclear factor-kappa B (NF-kappaB) and activator protein-1 (AP-1) in UVB-induced skin carcinogenesis. *Curr Cancer Drug Targets* **7:** 325-334.

Cuervo AM (2004). Autophagy: in sickness and in health. *Trends Cell Biol* **14:** 70-77.

Dailey LA, Jekel N, Fink L, Gessler T, Schmehl T, Wittmar M *et al* (2006). Investigation of the proinflammatory potential of biodegradable nanoparticle drug delivery systems in the lung. *Toxicol Appl Pharmacol* **215:** 100-108.

Darbre PD (2005). Aluminium, antiperspirants and breast cancer. *J Inorg Biochem* **99:** 1912-1919.

Darbre PD (2006). Environmental oestrogens, cosmetics and breast cancer. *Best Pract Res Clin Endocrinol Metab* **20:** 121-143.

de Gruijl FR (2000). Photocarcinogenesis: UVA vs UVB. *Methods Enzymol* **319:** 359-366.

de Souza-Pinto NC, Harris CC, Bohr VA (2004). p53 functions in the incorporation step in DNA base excision repair in mouse liver mitochondria. *Oncogene* **23:** 6559-6568.

Decraene D, Agostinis P, Bouillon R, Degreef H, Garmyn M (2002). Insulin-like growth factor-1-mediated AKT activation postpones the onset of ultraviolet B-induced apoptosis, providing more time for cyclobutane thymine dimer removal in primary human keratinocytes. *J Biol Chem* **277:** 32587-32595.

Decraene D, Smaers K, Gan D, Mammone T, Matsui M, Maes D *et al* (2004a). A Synthetic Superoxide Dismutase Catalase Mimetic (EUK-134) Inhibits Membrane-Damage-Induced Activation of Mitogen-Activated Protein Kinase Pathways and Reduces p53 Accumulation in Ultraviolet B-Exposed Primary Human Keratinocytes. *J Investig Dermatol* **122:** 484-491.

Decraene D, Van Laethem A, Agostinis P, De Peuter L, Degreef H, Bouillon R *et al* (2004b). AKT status controls susceptibility of malignant keratinocytes to the early-activated and UVB-induced apoptotic pathway. *J Investig Dermatol* **123:** 207-212.

Deliconstantinos G, Villiotou V, Stavrides JC (1996). Alterations of nitric oxide synthase and xanthine oxidase activities of human keratinocytes by ultraviolet B radiation. Potential role for peroxynitrite in skin inflammation. *Biochem Pharmacol* **51:** 1727-1738.

Deruy E, Gosselin K, Vercamer C, Martien S, Bouali F, Slomianny C *et al* (2010). MnSOD upregulation induces autophagic programmed cell death in senescent keratinocytes. *PLoS One* **5:** e12712.

Dhar SK, Lynn BC, Daosukho C, St Clair DK (2004). Identification of nucleophosmin as an NF-kappaB co-activator for the induction of the human SOD2 gene. *J Biol Chem* **279:** 28209-28219.

Dhar SK, Xu Y, Chen Y, St Clair DK (2006). Specificity protein 1-dependent p53-mediated suppression of human manganese superoxide dismutase gene expression. *J Biol Chem* **281:** 21698-21709.

Donaldson K, Tran CL (2002). Inflammation caused by particles and fibers. *Inhal Toxicol* **14:** 5-27.

Donaldson K, Stone V, Tran CL, Kreyling W, Borm PJ (2004). Nanotoxicology. *Occup Environ Med* **61:** 727-728.

Dong Z, Birrer MJ, Watts RG, Matrisian LM, Colburn NH (1994). Blocking of tumor promoter-induced AP-1 activity inhibits induced transformation in JB6 mouse epidermal cells. *Proc Natl Acad Sci U S A* **91:** 609-613.

Duttaroy A, Paul A, Kundu M, Belton A (2003). A Sod2 null mutation confers severely reduced adult life span in Drosophila. *Genetics* **165:** 2295-2299.

Egan D, Kim J, Shaw RJ, Guan KL (2011a). The autophagy initiating kinase ULK1 is regulated via opposing phosphorylation by AMPK and mTOR. *Autophagy* **7:** 643-644.

Egan DF, Shackelford DB, Mihaylova MM, Gelino S, Kohnz RA, Mair W *et al* (2011b). Phosphorylation of ULK1 (hATG1) by AMP-activated protein kinase connects energy sensing to mitophagy. *Science* **331:** 456-461.

el-Deiry WS, Tokino T, Velculescu VE, Levy DB, Parsons R, Trent JM *et al* (1993). WAF1, a potential mediator of p53 tumor suppression. *Cell* **75:** 817-825.

Elder A, Gelein R, Silva V, Feikert T, Opanashuk L, Carter J *et al* (2006). Translocation of inhaled ultrafine manganese oxide particles to the central nervous system. *Environ Health Perspect* **114:** 1172-1178.

Erster S, Mihara M, Kim RH, Petrenko O, Moll UM (2004). In Vivo Mitochondrial p53 Translocation Triggers a Rapid First Wave of Cell Death in Response to DNA Damage That Can Precede p53 Target Gene Activation. *Mol Cell Biol* **24:** 6728-6741.

Eskelinen EL (2005). Maturation of autophagic vacuoles in Mammalian cells. *Autophagy* **1:** 1-10.

Esworthy RS, Ho Y-S, Chu F-F (1997). TheGpx1Gene Encodes Mitochondrial Glutathione Peroxidase in the Mouse Liver. *Arch Biochem Biophys* **340:** 59-63.

Exley C (1998). Does antiperspirant use increase the risk of aluminium-related disease, including Alzheimer's disease? *Mol Med Today* **4:** 107-109.

Exley C (2004). The pro-oxidant activity of aluminum. *Free Radic Biol Med* **36:** 380-387.

Exley C, Charles LM, Barr L, Martin C, Polwart A, Darbre PD (2007). Aluminium in human breast tissue. *J Inorg Biochem* **101:** 1344-1346.

Feldmeyer L, Keller M, Niklaus G, Hohl D, Werner S, Beer HD (2007). The inflammasome mediates UVB-induced activation and secretion of interleukin-1beta by keratinocytes. *Curr Biol* **17:** 1140-1145.

Ferraro E, Cecconi F (2007). Autophagic and apoptotic response to stress signals in mammalian cells. *Arch Biochem Biophys* **462:** 210-219.

Ferrer-Sueta G, Batinic-Haberle I, Spasojevic I, Fridovich I, Radi R (1999). Catalytic scavenging of peroxynitrite by isomeric Mn(III) N-methylpyridylporphyrins in the presence of reductants. *Chem Res Toxicol* **12:** 442-449.

Fimia GM, Stoykova A, Romagnoli A, Giunta L, Di Bartolomeo S, Nardacci R *et al* (2007). Ambra1 regulates autophagy and development of the nervous system. *Nature* **447:** 1121-1125.

Flarend R, Bin T, Elmore D, Hem SL (2001). A preliminary study of the dermal absorption of aluminium from antiperspirants using aluminium-26. *Food Chem Toxicol* **39:** 163-168.

Flaten TP (2001). Aluminium as a risk factor in Alzheimer's disease, with emphasis on drinking water. *Brain Res Bull* **55:** 187-196.

Fliss MS, Usadel H, Caballero OL, Wu L, Buta MR, Eleff SM *et al* (2000). Facile detection of mitochondrial DNA mutations in tumors and bodily fluids. *Science* **287:** 2017-2019.

Fojta M, Kubicarova T, Vojtesek B, Palecek E (1999). Effect of p53 protein redox states on binding to supercoiled and linear DNA. *J Biol Chem* **274:** 25749-25755.

Fridlender B, Fry M, Bolden A, Weissbach A (1972). A new synthetic RNA-dependent DNA polymerase from human tissue culture cells (HeLa-fibroblast-synthetic oligonucleotides-template-purified enzymes). *Proc Natl Acad Sci U S A* **69:** 452-455.

Ganley IG, Lam du H, Wang J, Ding X, Chen S, Jiang X (2009). ULK1.ATG13.FIP200 complex mediates mTOR signaling and is essential for autophagy. *J Biol Chem* **284:** 12297-12305.

Garrido N, Griparic L, Jokitalo E, Wartiovaara J, van der Bliek AM, Spelbrink JN (2003). Composition and Dynamics of Human Mitochondrial Nucleoids. *Mol Biol Cell* **14:** 1583-1596.

Gloster HM, Jr., Brodland DG (1996). The epidemiology of skin cancer. *Dermatologic surgery : official publication for American Society for Dermatologic Surgery [et al]* **22:** 217-226.

Goldstein S, Lind J, Merenyi G (2005). Chemistry of peroxynitrites as compared to peroxynitrates. *Chemical reviews* **105:** 2457-2470.

Gonzalez-Garcia M, Perez-Ballestero R, Ding L, Duan L, Boise LH, Thompson CB *et al* (1994). bcl-XL is the major bcl-x mRNA form expressed during murine development and its product localizes to mitochondria. *Development* **120:** 3033-3042.

Gray H, Wong TW (1992). Purification and identification of subunit structure of the human mitochondrial DNA polymerase. *J Biol Chem* **267:** 5835-5841.

Graziewicz MA, Day BJ, Copeland WC (2002). The mitochondrial DNA polymerase as a target of oxidative damage. *Nucleic Acids Res* **30:** 2817-2824.

Graziewicz MA, Longley MJ, Bienstock RJ, Zeviani M, Copeland WC (2004). Structure-function defects of human mitochondrial DNA polymerase in autosomal dominant progressive external ophthalmoplegia. *Nat Struct Mol Biol* **11:** 770-776.

Graziewicz MA, Longley MJ, Copeland WC (2006). DNA polymerase γ in mitochondrial DNA replication and repair. *Chem Rev* **106:** 383-405.

Grillot DA, Gonzalez-Garcia M, Ekhterae D, Duan L, Inohara N, Ohta S *et al* (1997). Genomic organization, promoter region analysis, and chromosome localization of the mouse bcl-x gene. *J Immunol* **158:** 4750-4757.

Grutter MG (2000). Caspases: key players in programmed cell death. *Curr Opin Struct Biol* **10:** 649-655.

Gu Y, Wang C, Cohen A (2004). Effect of IGF-1 on the balance between autophagy of dysfunctional mitochondria and apoptosis. *FEBS Letters* **577:** 357-360.

Haldar S, Negrini M, Monne M, Sabbioni S, Croce CM (1994). Down-regulation of bcl-2 by p53 in breast cancer cells. *Cancer Res* **54:** 2095-2097.

Hall PA, McKee PH, Menage HD, Dover R, Lane DP (1993). High levels of p53 protein in UV-irradiated normal human skin. *Oncogene* **8:** 203-207.

Halliday GM, Lyons JG (2008). Inflammatory doses of UV may not be necessary for skin carcinogenesis. *Photochem Photobiol* **84:** 272-283.

Hamacher-Brady A, Brady NR, Gottlieb RA, Gustafsson AB (2006). Autophagy as a protective response to Bnip3-mediated apoptotic signaling in the heart. *Autophagy* **2:** 307-309.

Harbottle A, Birch-Machin MA (2006). Real-time PCR analysis of a 3895 bp mitochondrial DNA deletion in nonmelanoma skin cancer and its use as a quantitative marker for sunlight exposure in human skin. *Br J Cancer* **94:** 1887-1893.

Harper JW, Adami GR, Wei N, Keyomarsi K, Elledge SJ (1993). The p21 Cdk-interacting protein Cip1 is a potent inhibitor of G1 cyclin-dependent kinases. *Cell* **75:** 805-816.

Harris SL, Levine AJ (2005). The p53 pathway: positive and negative feedback loops. *Oncogene* **24:** 2899-2908.

Hayakawa H, Taketomi A, Sakumi K, Kuwano M, Sekiguchi M (1995). Generation and elimination of 8-oxo-7,8-dihydro-2'-deoxyguanosine 5'-triphosphate, a mutagenic substrate for DNA synthesis, in human cells. *Biochemistry* **34:** 89-95.

He C, Klionsky DJ (2009). Regulation mechanisms and signaling pathways of autophagy. *Annu Rev Genet* **43:** 67-93.

Hensley K, Robinson KA, Gabbita SP, Salsman S, Floyd RA (2000). Reactive oxygen species, cell signaling, and cell injury. *Free Radic Biol Med* **28:** 1456-1462.

Hernandez-Saavedra D, McCord JM (2003). Paradoxical effects of thiol reagents on Jurkat cells and a new thiol-sensitive mutant form of human mitochondrial superoxide dismutase. *Cancer Res* **63:** 159-163.

Hernandez-Saavedra D, McCord JM (2009). Association of a new intronic polymorphism of the SOD2 gene (G1677T) with cancer. *Cell Biochem Func* **27:** 223-227.

Herrling T, Jung K, Fuchs J (2006). Measurements of UV-generated free radicals/reactive oxygen species (ROS) in skin. *Spectrochimica acta Part A, Mol Biomol Spec* **63:** 840-845.

Heyne K, Mannebach S, Wuertz E, Knaup KX, Mahyar-Roemer M, Roemer K (2004). Identification of a putative p53 binding sequence within the human mitochondrial genome. *FEBS Lett* **578:** 198-202.

Ho YS, Crapo JD (1988). Isolation and characterization of complementary DNAs encoding human manganese-containing superoxide dismutase. *FEBS Lett* **229:** 256-260.

Holmgren A (1985). Thioredoxin. *Annu Rev Biochem* **54:** 237-271.

Holt IJ, Harding AE, Morgan-Hughes JA (1988). Deletions of muscle mitochondrial DNA in patients with mitochondrial myopathies. *Nature* **331:** 717-719.

Hubscher U, Kuenzle CC, Spadari S (1979). Functional roles of DNA polymerases beta and gamma. *Proc Natl Acad Sci U S A* **76:** 2316-2320.

Hussain AR, Uddin S, Bu R, Khan OS, Ahmed SO, Ahmed M *et al* (2011). Resveratrol suppresses constitutive activation of AKT via generation of ROS and induces apoptosis in diffuse large B cell lymphoma cell lines. *PLoS One* **6:** e24703.

Ide Y, Tsuchimoto D, Tominaga Y, Iwamoto Y, Nakabeppu Y (2003). Characterization of the genomic structure and expression of the mouse Apex2 gene. *Genomics* **81:** 47-57.

Imai S, Armstrong CM, Kaeberlein M, Guarente L (2000). Transcriptional silencing and longevity protein Sir2 is an NAD-dependent histone deacetylase. *Nature* **403:** 795-800.

Ischiropoulos H, Zhu L, Chen J, Tsai M, Martin JC, Smith CD *et al* (1992). Peroxynitrite-mediated tyrosine nitration catalyzed by superoxide dismutase. *Arch Biochem Biophys* **298:** 431-437.

Jacinto E, Hall MN (2003). Tor signalling in bugs, brain and brawn. *Nat Rev Mol Cell Biol* **4:** 117-126.

Jacks T, Remington L, Williams BO, Schmitt EM, Halachmi S, Bronson RT *et al* (1994). Tumor spectrum analysis in p53-mutant mice. *Curr Biol* **4:** 1-7.

Jang B, Han S (2006). Biochemical properties of cytochrome c nitrated by peroxynitrite. *Biochimie* **88:** 53-58.

Janssen AM, Bosman CB, van Duijn W, Oostendorp-van de Ruit MM, Kubben FJ, Griffioen G *et al* (2000). Superoxide dismutases in gastric and esophageal cancer and the prognostic impact in gastric cancer. *Clin Cancer Res* **6:** 3183-3192.

Jezek P, Hlavata L (2005). Mitochondria in homeostasis of reactive oxygen species in cell, tissues, and organism. *Int J Biochem Cell Biol* **37:** 2478-2503.

Jiang X, Wang X (2004). Cytochrome C-mediated apoptosis. *Annu Rev Biochem* **73:** 87-106.

Jin S (2006). Autophagy, mitochondrial quality control, and oncogenesis. *Autophagy* **2:** 80-84.

Johnatty SE, Nagle CM, Spurdle AB, Chen X, Webb PM, Chenevix-Trench G (2007). The MnSOD Val9Ala polymorphism, dietary antioxidant intake, risk and survival in ovarian cancer (Australia). *Gynecol Oncol* **107:** 388-391.

Johnson AA, Tsai Y, Graves SW, Johnson KA (2000). Human mitochondrial DNA polymerase holoenzyme: reconstitution and characterization. *Biochemistry* **39:** 1702-1708.

Johnson AA, Johnson KA (2001). Fidelity of nucleotide incorporation by human mitochondrial DNA polymerase. *J Biol Chem* **276:** 38090-38096.

Jung CH, Jun CB, Ro SH, Kim YM, Otto NM, Cao J *et al* (2009). ULK-Atg13-FIP200 complexes mediate mTOR signaling to the autophagy machinery. *Mol Biol Cell* **20:** 1992-2003.

Kaguni LS (2004). DNA polymerase γ, the mitochondrial replicase. *Annu Rev Biochem* **73:** 293-320.

Kasai H, Nishimura S (1983). Hydroxylation of the C-8 position of deoxyguanosine by reducing agents in the presence of oxygen. *Nucleic acids symposium series***:** 165-167.

Keller M, Ruegg A, Werner S, Beer HD (2008). Active caspase-1 is a regulator of unconventional protein secretion. *Cell* **132:** 818-831.

Kienhofer J, Haussler DJF, Ruckelshausen F, Muessig E, Weber K, Pimentel D *et al* (2009). Association of mitochondrial antioxidant enzymes with mitochondrial DNA as integral nucleoid constituents. *FASEB J* **23:** 2034-2044.

Kim EH, Sohn S, Kwon HJ, Kim SU, Kim MJ, Lee SJ *et al* (2007). Sodium selenite induces superoxide-mediated mitochondrial damage and subsequent autophagic cell death in malignant glioma cells. *Cancer Res* **67:** 6314-6324.

Kiningham KK, St Clair DK (1997). Overexpression of manganese superoxide dismutase selectively modulates the activity of Jun-associated transcription factors in fibrosarcoma cells. *Cancer Res* **57:** 5265-5271.

Kirkin V, McEwan DG, Novak I, Dikic I (2009). A role for ubiquitin in selective autophagy. *Mol Cell* **34:** 259-269.

Kobayashi N, Nakagawa A, Muramatsu T, Yamashina Y, Shirai T, Hashimoto MW *et al* (1998). Supranuclear melanin caps reduce ultraviolet induced DNA photoproducts in human epidermis. *J Investig Dermatol* **110:** 806-810.

Kondoh H, Lleonart ME, Gil J, Wang J, Degan P, Peters G *et al* (2005). Glycolytic enzymes can modulate cellular life span. *Cancer Res* **65:** 177-185.

Kops GJ, Dansen TB, Polderman PE, Saarloos I, Wirtz KW, Coffer PJ *et al* (2002). Forkhead transcription factor FOXO3a protects quiescent cells from oxidative stress. *Nature* **419:** 316-321.

Kovalenko OA, Santos JH (2009). *Analysis of Oxidative Damage by Gene-Specific Quantitative PCR*. John Wiley & Sons, Inc.

Krauss S (2001). Mitochondria: Structure and Role in Respiration. *eLS*. John Wiley & Sons, Ltd.

Kreilgaard M (2002). Influence of microemulsions on cutaneous drug delivery. *Adv Drug Deliv Rev* **54 Suppl 1:** S77-98.

Krishnan KJ, Harbottle A, Birch-Machin MA (2004). The Use of a 3895 bp Mitochondrial DNA Deletion as a Marker for Sunlight Exposure in Human Skin. *J Investig Dermatol* **123:** 1020-1024.

Kroemer G, Marino G, Levine B (2010). Autophagy and the integrated stress response. *Molecular cell* **40:** 280-293.

Krysko DV, Agostinis P, Krysko O, Garg AD, Bachert C, Lambrecht BN *et al* (2011). Emerging role of damage-associated molecular patterns derived from mitochondria in inflammation. *Trends Immunol* **32:** 157-164.

Kuhn C, Hurwitz SA, Kumar MG, Cotton J, Spandau DF (1999). Activation of the insulin-like growth factor-1 receptor promotes the survival of human keratinocytes following ultraviolet B irradiation. *Int J Cancer* **80:** 431-438.

Kujoth GC, Hiona A, Pugh TD, Someya S, Panzer K, Wohlgemuth SE *et al* (2005). Mitochondrial DNA Mutations, Oxidative Stress, and Apoptosis in Mammalian Aging. *Science* **309:** 481-484.

Kulawiec M, Ayyasamy V, Singh KK (2009). p53 regulates mtDNA copy number and mitocheckpoint pathway. *J Carcinog* **8:** 8.

Kulms D, Schwarz T (2002). Independent contribution of three different pathways to ultraviolet-B-induced apoptosis. *Biochem Pharmacol* **64:** 837-841.

Kunisada M, Sakumi K, Tominaga Y, Budiyanto A, Ueda M, Ichihashi M *et al* (2005). 8-Oxoguanine formation induced by chronic UVB exposure makes Ogg1 knockout mice susceptible to skin carcinogenesis. *Cancer Res* **65:** 6006-6010.

Lademann J, Weigmann H, Rickmeyer C, Barthelmes H, Schaefer H, Mueller G *et al* (1999). Penetration of titanium dioxide microparticles in a sunscreen formulation into the horny layer and the follicular orifice. *Skin Pharmacol Appl Skin Physiol* **12:** 247-256.

Lane DP (1992). Cancer. p53, guardian of the genome. *Nature* **358:** 15-16.

Langley E, Pearson M, Faretta M, Bauer UM, Frye RA, Minucci S *et al* (2002). Human SIR2 deacetylates p53 and antagonizes PML/p53-induced cellular senescence. *Embo J* **21:** 2383-2396.

Lebedeva MA, Eaton JS, Shadel GS (2009). Loss of p53 causes mitochondrial DNA depletion and altered mitochondrial reactive oxygen species homeostasis. *Biochimica et biophysica acta* **1787:** 328-334.

Lebovitz RM, Zhang H, Vogel H, Cartwright J, Jr., Dionne L, Lu N *et al* (1996). Neurodegeneration, myocardial injury, and perinatal death in mitochondrial superoxide dismutase-deficient mice. *Proc Natl Acad Sci U S A* **93:** 9782-9787.

Lecrenier N, Van Der Bruggen P, Foury F (1997). Mitochondrial DNA polymerases from yeast to man: a new family of polymerases. *Gene* **185:** 147-152.

Lee JW, Park S, Takahashi Y, Wang HG (2010). The association of AMPK with ULK1 regulates autophagy. *PLoS One* **5:** e15394.

Lee YS, Kennedy WD, Yin YW (2009). Structural insight into processive human mitochondrial DNA synthesis and disease-related polymerase mutations. *Cell* **139:** 312-324.

Legros F, Malka F, Frachon P, Lombes A, Rojo M (2004). Organization and dynamics of human mitochondrial DNA. *J Cell Sci* **117:** 2653-2662.

Lenaz G, Baracca A, Barbero G, Bergamini C, Dalmonte ME, Del Sole M *et al* (2010). Mitochondrial respiratory chain super-complex I-III in physiology and pathology. *Biochimica et biophysica acta* **1797:** 633-640.

Lenaz G, Genova ML (2010). Structure and organization of mitochondrial respiratory complexes: a new understanding of an old subject. *Antioxid Redox Signal* **12:** 961-1008.

Leu JI, Dumont P, Hafey M, Murphy ME, George DL (2004). Mitochondrial p53 activates Bak and causes disruption of a Bak-Mcl1 complex. *Nature Cell Biol* **6:** 443-450.

Levine AJ, Momand J, Finlay CA (1991). The p53 tumour suppressor gene. *Nature* **351:** 453-456.

Levine B, Klionsky DJ (2004). Development by self-digestion: molecular mechanisms and biological functions of autophagy. *Developmental cell* **6:** 463-477.

Lewis W, Day BJ, Kohler JJ, Hosseini SH, Chan SSL, Green EC *et al* (2006). Decreased mtDNA, oxidative stress, cardiomyopathy, and death from transgenic cardiac targeted human mutant polymerase γ. *Lab Invest* **87:** 326-335.

Lewis W, Day BJ, Kohler JJ, Hosseini SH, Chan SS, Green EC *et al* (2007). Decreased mtDNA, oxidative stress, cardiomyopathy, and death from transgenic cardiac targeted human mutant polymerase γ. *Lab Invest* **87:** 326-335.

Li G, Mitchell DL, Ho VC, Reed JC, Tron VA (1996). Decreased DNA repair but normal apoptosis in ultraviolet-irradiated skin of p53-transgenic mice. *Am J Pathol* **148:** 1113-1123.

Li G, Ho VC, Mitchell DL, Trotter MJ, Tron VA (1997). Differentiation-dependent p53 regulation of nucleotide excision repair in keratinocytes. *Am J Pathol* **150:** 1457-1464.

Li G, Ho VC (1998). p53-dependent DNA repair and apoptosis respond differently to high- and low-dose ultraviolet radiation. *Br J Dermatol* **139:** 3-10.

Li JJ, Colburn NH, Oberley LW (1998). Maspin gene expression in tumor suppression induced by overexpressing manganese-containing superoxide dismutase cDNA in human breast cancer cells. *Carcinogenesis* **19:** 833-839.

Li Y, Huang TT, Carlson EJ, Melov S, Ursell PC, Olson JL *et al* (1995). Dilated cardiomyopathy and neonatal lethality in mutant mice lacking manganese superoxide dismutase. *Nat Genet* **11:** 376-381.

Liang C, Feng P, Ku B, Dotan I, Canaani D, Oh BH *et al* (2006). Autophagic and tumour suppressor activity of a novel Beclin1-binding protein UVRAG. *Nature cell biology* **8:** 688-699.

Lim CS (2006). SIRT1: tumor promoter or tumor suppressor? *Med Hypotheses* **67:** 341-344.

Lim SE, Longley MJ, Copeland WC (1999). The mitochondrial p55 accessory subunit of human DNA polymerase γ enhances DNA binding, promotes processive DNA synthesis, and confers N-ethylmaleimide resistance. *J Biol Chem* **274:** 38197-38203.

Lim SE, Ponamarev MV, Longley MJ, Copeland WC (2003). Structural Determinants in Human DNA Polymerase γ Account for Mitochondrial Toxicity from Nucleoside Analogs. *J Mol Biol* **329:** 45-57.

Lippens S, Denecker G, Ovaere P, Vandenabeele P, Declercq W (2005). Death penalty for keratinocytes: apoptosis versus cornification. *Cell death and Differ* **12 Suppl 2:** 1497-1508.

Liu B, Chen Y, St Clair DK (2008). ROS and p53: a versatile partnership. *Free Radic Biol Med* **44:** 1529-1535.

Liu M, Dhanwada KR, Birt DF, Hecht S, Pelling JC (1994). Increase in p53 protein half-life in mouse keratinocytes following UV-B irradiation. *Carcinogenesis* **15:** 1089-1092.

Longley MJ, Prasad R, Srivastava DK, Wilson SH, Copeland WC (1998). Identification of 5'-deoxyribose phosphate lyase activity in human DNA polymerase γ and its role in mitochondrial base excision repair in vitro. *Proc Natl Acad Sci U S A* **95:** 12244-12248.

Longley MJ, Copeland WC (2002). Purification, separation, and identification of the human mtDNA polymerase with and without its accessory subunit. *Methods Mol Biol* **197:** 245-257.

Lotti LV, Rotolo S, Francescangeli F, Frati L, Torrisi MR, Marchese C (2007). AKT and MAPK signaling in KGF-treated and UVB-exposed human epidermal cells. *J Cell Physiol* **212:** 633-642.

Luo J, Su F, Chen D, Shiloh A, Gu W (2000). Deacetylation of p53 modulates its effect on cell growth and apoptosis. *Nature* **408:** 377-381.

Luo J, Nikolaev AY, Imai S, Chen D, Su F, Shiloh A *et al* (2001). Negative control of p53 by Sir2alpha promotes cell survival under stress. *Cell* **107:** 137-148.

Luo N, Kaguni LS (2005). Mutations in the spacer region of Drosophila mitochondrial DNA polymerase affect DNA binding, processivity, and the balance between Pol and Exo function. *J Biol Chem* **280:** 2491-2497.

Lymar SV, Hurst JK (1998). Radical nature of peroxynitrite reactivity. *Chem Res Toxicol* **11:** 714-715.

MacMillan-Crow LA, Crow JP, Kerby JD, Beckman JS, Thompson JA (1996). Nitration and inactivation of manganese superoxide dismutase in chronic rejection of human renal allografts. *Proc Natl Acad Sci U S A* **93:** 11853-11858.

MacMillan-Crow LA, Crow JP, Thompson JA (1998). Peroxynitrite-mediated inactivation of manganese superoxide dismutase involves nitration and oxidation of critical tyrosine residues. *Biochemistry* **37:** 1613-1622.

MacMillan-Crow LA, Thompson JA (1999). Tyrosine modifications and inactivation of active site manganese superoxide dismutase mutant (Y34F) by peroxynitrite. *Arch Biochem Biophys* **366:** 82-88.

Maeda T, Hanna AN, Sim AB, Chua PP, Chong MT, Tron VA (2002). GADD45 regulates G2/M arrest, DNA repair, and cell death in keratinocytes following ultraviolet exposure. *J Invest Dermatol* **119:** 22-26.

Maglio DHG, Paz ML, Ferrari A, Weill FS, Czerniczyniec A, Leoni J *et al* (2005). Skin damage and mitochondrial dysfunction after acute ultraviolet B irradiation: relationship with nitric oxide production. *Photodermatol Photoimmunol Photomed* **21:** 311-317.

Malafa M, Margenthaler J, Webb B, Neitzel L, Christophersen M (2000). MnSOD expression is increased in metastatic gastric cancer. *The Journal of surgical research* **88:** 130-134.

Mammone T, Gan D, Collins D, Lockshin RA, Marenus K, Maes D (2000). Successful separation of apoptosis and necrosis pathways in HaCaT keratinocyte cells induced by UVB irradiation. *Cell Biol Toxicol* **16:** 293-302.

Mammucari C, Milan G, Romanello V, Masiero E, Rudolf R, Del Piccolo P *et al* (2007). FoxO3 controls autophagy in skeletal muscle in vivo. *Cell metabolism* **6:** 458-471.

Manning BD, Cantley LC (2007). AKT/PKB signaling: navigating downstream. *Cell* **129:** 1261-1274.

Marchenko ND, Zaika A, Moll UM (2000). Death signal-induced localization of p53 protein to mitochondria. A potential role in apoptotic signaling. *J Biol Chem* **275:** 16202-16212.

Marchenko ND, Wolff S, Erster S, Becker K, Moll UM (2007). Monoubiquitylation promotes mitochondrial p53 translocation. *Embo J* **26:** 923-934.

Martindale JL, Holbrook NJ (2002). Cellular response to oxidative stress: signaling for suicide and survival. *J Cell Physiol* **192:** 1-15.

Mason JM, Schmitz MA, Muller KM, Arndt KM (2006). Semirational design of Jun-Fos coiled coils with increased affinity: Universal implications for leucine zipper prediction and design. *Proc Natl Acad Sci U S A* **103:** 8989-8994.

Matoba S, Kang JG, Patino WD, Wragg A, Boehm M, Gavrilova O *et al* (2006). p53 regulates mitochondrial respiration. *Science* **312:** 1650-1653.

Matsumura Y, Ananthaswamy HN (2002). Short-term and long-term cellular and molecular events following UV irradiation of skin: implications for molecular medicine. *Expert Rev Mol Med* **4:** 1-22.

Matsunaga K, Saitoh T, Tabata K, Omori H, Satoh T, Kurotori N *et al* (2009). Two Beclin 1-binding proteins, Atg14L and Rubicon, reciprocally regulate autophagy at different stages. *Nature Cell Biol* **11:** 385-396.

McLennan HR, Degli Esposti M (2000). The contribution of mitochondrial respiratory complexes to the production of reactive oxygen species. *J Bioenerg Biomembr* **32:** 153-162.

McNeil SE (2005). Nanotechnology for the biologist. *J Leukoc Biol* **78:** 585-594.

Medina C, Santos-Martinez MJ, Radomski A, Corrigan OI, Radomski MW (2007). Nanoparticles: pharmacological and toxicological significance. *Br J Pharmacol* **150:** 552-558.

Melov S, Coskun P, Patel M, Tuinstra R, Cottrell B, Jun AS *et al* (1999). Mitochondrial disease in superoxide dismutase 2 mutant mice. *Proc Natl Acad Sci U S A* **96:** 846-851.

Mihara M, Erster S, Zaika A, Petrenko O, Chittenden T, Pancoska P *et al* (2003). p53 Has a Direct Apoptogenic Role at the Mitochondria. *Molecular cell* **11:** 577-590.

Mihara M, Moll UM (2003). Detection of mitochondrial localization of p53. *Methods Mol Biol* **234:** 203-209.

Miyashita T, Reed JC (1995). Tumor suppressor p53 is a direct transcriptional activator of the human bax gene. *Cell* **80:** 293-299.

Mizushima N (2007). Autophagy: process and function. *Genes Dev* **21:** 2861-2873.

Mizushima N, Levine B, Cuervo AM, Klionsky DJ (2008). Autophagy fights disease through cellular self-digestion. *Nature* **451:** 1069-1075.

Moll UM, Zaika A (2001). Nuclear and mitochondrial apoptotic pathways of p53. *FEBS Lett* **493:** 65-69.

Momand J, Wu HH, Dasgupta G (2000). MDM2--master regulator of the p53 tumor suppressor protein. *Gene* **242:** 15-29.

Mustafa AG, Singh IN, Wang J, Carrico KM, Hall ED (2010). Mitochondrial protection after traumatic brain injury by scavenging lipid peroxyl radicals. *J Neurochem* **114:** 271-280.

Naderi-Hachtroudi L, Peters T, Brenneisen P, Meewes C, Hommel C, Razi-Wolf Z *et al* (2002). Induction of manganese superoxide dismutase in human dermal fibroblasts: a UV-B-mediated paracrine mechanism with the release of epidermal interleukin 1 alpha, interleukin 1 beta, and tumor necrosis factor alpha. *Arch Dermatol* **138:** 1473-1479.

Nakabeppu Y (2001). Regulation of intracellular localization of human MTH1, OGG1, and MYH proteins for repair of oxidative DNA damage. *Prog Nucleic Acid Res Mol Biol* **68:** 75-94.

Nakahira K, Haspel JA, Rathinam VA, Lee SJ, Dolinay T, Lam HC *et al* (2011). Autophagy proteins regulate innate immune responses by inhibiting the release of mitochondrial DNA mediated by the NALP3 inflammasome. *Nat Immunol* **12:** 222-230.

Nakano K, Vousden KH (2001). PUMA, a novel proapoptotic gene, is induced by p53. *Mol Cell* **7:** 683-694.

Nalwaya N, Deen WM (2005). Nitric oxide, oxygen, and superoxide formation and consumption in macrophage cultures. *Chem Res Toxicol* **18:** 486-493.

Nemes Z, Steinert PM (1999). Bricks and mortar of the epidermal barrier. *Exp Mol Med* **31:** 5-19.

Nemoto S, Fergusson MM, Finkel T (2005). SIRT1 functionally interacts with the metabolic regulator and transcriptional coactivator PGC-1{alpha}. *J Biol Chem* **280:** 16456-16460.

Nestle FO, Di Meglio P, Qin JZ, Nickoloff BJ (2009). Skin immune sentinels in health and disease. *Nat Rev Immunol* **9:** 679-691.

Nicholson S, Exley C (2007). Aluminum: A potential pro-oxidant in sunscreens/sunblocks? *Free Radic Biol Med* **43:** 1216-1217.

O'Brien KM, Dirmeier R, Engle M, Poyton RO (2004). Mitochondrial Protein Oxidation in Yeast Mutants Lacking Manganese-(MnSOD) or Copper- and Zinc-containing Superoxide Dismutase (CuZnSOD). *J Biol Chem* **279:** 51817-51827.

Oberdorster G, Maynard A, Donaldson K, Castranova V, Fitzpatrick J, Ausman K *et al* (2005a). Principles for characterizing the potential human health effects from exposure to nanomaterials: elements of a screening strategy. *Part Fibre Toxicol* **2:** 8.

Oberdorster G, Oberdorster E, Oberdorster J (2005b). Nanotoxicology: an emerging discipline evolving from studies of ultrafine particles. *Environ Health Perspect* **113:** 823-839.

Oberley LW, Bize IB, Sahu SK, Leuthauser SW, Gruber HE (1978). Superoxide dismutase activity of normal murine liver, regenerating liver, and H6 hepatoma. *J Natl Cancer Inst* **61:** 375-379.

Oberley LW, Buettner GR (1979). Role of superoxide dismutase in cancer: a review. *Cancer Res* **39:** 1141-1149.

Oberley LW (2005). Mechanism of the tumor suppressive effect of MnSOD overexpression. *Biomed Pharmacother* **59:** 143-148.

Oberley TD, Xue Y, Zhao Y, Kiningham K, Szweda LI, St Clair DK (2004). In situ reduction of oxidative damage, increased cell turnover, and delay of mitochondrial injury by overexpression of manganese superoxide dismutase in a multistage skin carcinogenesis model. *Antioxid Redox Signal* **6:** 537-548.

Oda E, Ohki R, Murasawa H, Nemoto J, Shibue T, Yamashita T *et al* (2000a). Noxa, a BH3-only member of the Bcl-2 family and candidate mediator of p53-induced apoptosis. *Science* **288:** 1053-1058.

Oda K, Arakawa H, Tanaka T, Matsuda K, Tanikawa C, Mori T *et al* (2000b). p53AIP1, a potential mediator of p53-dependent apoptosis, and its regulation by Ser-46-phosphorylated p53. *Cell* **102:** 849-862.

Okamoto K, Shaw JM (2005). Mitochondrial morphology and dynamics in yeast and multicellular eukaryotes. *Annu Rev Genet* **39:** 503-536.

Ouhtit A, Muller HK, Davis DW, Ullrich SE, McConkey D, Ananthaswamy HN (2000). Temporal Events in Skin Injury and the Early Adaptive Responses in Ultraviolet-Irradiated Mouse Skin. *Am J Pathol* **156:** 201-207.

Owen-Schaub LB, Zhang W, Cusack JC, Angelo LS, Santee SM, Fujiwara T *et al* (1995). Wild-type human p53 and a temperature-sensitive mutant induce Fas/APO-1 expression. *Mol Cell Biol* **15:** 3032-3040.

Ozden O, Park SH, Kim HS, Jiang H, Coleman MC, Spitz DR *et al* (2011). Acetylation of MnSOD directs enzymatic activity responding to cellular nutrient status or oxidative stress. *Aging (Albany NY)* **3:** 102-107.

Pani G, Bedogni B, Anzevino R, Colavitti R, Palazzotti B, Borrello S *et al* (2000). Deregulated manganese superoxide dismutase expression and resistance to oxidative injury in p53-deficient cells. *Cancer Res* **60:** 4654-4660.

Pattingre S, Tassa A, Qu X, Garuti R, Liang XH, Mizushima N *et al* (2005). Bcl-2 antiapoptotic proteins inhibit Beclin 1-dependent autophagy. *Cell* **122:** 927-939.

Paul A, Belton A, Nag S, Martin I, Grotewiel MS, Duttaroy A (2007). Reduced mitochondrial SOD displays mortality characteristics reminiscent of natural aging. *Mech Ageing Dev* **128:** 706-716.

Paunesku T, Mittal S, Protic M, Oryhon J, Korolev SV, Joachimiak A *et al* (2001). Proliferating cell nuclear antigen (PCNA): ringmaster of the genome. *Int J Radiat Biol* **77:** 1007-1021.

Petit C, Sancar A (1999). Nucleotide excision repair: from E. coli to man. *Biochimie* **81:** 15-25.

Peus D, Vasa RA, Meves A, Pott M, Beyerle A, Squillace K *et al* (1998). H2O2 is an important mediator of UVB-induced EGF-receptor phosphorylation in cultured keratinocytes. *J Invest Dermatol* **110:** 966-971.

Pfeifer GP (1997). Formation and processing of UV photoproducts: effects of DNA sequence and chromatin environment. *Photochem Photobiol* **65:** 270-283.

Pinz KG, Bogenhagen DF (1998). Efficient repair of abasic sites in DNA by mitochondrial enzymes. *Mol Cell Biol* **18:** 1257-1265.

Ponamarev MV, Longley MJ, Nguyen D, Kunkel TA, Copeland WC (2002). Active site mutation in DNA polymerase γ associated with progressive external ophthalmoplegia causes error-prone DNA synthesis. *J Biol Chem* **277:** 15225-15228.

Porntadavity S, Xu Y, Kiningham K, Rangnekar VM, Prachayasittikul V, St Clair DK (2001). TPA-activated transcription of the human MnSOD gene: role of transcription factors Sp-1 and Egr-1. *DNA Cell Biol* **20:** 473-481.

Prives C, Hall PA (1999). The p53 pathway. *J Pathol* **187:** 112-126.

Quijano C, Alvarez B, Gatti RM, Augusto O, Radi R (1997). Pathways of peroxynitrite oxidation of thiol groups. *Biochem J* **322 (Pt 1):** 167-173.

Quijano C, Romero N, Radi R (2005). Tyrosine nitration by superoxide and nitric oxide fluxes in biological systems: modeling the impact of superoxide dismutase and nitric oxide diffusion. *Free Radic Biol Med* **39:** 728-741.

Radi R, Rodriguez M, Castro L, Telleri R (1994). Inhibition of mitochondrial electron transport by peroxynitrite. *Arch Biochem Biophys* **308:** 89-95.

Radi R (1998). Peroxynitrite reactions and diffusion in biology. *Chemical Res Toxicol* **11:** 720-721.

Radi R, Peluffo G, Alvarez MN, Naviliat M, Cayota A (2001). Unraveling peroxynitrite formation in biological systems. *Free Radic Biol Med* **30:** 463-488.

Raivich G, Behrens A (2006). Role of the AP-1 transcription factor c-Jun in developing, adult and injured brain. *Prog Neurobiol* **78:** 347-363.

Ravikumar B, Sarkar S, Davies JE, Futter M, Garcia-Arencibia M, Green-Thompson ZW *et al* (2010). Regulation of mammalian autophagy in physiology and pathophysiology. *Physiological reviews* **90:** 1383-1435.

Ray AJ, Turner R, Nikaido O, Rees JL, Birch-Machin MA (2000). The Spectrum of Mitochondrial DNA Deletions is a Ubiquitous Marker of Ultraviolet Radiation Exposure in Human Skin. *J Investig Dermatol* **115:** 674-679.

Renzing J, Hansen S, Lane D (1996). Oxidative stress is involved in the UV activation of p53. *J Cell Sci* **109:** 1105-1112.

Rigel DS (2008). Cutaneous ultraviolet exposure and its relationship to the development of skin cancer. *J Am Acad Dermatol* **58:** S129-132.

Robles AI, Bemmels NA, Foraker AB, Harris CC (2001). APAF-1 is a transcriptional target of p53 in DNA damage-induced apoptosis. *Cancer Res* **61:** 6660-6664.

Romero N, Radi R, Linares E, Augusto O, Detweiler CD, Mason RP *et al* (2003). Reaction of human hemoglobin with peroxynitrite. Isomerization to nitrate and secondary formation of protein radicals. *J Biol Chem* **278:** 44049-44057.

Ropp PA, Copeland WC (1996). Cloning and characterization of the human mitochondrial DNA polymerase, DNA polymerase γ. *Genomics* **36:** 449-458.

Rosenblum JS, Gilula NB, Lerner RA (1996). On signal sequence polymorphisms and diseases of distribution. *Proc Natl Acad Sci U S A* **93:** 4471-4473.

Sabatini DM (2006). mTOR and cancer: insights into a complex relationship. *Nature Rev Cancer* **6:** 729-734.

Sakaguchi K, Herrera JE, Saito S, Miki T, Bustin M, Vassilev A *et al* (1998). DNA damage activates p53 through a phosphorylation-acetylation cascade. *Genes Dev* **12:** 2831-2841.

Salvatorelli E, Guarnieri S, Menna P, Liberi G, Calafiore AM, Mariggio MA *et al* (2006). Defective one- or two-electron reduction of the anticancer anthracycline epirubicin in human heart. Relative importance of vesicular sequestration and impaired efficiency of electron addition. *J Biol Chem* **281:** 10990-11001.

Scherz-Shouval R, Elazar Z (2007). ROS, mitochondria and the regulation of autophagy. *Trends Cell Biol* **17:** 422-427.

Schwarten M, Mohrluder J, Ma P, Stoldt M, Thielmann Y, Stangler T *et al* (2009). Nix directly binds to GABARAP: a possible crosstalk between apoptosis and autophagy. *Autophagy* **5:** 690-698.

Schweers RL, Zhang J, Randall MS, Loyd MR, Li W, Dorsey FC *et al* (2007). NIX is required for programmed mitochondrial clearance during reticulocyte maturation. *Proc Natl Acad Sci U S A* **104:** 19500-19505.

Shaw RJ (2009). LKB1 and AMP-activated protein kinase control of mTOR signalling and growth. *Acta physiologica* **196:** 65-80.

Shibutani S, Takeshita M, Grollman AP (1991). Insertion of specific bases during DNA synthesis past the oxidation-damaged base 8-oxodG. *Nature* **349:** 431-434.

Shokolenko I, Venediktova N, Bochkareva A, Wilson GL, Alexeyev MF (2009). Oxidative stress induces degradation of mitochondrial DNA. *Nucl Acids Res* **37:** 2539-2548.

Siemiatycki J, Richardson L, Straif K, Latreille B, Lakhani R, Campbell S *et al* (2004). Listing occupational carcinogens. *Environ Health Perspect* **112:** 1447-1459.

Sluyter R, Halliday GM (2000). Enhanced tumor growth in UV-irradiated skin is associated with an influx of inflammatory cells into the epidermis. *Carcinogenesis* **21:** 1801-1807.

Sluyter R, Halliday GM (2001). Infiltration by inflammatory cells required for solar-simulated ultraviolet radiation enhancement of skin tumor growth. *Cancer Immunol Immunother* **50:** 151-156.

Smith J (2002). Human Sir2 and the 'silencing' of p53 activity. *Trends Cell Biol* **12:** 404-406.

Smith ML, Chen IT, Zhan Q, Bae I, Chen CY, Gilmer TM *et al* (1994). Interaction of the p53-regulated protein Gadd45 with proliferating cell nuclear antigen. *Science* **266:** 1376-1380.

Smith PS, Zhao W, Spitz DR, Robbins ME (2007). Inhibiting catalase activity sensitizes 36B10 rat glioma cells to oxidative stress. *Free Radic Biol Med* **42:** 787-797.

Spitz DR, Oberley LW (1989). An assay for superoxide dismutase activity in mammalian tissue homogenates. *Anal Biochem* **179:** 8-18.

St Clair DK, Oberley TD, Muse KE, St Clair WH (1994). Expression of manganese superoxide dismutase promotes cellular differentiation. *Free Radic Biol Med* **16:** 275-282.

Stadtman ER (1990). Metal ion-catalyzed oxidation of proteins: biochemical mechanism and biological consequences. *Free Radic Biol Med* **9:** 315-325.

Storz P (2006). Reactive oxygen species-mediated mitochondria-to-nucleus signaling: a key to aging and radical-caused diseases. *Science's STKE : signal transduction knowledge environment* **2006:** re3.

Stuart JA, Karahalil B, Hogue BA, Souza-Pinto NC, Bohr VA (2004). Mitochondrial and nuclear DNA base excision repair are affected differently by caloric restriction. *FASEB J*: 03-0890fje.

Sutton A, Khoury H, Prip-Buus C, Cepanec C, Pessayre D, Degoul F (2003). The Ala16Val genetic dimorphism modulates the import of human manganese superoxide dismutase into rat liver mitochondria. *Pharmacogenetics* **13:** 145-157.

Szabo C, Ohshima H (1997). DNA damage induced by peroxynitrite: subsequent biological effects. *Nitric oxide : biology and chemistry / official journal of the Nitric Oxide Society* **1:** 373-385.

Szabo C, Ischiropoulos H, Radi R (2007). Peroxynitrite: biochemistry, pathophysiology and development of therapeutics. *Nature Rev Drug Discov* **6:** 662-680.

Taanman JW, Heiske M, Letellier T (2010). Measurement of kinetic parameters of human platelet DNA polymerase γ. *Methods* **51:** 374-378.

Takasawa R, Nakamura H, Mori T, Tanuma S (2005). Differential apoptotic pathways in human keratinocyte HaCaT cells exposed to UVB and UVC. *Apoptosis :* **10:** 1121-1130.

Takeshige K, Minakami S (1979). NADH- and NADPH-dependent formation of superoxide anions by bovine heart submitochondrial particles and NADH-ubiquinone reductase preparation. *Biochem J* **180:** 129-135.

Takeuchi S, Zhang W, Wakamatsu K, Ito S, Hearing VJ, Kraemer KH *et al* (2004). Melanin acts as a potent UVB photosensitizer to cause an atypical mode of cell death in murine skin. *Proc Natl Acad Sci U S A* **101:** 15076-15081.

Tanaka Y, Guhde G, Suter A, Eskelinen EL, Hartmann D, Lullmann-Rauch R *et al* (2000). Accumulation of autophagic vacuoles and cardiomyopathy in LAMP-2-deficient mice. *Nature* **406:** 902-906.

Tao R, Coleman MC, Pennington JD, Ozden O, Park SH, Jiang H *et al* (2010). Sirt3-mediated deacetylation of evolutionarily conserved lysine 122 regulates MnSOD activity in response to stress. *Mol Cell* **40:** 893-904.

Tinkle SS, Antonini JM, Rich BA, Roberts JR, Salmen R, DePree K *et al* (2003). Skin as a route of exposure and sensitization in chronic beryllium disease. *Environ Health Perspect* **111:** 1202-1208.

Tornaletti S, Pfeifer GP (1996). UV damage and repair mechanisms in mammalian cells. *BioEssays : news and reviews in molecular, cellular and developmental biology* **18:** 221-228.

Tracy K, Dibling BC, Spike BT, Knabb JR, Schumacker P, Macleod KF (2007). BNIP3 is an RB/E2F target gene required for hypoxia-induced autophagy. *Mol Cell Biol* **27:** 6229-6242.

Trifunovic A, Wredenberg A, Falkenberg M, Spelbrink JN, Rovio AT, Bruder CE *et al* (2004). Premature ageing in mice expressing defective mitochondrial DNA polymerase. *Nature* **429:** 417-423.

Tron VA, Trotter MJ, Tang L, Krajewska M, Reed JC, Ho VC *et al* (1998). p53-Regulated Apoptosis Is Differentiation Dependent in Ultraviolet B-Irradiated Mouse Keratinocytes. *Am J Pathol* **153:** 579-585.

Trouba KJ, Hamadeh HK, Amin RP, Germolec DR (2002). Oxidative stress and its role in skin disease. *Antioxid Redox Signal* **4:** 665-673.

Tsuchimoto D, Sakai Y, Sakumi K, Nishioka K, Sasaki M, Fujiwara T *et al* (2001). Human APE2 protein is mostly localized in the nuclei and to some extent in the mitochondria, while nuclear APE2 is partly associated with proliferating cell nuclear antigen. *Nucleic Acids Res* **29:** 2349-2360.

Tsujimoto Y, Cossman J, Jaffe E, Croce CM (1985). Involvement of the bcl-2 gene in human follicular lymphoma. *Science* **228:** 1440-1443.

Tsujimoto Y (1998). Role of Bcl-2 family proteins in apoptosis: apoptosomes or mitochondria? *Genes Cells* **3:** 697-707.

Tsujimoto Y, Shimizu S (2000). Bcl-2 family: life-or-death switch. *FEBS Lett* **466:** 6-10.

Tsujimoto Y, Shimizu S (2005). Another way to die: autophagic programmed cell death. *Cell Death Differ* **12 Suppl 2:** 1528-1534.

van der Voet GB, de Wolff FA (1985). Distribution of aluminium between plasma and erythrocytes. *Hum Toxicol* **4:** 643-648.

Van Goethem G, Dermaut B, Lofgren A, Martin J-J, Van Broeckhoven C (2001). Mutation of POLG is associated with progressive external ophthalmoplegia characterized by mtDNA deletions. *Nat Genet* **28:** 211-212.

van Hoffen A, Venema J, Meschini R, van Zeeland AA, Mullenders LH (1995). Transcription-coupled repair removes both cyclobutane pyrimidine dimers and 6-4 photoproducts with equal efficiency and in a sequential way from transcribed DNA in xeroderma pigmentosum group C fibroblasts. *EMBO J* **14:** 360-367.

Van Remmen H, Salvador C, Yang H, Huang TT, Epstein CJ, Richardson A (1999). Characterization of the Antioxidant Status of the Heterozygous Manganese Superoxide Dismutase Knockout Mouse. *Arch Biochem Biophys* **363:** 91-97.

Van Remmen H, Ikeno Y, Hamilton M, Pahlavani M, Wolf N, Thorpe SR *et al* (2003). Life-long reduction in MnSOD activity results in increased DNA damage and higher incidence of cancer but does not accelerate aging. *Physiol Genomics* **16:** 29-37.

Vaseva AV, Moll UM (2009). The mitochondrial p53 pathway. *Biochim Biophys Acta* **1787:** 414-420.

Vaziri H, Dessain SK, Ng Eaton E, Imai SI, Frye RA, Pandita TK *et al* (2001). hSIR2(SIRT1) functions as an NAD-dependent p53 deacetylase. *Cell* **107:** 149-159.

Vermulst M, Wanagat J, Kujoth GC, Bielas JH, Rabinovitch PS, Prolla TA *et al* (2008). DNA deletions and clonal mutations drive premature aging in mitochondrial mutator mice. *Nat Genet* **40:** 392-394.

Vickers SM, MacMillan-Crow LA, Green M, Ellis C, Thompson JA (1999). Association of increased immunostaining for inducible nitric oxide synthase and nitrotyrosine with fibroblast growth factor transformation in pancreatic cancer. *Arch Surg* **134:** 245-251.

Vousden KH, Lu X (2002). Live or let die: the cell's response to p53. *Nature Rev Cancer* **2:** 594-604.

Wallace DC, Singh G, Lott MT, Hodge JA, Schurr TG, Lezza AM *et al* (1988). Mitochondrial DNA mutation associated with Leber's hereditary optic neuropathy. *Science* **242:** 1427-1430.

Wallace DC (1999). Mitochondrial diseases in man and mouse. *Science* **283:** 1482-1488.

Wan XS, Devalaraja MN, St Clair DK (1994). Molecular structure and organization of the human manganese superoxide dismutase gene. *DNA Cell Biol* **13:** 1127-1136.

Wang LI, Miller DP, Sai Y, Liu G, Su L, Wain JC *et al* (2001). Manganese superoxide dismutase alanine-to-valine polymorphism at codon 16 and lung cancer risk. *J Natl Cancer Inst* **93:** 1818-1821.

Wang Y, Farr CL, Kaguni LS (1997). Accessory subunit of mitochondrial DNA polymerase from Drosophila embryos. Cloning, molecular analysis, and association in the native enzyme. *J Biol Chem* **272:** 13640-13646.

Wang Y, Kaguni LS (1999). Baculovirus expression reconstitutes Drosophila mitochondrial DNA polymerase. *J Biol Chem* **274:** 28972-28977.

Warheit DB, Brock WJ, Lee KP, Webb TR, Reed KL (2005). Comparative pulmonary toxicity inhalation and instillation studies with different TiO2 particle formulations: impact of surface treatments on particle toxicity. *Toxicol Sci* **88:** 514-524.

Waster PK, Ollinger KM (2009). Redox-Dependent Translocation of p53 to Mitochondria or Nucleus in Human Melanocytes after UVA- and UVB-Induced Apoptosis. *J Investig Dermatol* **129:** 1769-1781.

Willis I, Menter JM, Whyte HJ (1981). The rapid induction of cancers in the hairless mouse utilizing the principle of photoaugmentation. *J Investig Dermatol* **76:** 404-408.

Wisdom R (1999). AP-1: one switch for many signals. *Exp Cell Res* **253:** 180-185.

Wong TS, Rajagopalan S, Townsley FM, Freund SM, Petrovich M, Loakes D *et al* (2009). Physical and functional interactions between human mitochondrial single-stranded DNA-binding protein and tumour suppressor p53. *Nucleic Acids Res* **37:** 568-581.

Woodson K, Tangrea JA, Lehman TA, Modali R, Taylor KM, Snyder K *et al* (2003). Manganese superoxide dismutase (MnSOD) polymorphism, alpha-tocopherol supplementation and prostate cancer risk in the alpha-tocopherol, beta-carotene cancer prevention study (Finland). *Cancer causes & control : CCC* **14:** 513-518.

Wu GS, Burns TF, McDonald ER, 3rd, Jiang W, Meng R, Krantz ID *et al* (1997). KILLER/DR5 is a DNA damage-inducible p53-regulated death receptor gene. *Nat Genet* **17:** 141-143.

Wu S, Wang L, Jacoby AM, Jasinski K, Kubant R, Malinski T (2010). Ultraviolet B Light-induced Nitric Oxide/Peroxynitrite Imbalance in Keratinocytes—Implications for Apoptosis and Necrosis. *Photochem Photobiol* **86:** 389-396.

Xia T, Kovochich M, Brant J, Hotze M, Sempf J, Oberley T *et al* (2006). Comparison of the Abilities of Ambient and Manufactured Nanoparticles to Induce Cellular Toxicity According to an Oxidative Stress Paradigm. *Nano Letters* **6:** 1794-1807.

Xu Q, Ming Z, Dart AM, Du XJ (2007a). Optimizing dosage of ketamine and xylazine in murine echocardiography. *Clin Exp Pharmacol Physiol* **34:** 499-507.

Xu Y, Kiningham KK, Devalaraja MN, Yeh CC, Majima H, Kasarskis EJ *et al* (1999a). An intronic NF-kappaB element is essential for induction of the human manganese superoxide dismutase gene by tumor necrosis factor-alpha and interleukin-1beta. *DNA Cell Biol* **18:** 709-722.

Xu Y, Krishnan A, Wan XS, Majima H, Yeh CC, Ludewig G *et al* (1999b). Mutations in the promoter reveal a cause for the reduced expression of the human manganese superoxide dismutase gene in cancer cells. *Oncogene* **18:** 93-102.

Xu Y, Porntadavity S, St Clair DK (2002). Transcriptional regulation of the human manganese superoxide dismutase gene: the role of specificity protein 1 (Sp1) and activating protein-2 (AP-2). *Biochem J* **362:** 401-412.

Xu Y, Fang F, Dhar SK, St Clair WH, Kasarskis EJ, St Clair DK (2007b). The role of a single-stranded nucleotide loop in transcriptional regulation of the human sod2 gene. *J Biol Chem* **282:** 15981-15994.

Xu Y, Fang F, Dhar SK, Bosch A, St Clair WH, Kasarskis EJ *et al* (2008). Mutations in the SOD2 promoter reveal a molecular basis for an activating protein 2-dependent dysregulation of manganese superoxide dismutase expression in cancer cells. *Mol Cancer Res* **6:** 1881-1893.

Yaar M, Gilchrest BA (2001). Ageing and photoageing of keratinocytes and melanocytes. *Clin Exp Dermatol* **26:** 583-591.

Yakes FM, Van Houten B (1997). Mitochondrial DNA damage is more extensive and persists longer than nuclear DNA damage in human cells following oxidative stress. *Proc Natl Acad Sci U S A* **94:** 514-519.

Yakubovskaya E, Chen Z, Carrodeguas JA, Kisker C, Bogenhagen DF (2006). Functional human mitochondrial DNA polymerase γ forms a heterotrimer. *J Biol Chem* **281:** 374-382.

Yakubovskaya E, Lukin M, Chen Z, Berriman J, Wall JS, Kobayashi R *et al* (2007). The EM structure of human DNA polymerase γ reveals a localized contact between the catalytic and accessory subunits. *EMBO J* **26:** 4283-4291.

Yamakura F, Taka H, Fujimura T, Murayama K (1998). Inactivation of human manganese-superoxide dismutase by peroxynitrite is caused by exclusive nitration of tyrosine 34 to 3-nitrotyrosine. *J Biol Chem* **273:** 14085-14089.

Yang JH, Lee HC, Lin KJ, Wei YH (1994). A specific 4977-bp deletion of mitochondrial DNA in human ageing skin. *Arch Dermatol Res* **286:** 386-390.

Yen WL, Klionsky DJ (2008). How to live long and prosper: autophagy, mitochondria, and aging. *Physiology (Bethesda)* **23:** 248-262.

Yokel RA, McNamara PJ (2001). Aluminium toxicokinetics: an updated minireview. *Pharmacol Toxicol* **88:** 159-167.

Zhang L, Yu L, Yu CA (1998). Generation of superoxide anion by succinate-cytochrome c reductase from bovine heart mitochondria. *J Biol Chem* **273:** 33972-33976.

Zhang Q, Raoof M, Chen Y, Sumi Y, Sursal T, Junger W *et al* (2010). Circulating mitochondrial DAMPs cause inflammatory responses to injury. *Nature* **464:** 104-107.

Zhang W, Remenyik E, Zelterman D, Brash DE, Wikonkal NM (2001). Escaping the stem cell compartment: sustained UVB exposure allows p53-mutant keratinocytes to colonize adjacent epidermal proliferating units without incurring additional mutations. *Proc Natl Acad Sci U S A* **98:** 13948-13953.

Zhao Y, Xue Y, Oberley TD, Kiningham KK, Lin SM, Yen HC *et al* (2001). Overexpression of manganese superoxide dismutase suppresses tumor formation by modulation of activator protein-1 signaling in a multistage skin carcinogenesis model. *Cancer Res* **61:** 6082-6088.

Zhao Y, Oberley TD, Chaiswing L, Lin SM, Epstein CJ, Huang TT *et al* (2002). Manganese superoxide dismutase deficiency enhances cell turnover via tumor promoter-induced alterations in AP-1 and p53-mediated pathways in a skin cancer model. *Oncogene* **21:** 3836-3846.

Zhao Y, Chaiswing L, Oberley TD, Batinic-Haberle I, St Clair W, Epstein CJ *et al* (2005a). A mechanism-based antioxidant approach for the reduction of skin carcinogenesis. *Cancer Res* **65:** 1401-1405.

Zhao Y, Chaiswing L, Velez JM, Batinic-Haberle I, Colburn NH, Oberley TD *et al* (2005b). p53 Translocation to Mitochondria Precedes Its Nuclear Translocation and Targets Mitochondrial Oxidative Defense Protein-Manganese Superoxide Dismutase. *Cancer Res* **65:** 3745-3750.

Zhong W, Yan T, Lim R, Oberley LW (1999). Expression of superoxide dismutases, catalase, and glutathione peroxidase in glioma cells. *Free Radic Biol Med* **27:** 1334-1345.

Zhou Q, Mrowietz U, Rostami-Yazdi M (2009). Oxidative stress in the pathogenesis of psoriasis. *Free Radic Biol Med* **47:** 891-905.

Zhou R, Yazdi AS, Menu P, Tschopp J (2011). A role for mitochondria in NLRP3 inflammasome activation. *Nature* **469:** 221-225.

Ziegler A, Leffell DJ, Kunala S, Sharma HW, Gailani M, Simon JA *et al* (1993). Mutation hotspots due to sunlight in the p53 gene of nonmelanoma skin cancers. *Proc Natl Acad Sci U S A* **90:** 4216-4220.

Ziegler A, Jonason AS, Leffell DJ, Simon JA, Sharma HW, Kimmelman J *et al* (1994). Sunburn and p53 in the onset of skin cancer. *Nature* **372:** 773-776.

Zitvogel L, Kepp O, Kroemer G (2010). Decoding cell death signals in inflammation and immunity. *Cell* **140:** 798-804.

Vita

PERSONAL INFORMATION

Name   Vasudevan Bakthavatchalu

Date of Birth   05/19/1977

Place of Birth   Arakkonam, India

EDUCATION

2010- Present   Post-Doctoral Scholar, UKVDL, College of Agriculture, University of Kentucky, Lexington, Kentucky

2003-2004   Post-Doctoral Scholar, Center for Oral Health Research, College of Dentistry, University of Kentucky, Lexington, Kentucky

2001 – 2003   Masters in Veterinary Science (MVSc., - Veterinary Pathology)
Tamil Nadu Veterinary and Animal Sciences University, Tamil Nadu, India

1995-2001   Bachelors in Veterinary Science (BVSc.,)
Tamil Nadu Veterinary and Animal Sciences University, Tamil Nadu, India

RESEARCH ACTIVITIES

2001-2003   MVSc., Thesis Research on "Cytological and pathological studies of canine mammary tumours"
Tamil Nadu Veterinary and Animal Sciences University, Tamil Nadu, India

HONORS AND AWARDS

Travel Award for the 16th Annual conference of Society of Free Radical Biology and Medicine, 2009

Research Challenge Trust Fund (RCTF) fellowship – University of Kentucky

University Merit Scholarship during BVSc., and MVSc.,

PUBLICATIONS AND PRESENTATIONS

Holley AK **Bakthavatchalu V**, Velez-Roman JM, and St Clair DK. (2011).Manganese superoxide dismutase: guardian of the powerhouse. Int J Mol Sci 12(10): 7114-62.

Bakthavatchalu V, Dey S, Xu Y, Noel T, Jungsuwadee P, Holley AK, Dhar SK, Batinic-Haberle I, and St Clair DK. (2011).Manganese superoxide dismutase is a mitochondrial fidelity protein that protects Polγ against UV-induced inactivation. Oncogene.

Bakthavatchalu V, Meka A, Mans JJ, Sathishkumar S, Lopez MC, Bhattacharyya I, Boyce BF, Baker HV, Lamont RJ, Ebersole JL and Kesavalu L. (2010). Polymicrobial periodontal transcriptomes in calvarial bone and soft tissue. Mol. Oral. Microbiol. 26(5): 303-20

Bakthavatchalu V, Meka A, Sathishkumar S, Lopez MC, Bhattacharyya I, Boyce BF, Mans JJ, Lamont RJ, Baker HV, Ebersole JL and Kesavalu L. (2010). Tannerella forsythia infection-induced calvarial bone and soft tissue transcription profiles. Mol. Oral. Microbiol. 25(5): 317-30

Bakthavatchalu V, Meka A, Sathishkumar S, Lopez MC, Verma RK, Wallet SM, Bhattacharyya I, Boyce BF, Mans JJ, Lamont RJ, Baker HV, Ebersole JL and Kesavalu L. (2010). Molecular characterization of *Treponema denticola* infection-induced bone and soft tissue transcription profiles. Mol. Oral. Microbiol. 25(4): 260-74

Meka A, **Bakthavatchalu V**, Sathishkumar S, Lopez MC, Verma RK, Wallet SM, Bhattacharyya I, Boyce BF, Handfield M, Lamont RJ, Baker HV, Ebersole JL and Kesavalu L. (2010). *Porphyromonas gingivalis* infection-induced tissue and bone transcriptional profiles. Mol. Oral. Microbiol. 25(1): 61-74

Xu Y, Josson S, Fang F, Oberley TD, St Clair DK, Wan XS, Sun Y, **Bakthavatchalu V**, Muthuswamy A and St Clair WH. (2009). RelB enhances prostate cancer growth: implications for the role of the nuclear factor-kappa B alternative pathway in tumorigenicity. Cancer Res. 69(8): 3267-3271

Dey S*, **Bakthavatchalu V***, Tseng MT, Wu P, Florence R, Grulke EA, Yokel R, Dhar SK, Yang HS, Chen Y and St Clair DK. (2008). Interactions between SIRT1 and AP-1 reveal a mechanistic insight into the growth promoting properties of alumina (Al2O3) nanoparticles in mouse skin epithelial cells. Carcinogenesis. 29(10): 1920-1929

Kesavalu L, **Bakthavatchalu V**, Rahman MM, Su J, Raghu B, Dawson D, Fernandes G and Ebersole JL. (2007). Omega-3 fatty acid regulates inflammatory cytokine/mediator messenger RNA expression in *P. gingivalis*-induced experimental periodontal disease. Oral Microbiol. Immunol. 22(4): 232-239

Kesavalu L, Sathishkumar S, **Bakthavatchalu V**, Matthews C, Dawson D, Steffen M and Ebersole JL. (2007). Rat model of polymicrobial infection, immunity, and alveolar bone resorption in periodontal disease. Infect. Immun. 75(4): 1704-1712

Zhao Y, Chaiswing L, **Bakthavatchalu V**, Oberley TD and St Clair DK. (2006). Ras mutation promotes p53 activation and apoptosis of skin keratinocytes. Carcinogenesis; 27(8): 1692-1698

Kesavalu L, **Vasudevan B**, Raghu B, Browning E, Dawson D, Novak JM, Corell MC, Steffen MJ, Bhattacharya A, Fernandes G and Ebersole JL. (2006). Omega-3 fatty acid effect on alveolar bone loss in rats. J. Dent. Res. 85(7): 648-652

Vasudevan B, Raghul J, Madheswaran R, Murali Manohar B and Balachandran C. (2004). Cytological and histopathological diagnosis of canine skin tumors. Indian Journal of Veterinary Pathology. 28(2): 130-133

Vasudevan B, Zaheer Abbas K, Nayeem Md, and Balachandran C. (2003). Effect of cigarette smoke on rats under hypobaric condition. Cheiron. 32(5&6): 107-110

Bakthavatchalu V and Daret K St. Clair (2009). MnSOD links oxidative stress and mitochondrial DNA repair by interacting with p53 and DNA pol γ. Presented at the 16th Annual meeting of Society of Free Radical Biology and Medicine, San Francisco CA.

Bakthavatchalu V and Daret K St. Clair (2010). Manganese Superoxide Dismutase protects Polγ against UV induced inactivation: Implication for DNA repair. Presented at the 17th Annual meeting of Society of Free Radical Biology and Medicine, Orlando FL.

Vasudevan Bakthavatchalu

04-18-12